DOCTORAL THESIS

Development and Analysis of Carbon-Based Dry-Contact Electrodes for Bioimpedance Measurements

Hip Kõiv

Development and Analysis of Carbon-Based Dry-Contact Electrodes for Bioimpedance Measurements

HIP KÕIV

TAL
TECH
PRESS

TALLINN UNIVERSITY OF TECHNOLOGY
School of Information Technologies
Thomas Johann Seebeck Department of Electronics

The dissertation was accepted for the defence of the degree of Doctor of Philosophy on 21 November 2022.

Supervisor: Professor Emeritus Dr Mart Min,
Thomas Johann Seebeck Department of Electronics,
Tallinn University of Technology,
Tallinn, Estonia

Co-supervisor: Dr Raul Land,
Thomas Johann Seebeck Department of Electronics,
Tallinn University of Technology,
Tallinn, Estonia

Co-supervisor: Associate Professor Dr Indrek Must,
Institute of Technology,
University of Tartu
Tartu, Estonia

Opponents: Professor Dr Ørjan Grøttem Martinsen,
Department of Physics,
University of Oslo,
Oslo, Norway

Associate Professor Dr Jari Viik,
Institute of Biosciences and Medical Technology (BioMediTech),
University of Tampere,
Tampere, Finland

Defence of the thesis: 20 January 2023, Tallinn

Declaration:
Hereby I declare that this doctoral thesis, my original investigation and achievement, submitted for the doctoral degree at Tallinn University of Technology, has not been submitted for any academic degree elsewhere.

Hip Kõiv

_____
signature

European Union
European Regional
Development Fund

Investing
in your future

Süsinikmaterjalil põhinevate kuivkontakt-elektroodide arendus ja analüüs bioimpedantsi mõõtmiseks

HIP KÕIV

TAL
TECH
KIRJASTUS

Contents

List of publications

The thesis is based on the following publications by the author:

I   H. Kõiv, K. Pesti, M. Min, R. Land.   Investigation of cost-effective carbon nanofiber/carbon fiber and silicone polymer composite material for wearable bioimpedance device. In IEEE Sensors Applications Symposium (SAS) proceedings, pages 1-6. IEEE, 2019.

II H. Kõiv, K. Pesti, M. Min, R. Land, I. Must. Comparison of the carbon nanofiber-/fiber- and silicone-based electrodes for bioimpedance measurements. In IEEE Transactions on Instrumentation and Measurement, vol. 69, no. 4, pages 1455-1463. IEEE, 2020.

III H. Kõiv, M. Rist, M. Min. Development of bioimpedance sensing device for wearable monitoring of the aortic blood pressure curve. In tm - Technisches Messen, vol. 85, no. 5, pages 366-377. De Gruyter/Oldenbourg, 2018.

Contribution to the aforementioned publications in this thesis are:

I   In I, I developed the carbon-PDSM material, carried out the data collection and analyzed the electrical conductivity results under compressive load and stretching, prepared the figures, and wrote the manuscript.

II In II, I prepared different electrodes and methods to measure and analyze the best and optimal possible solution for bioimpedance measurements on the human forearm, carried out the data collection and evaluated the results, prepared the figures, and wrote the manuscript.

III In III, I researched and wrote the literature review, fabricated the phantom material, conducted the multipoint measurements, prepared the figures, and analyzed the results.

Other related publications

IV M. Min, H. Kõiv, E. Priidel, K. Pesti, P. Annus. Non-invasive acquisition of the aortic blood pressure waveform. In Wearable Devices – the Big Wave of Innovation, N. Nasiri (Ed.). London: IntechOpen, 2019.

V M. Metshein, H. Kõiv, P. Annus, M. Min. Electrode optimization for bioimpedance based central aortic blood pressure estimation. In World Congress on Medical Physics and Biomedical Engineering, IFMBE Proceedings, vol 68/2, pages 497-501. Springer, 2018.

VI M. Min, P. Annus, A. Krivošei, J. Lamp, H. Kõiv, T. Uuetoa. Bioimpedance sensing – a viable alternative for tonometry in non-invasive assessment of central aortic blood pressure. In IEEE International Symposium on Medical Measurements and Applications (MeMeA), pages 373-378. IEEE, 2017.

VII H. Kõiv, K. Pesti, R. Gordon. Electric impedance measurement of tissue phantom materials for development of medical diagnostic systems. In Progress reports on impedance spectroscopy: Measurements, Modeling and Applications, pages 131-137. De Gruyter/Oldenbourg, 2016.

Abbreviations

CF	Carbon fiber
ChAc	Choline acetate
CMRR	Common mode rejection ratio
CNF	Carbon nanofiber
CNT	Carbon nanotubes
DNA	Deoxyribonucleic acid
ECG	Electrocardiography
EDA	Electrodermal activity
EDL	Electrical double layer
EEG	Electroencephalography
EIS	Electrical impedance spectroscopy
EIT	Electrical impedance tomography
EMG	Electromyography
GPIO	General-purpose input/output
HAc	Acetic acid
HMDSO	Hexamethyldisiloxane
ICG	Impedance cardiography
IL	Ionic liquid
IPA	Isopropyl alcohol
IPG	Electrical impedance plethysmography
KAc	Potassium acetate
MWCNT	Multi-walled carbon nanotubes
PDMS	Polydimethylsiloxane
PEDOT:PSS	Poly(3,4-ethylenedioxythiphene) poly(styrene sulfonate)
PET	Polyethylene terephthalate
PI	Polyimide
PVA	Polyvinyl alcohol
PVC	Polyvinyl chloride
SC	Stratum corneum
SCR	Skin conductance response
STMP	Sodium trimetaphosphate
SWCNT	Single-walled carbon nanotubes
TIP	Transthoracic impedance pneumography

1 Introduction

1.1 Non-invasive health monitoring

75% to 85% of the healthcare-related costs in developed countries are spent on cardiovascular disease, diabetes, cancer, and obesity [1]. One solution to reduce these costs and achieve better health for people is to monitor and treat patients before their symptoms become acute.

European Framework Program "Horizon Europe" for research and innovation consists of six main clusters, one of which is health. This cluster aims to contribute to the well-being and accessible healthcare with high quality; more specifically, one of the expected impacts, as set out by the strategic plan, is "staying healthy in a rapidly changing society" [2]. To reach this goal, patients and not-yet-patients need to be involved in their care as much as possible by measuring their own physical health parameters, evaluating symptoms, or analyzing their daily activities. Undoubtedly, one prerequisite is reliable self-monitoring wearable devices paired with a system recording the needed data.

Wearable electronics is an emerging field, and the market has experienced rapid growth in recent years – an almost 60% increase in the number of devices sold from 2018 to 2021 [3]. Furthermore, the market size is expected to reach 118.16 billion USD by 2028 as growing health awareness among consumers leads to increased interest in fitness activities [4]. When classifying wearables by end-use, the most common application segments are sports, remote patient monitoring, and home healthcare [3]. These wearables have numerous sensors that can collect, store and transmit physiological data to provide a wide range of necessary measures, such as heart rate, body temperature, sleep, movement/activity, oxygen saturation, respiratory rate, galvanic skin response, blood pressure, etc. [1]. All these parameters would be immensely useful to gather together and use in the patient-centered approach called "personalized health". This concept, considered part of the future healthcare regime, requires wearable remote monitoring tools for early diagnosis.

Wearable technologies promise to redefine the assessment of health behaviors, yet their clinical implementation remains a challenge. There is a need for data standardization between the devices and sensor locations; also, the measurement accuracy of the acquisition of many physiological parameters is poor [5]. Registering physical activity and estimating heart rate are the two most common measurements provided by current commercial wearable devices but incorporating blood pressure measurements with a wearable is the new trend [6]. Numerous prestigious companies like Valencell [7], Omron [8], and Garmin [9] are developing blood pressure monitor watches to keep up with the movement.

High blood pressure (hypertension) is a serious medical condition, which can lead to severe health complications and increase the risk factor for cardiovascular disease. It affects 1.28 billion people worldwide and an estimated 46% of adults with hypertension are unaware that they have the condition [10]. This is because high blood pressure develops slowly over time and often does not cause any overt symptoms. Consequently, hypertension is also called a "silent killer". Exactly for this reason measuring blood pressure regularly during the day and between the days is an effective way to detect problems and act on them at an early stage. Currently, our workgroup is developing a bioimpedance measurement system to estimate blood pressure from the wrist area non-invasively.

1.2 Problem statement

The electrode is a crucial part of the bioimpedance measurement system. If not correctly designed and applied, the registered signals can be attenuated or superimposed with artifacts from the electrodes. Bioimpedance measurements are often performed using silver/silver chloride (Ag/AgCl) gel electrodes. In this case, the skin is exposed to an electrolytic gel to establish an electrically continuous domain, i.e., ionic conductivity is facilitated across the skin and the gel. The gel, in turn, is in contact with a solid layer of silver and silver chloride to transduce between ionic and electronic currents. The electric circuit from the silver layer to the measurement instrument is typically completed via snap connectors.

Ag/AgCl electrodes are used due to being non-polarizable, having low interface impedance, and more stable contact potential, consequently, better noise behavior [11]. Unfortunately, gel/wet electrodes are unsuitable for wearables as they are not reusable, and the irritation problem from highly electrolytic gel makes them inconvenient for the wearer. Dry stretchable electrodes could be an exciting alternative and have been gaining popularity in recent years [12]-[14], but using dry electrodes for bioimpedance measurements is limited. The outermost, very dry layer of the skin, the stratum corneum (SC), is highly resistive and contributes greatly to electrode-skin interface impedance. This, in turn, results in poor signal quality. Dry microneedle electrodes can minimize the effect of insulating SC as they can pierce this thin layer and make direct contact with the highly conductive epidermal layers [15]. Unfortunately, in addition to the costly and complicated fabrication process, skin-piercing microneedles can cause discomfort to the patient [16]. Another possibility could be semi-dry ionogel electrodes, which have all the advantages of dry electrodes, but also the surface's slight stickiness, improving highly problematic interfacial impedance issues. In addition, intermediary solutions exist, where microneedle-like electrodes with flexible and soft strands naturally press against the skin to reduce the interface impedance. However, contacting performance as the sole is insufficient: a successful electrode solution also anticipates an effective fabrication procedure, preferably compatible with the existing wearable technology, potentially even with textiles.

The lack of universally accepted metrics and standard characterization techniques prohibits developers from properly benchmarking the electrodes. Several previous studies [1], [17], [18] have used the interface impedance to evaluate the performance of a new electrode or compare it with standard commercial electrodes but the methods and metrics used are all slightly varying. Assessing electrode-skin interface impedance (introduced in Chapter 4.1.2) has not considered the full potential of these measurements to compare electrodes' capabilities to register bioimpedance. With current methods, it is not possible to register the interfacial impedance of different electrodes and provide tissue impedance characterization without repositioning the electrodes between the measurements. This is a severe disadvantage as it is important to have the same conditions when making comparative studies because substant errors can be introduced by changing the initial parameters (time, pressure, and placement on the skin surface).

This dissertation focuses on fabricating, testing, and evaluating microneedle-like dry and semi-dry carbon-based electrodes for bioimpedance measurements, with particular emphasis on developing interfacial impedance measurement metrics and using phantom models for increased repeatability and comparative assessment.

1.3 Aim

Develop practical electrodes for bioimpedance-based applications, fostering prolonged health with monitoring and diagnostics.

1.4 Objectives and research questions

Objective #1: Design dry/semi-dry electrodes with an effective and straightforward method.

1. *How to cost-effectively produce a carbon-polydimethylsiloxane (PDMS) composite with a good distribution of carbon fillers inside the PDMS matrix for electrical conductivity?*

Objective #2: Decrease skin-electrode contact impedance, as it is expected to give a major contribution and source for parasitic signals, artifacts, etc.

2. *How to improve the contact between the skin and the (dry) electrode?*

Objective #3: To evaluate ionic liquids as composite electrode constituents for decreased contact impedance and increased time stability.

3. *How to combine carbon-PDMS electrodes with ionic liquid gel to prepare semi-dry ionogel electrodes?*

    3.1 *Explore the trade-off between contact impedance and repositioning in semi-dry electrodes.*

Objective #4: To propose an effective contact impedance measurement method for electrode quality assessment.

4. *How to develop appropriate and applicable metrics to evaluate the quality of dry and semi-dry ionogel electrodes?*

Objective #5: To develop a multifunctional test phantom for bioimpedance electrode evaluation.

5. *Choice of representative test bodies. Specifically, is PVA-gelatin phantom sufficient in interface impedance comparative study?*

Objective #6: As a case study, test the developed dry electrodes in a real application to detect heart rate from the wrist.

6. *Are developed CNF/CF-PDMS electrodes usable in bioimpedance measurements on the wrist to detect heart rate?*

    6.1 *Are the results comparable to commercially available electrodes?*

The mapping of research questions (RQs) to the corresponding publication and thesis chapter, where the question is analyzed and answered, is presented in Table 1.

Table 1. Mapping of research questions and publications.

Research question	Publication	Chapter number	Main content
RQ 1	Publication I	3	Carbon-PDMS material and characterization.
RQ 2	Publication II	4	Improving the contact between the skin and the electrode.
RQ 3, 3.1	Thesis	5	Ionic liquid electrolyte (ionogel) preparation and interface impedance assessment.
RQ 4	Publication II	4	Interface impedance method.
RQ 5	Publication III	5	Test PVA-gelatin phantom.
RQ 6, 6.1	Publication II	4	Bioimpedance measurements on the wrist.

1.5 Research methodology

An adjusted quantitative methodology is mainly used in this study, meaning that the results are based on and assessed by comparing the data acquired. The work hypothesizes about the contact interface impedance dependencies:

- The soft microneedle-like surface of electrodes lowers the interface impedance, and consequently bioimpedance signal has a higher signal-to-noise ratio.

- The ionic liquid and hygroscopic salt gels (ionogels) make an effective layer between the dry electrode and skin surface to reduce the interface impedance.

These dependencies are investigated by the following experimental methods to make generalizations:

- fabricating electrode materials;

- developing ionogel carbon-based electrodes: the casting of composite gels;

- characterizing electrode materials: pressure loading, stress-strain tests, impedance change over time;

- characterization of electrodes: evaluating electrode-skin interface impedance changes under different circumstances (time, pressure, frequency, abrasion);

- test phantom preparation: design and validation;

- signal processing towards standardized methodology in dry electrode characterization: data conditioning, filtering, extrapolation, feature extraction, fitting/parameter extracting.

1.6 Contribution of the thesis

Overall, this research contributes to bioimpedance monitoring by suggesting dry and semi-dry carbon-based electrodes of decreased skin-electrode impedance for biosignal sensing and developing an effective interface impedance measurement method.

1. Development of a recipe to fabricate flexible and cost-effective carbon-PDMS composite with a low electrical percolation threshold (between 2-4 wt%).

2. Development of hybrid carbon fiber and nanofiber-PDMS composite microneedle-like electrodes for bioimpedance measurements with interface impedance values comparable to Ag/AgCl or carbon fiber adhesive hydrogel-free electrodes (averagely around 3 kOhm at 10 kHz).

3. Working out a novel method to effectively measure and evaluate different electrodes' electrode-skin interface impedance without repositioning the electrodes (as opposed to other popular methods) and therefore fulfilling the requirements for the consistency of initial parameters (skin contact time, contact condition). The main advantage is that the primary task (tissue characterization, i.e., static and dynamic impedance) can be done simultaneously, along with the electrode contact quality check (electrode-skin interface impedance).

4. Introducing new ionic gel electrodes as a semi-dry ionogel option for bioimpedance electrodes, which have similar interface impedance as conventional Ag/AgCl pre-gelled electrodes (2 kOhm at 10 kHz).

5. Developing a low-cost, reliable, and stable PVA-gelatin phantom with a mock artery as a test bench for multiple bioimpedance-based measurements in need of ionic conduction and changing pulsating impedance.

1.7 Outline of the thesis

The thesis is divided into 6 main chapters. The introductory chapter provides a brief overview of the challenges in combining healthcare and wearables, as well as the thesis's aims, objectives, research questions, methods, and contribution. Chapter 2 gives a broad overview of bioimpedance measurements, fabricating carbon-based PDMS composites, and the importance of interface impedance. In addition, this chapter briefly introduces ionic liquids and hygroscopic potassium salt for semi-dry solid-gel electrodes.

The third chapter describes two methods and recipes to fabricate carbon-PDMS composites. Also, fabricated material impedance is experimentally evaluated under the compressive loading and unloading process.

The fourth chapter focuses on different electrodes made for the experiment and compares them to each other using electrode-skin interface impedance with the proposed novel measurement method.

The fifth chapter focuses on ionic liquid gel electrodes as a semi-dry ionogel electrode option, and developed phantom material is implemented to test prepared ionic liquid electrodes.

Chapter 6 summarizes the work and outlines further work.

2 Background and challenges

2.1 State-of-the-art

Currently, medically qualified personnel are using mercury sphygmomanometers to measure blood pressure - a technology that has remained practically unchanged since the 19th century. An inflatable cuff presses the artery (usually brachial) shut, and then it is released in a controlled manner. Meanwhile, pressure is indicated with a column of mercury, and trained practitioners use a stethoscope for auscultation to detect Korotkoff sounds. There are alternative methods for blood pressure devices like aneroid sphygmomanometer and digital meters that use oscillometric measurements, but the mercury sphygmomanometer, when used properly, is the most accurate technology in use and a gold standard in medicine [19].

125 years ago, in 1896, Italian pediatrician Scipione Riva-Rocci reported the inflatable cuff method upon which the present-day technique is entirely based [20]. The method was improved in 1905 when Russian surgeon Nikolai Korotkoff placed a stethoscope over the brachial artery when Riva-Rocci's sleeve was around the arm and detected sounds that measured systolic and diastolic arterial pressure levels [21]. Riva-Rocci and Korotkoff's technique is still used a century later, with almost no changes made to it. Consequently, the motivation to develop modern blood pressure measurement devices is high. The currently used method has stood the test of time, but the technique is undeniably physically inconvenient for the patient with its inflatable cuff pressing on the hand.

Wearables that monitor blood pressure and cause little or no discomfort to the wearer are being developed by numerous tech giants like Apple [22], Samsung [23], Garmin [24], Aktiia [25], Valencell [26], and Omron [8], to name a few. While most smartwatches use photoplethysmography to detect heart rate and indirectly calculate blood pressure, Omron HeartGuide is a cuff-based blood pressure wristband. It has a similar pressure sensor technology as found in a brachial sphygmomanometer but in the size of a wristwatch. Unfortunately, it is bulky and can cause discomfort during measurement; nevertheless, currently, it is the most accurate blood pressure wearable on the market [27].

Devices used for medical purposes that use bioimpedance (mentioned in Chapter 2.2) are often developed at the research level, but few have become commercially available. The most successful technique is bioelectrical impedance analysis (BIA) for estimating body composition, frequently used in fitness communities. There are already multiple devices on the market sold by successful companies like Akern [28], ImpediMed [29], Bodystat [30], Seca [31], etc. Other, less known bioimpedance-based devices are, for example, characterization probe of cancerous tissues (Nevisense by SciBase [32]), real-time bioimpedance-based biopsy needle to identify tissue types (Injeq IQ-Biopsy [33]), fast impedance spectrometer, Quadra [34] (developed in Tallinn University of Technology), and first electrical impedance tomography device for lung monitoring for everyday clinical use made by Dräger Medical (PulmoVista 500) [35]. Some wearables are also available, like the CoVa Monitoring system in a necklace form that measures thoracic bioimpedance to detect heart failure [36], a single-use BX100 biosensor patch by Philips N.V. to assess respiration [37], and Auraband wristband [38], which should analyze body composition.

In addition to already commercialized products, bioimpedance's research and development side are extensive. Scientific publications related to impedance technology are now published already more than 1500 per year [39]. What is worth noting is that bioimpedance research is particularly strong in Estonia. The top three prolific institutions in bioimpedance publishing are the University of Queensland in Australia, Universitat Politècnica de Catalunya in Barcelona, and Tallinn University of Technology [40].

Our team's approach to measuring the impedance change of pulsating artery in the wrist and figuring out the aortic blood pressure has not been widely reported. Nevertheless, big corporate Microsoft Technologies patented a bioimpedance-based pulse waveform sensing system/sensor in 2018 [41], which has a similar end goal – a portable sensing device worn continuously over an artery at the wrist to determine a pulse waveform by using bioimpedance measurements and pressure transducer. Also, Rachim et al. [42] reported in 2019 a multimodal biosensor for a continuous blood pressure monitoring system, which uses photo-plethysmography (PPG) and impedance plethysmography (IPG) signals simultaneously from the patient's wrist. In addition, Wang et al. [43] proposed in 2022 a proof-of-concept wearable (placed on the neck), an intelligent bioimpedance system, which includes IPG sensing and artificial intelligence based blood pressure estimation. These recent researches give reassurance that our team's work is significant and impactful for public health.

2.2 Bioimpedance measurements

Biological impedance is defined as the ability of biological tissue to impede electrical current [44]. This means that when externally applied small electric current flows through the tissue, it will have some kind of opposition – impedance, which is reciprocal of conductance. If harmless and very low-intensity alternating electric current (or voltage) is injected into the human body, the response signal (voltage or current) between the two electrodes can be registered. Tissues exhibit dispersive characteristics, and the electrical response depends on the frequency at which they are measured. Complex bioimpedance, $Z(\omega)$, can be represented as a combination of electric resistance, $R(\omega)$, as a real part, and reactance, $X(\omega)$, as an imaginary part.

$$Z(\omega) = R(\omega) + jX(\omega) \tag{1}$$

Equation (1) characterizes the relationship between resistive and reactive components of bioimpedance where ω is the signal frequency, and j represents the imaginary quantity $\sqrt{-1}$. The resistance part of the equation is typically associated with the ability of a tissue to carry a charge and dissipate energy (i.e., current flow through ionic solutions, both intra- and extracellular), while reactance is associated with the ability of a tissue to store charge (i.e., the capacitive nature of a cell's double membrane) [45].

2.2.1 Electrical equivalent circuit of tissue

From an electrical point of view, a living organism is a conductor as it is predominantly made of water (i.e., aqueous electrolytes). Still, every tissue has different hydration levels, and consequently, the conductivity varies. For example, the conductivity of fat tissue is about 14 times lower than blood conductivity [46]. Besides the varying conductivities between tissue types (possibly at a different hydration level), the air in our lungs and changes in blood volume inside arteries can also affect the conductivity (via geometric transformations). These variations are effectively exploited in many applications that use methods like impedance cardiography (ICG), transthoracic impedance pneumography (TIP), electrical impedance tomography (EIT), skin conductance response (SCR), electrical impedance plethysmography (IPG), electrical impedance spectroscopy (EIS), and body composition assessment (bioelectrical impedance analysis – BIA) [47].

As blood volume variates in the arteries during the heart beat cycle, the electrodes placed on the skin can detect the changing bioimpedance and register the heart pulse in impedance form. What is phenomenal is that the impedance curve is very similar to

the blood pressure curve. The term "measuring bioimpedance" can be interpreted as a bioimpedance spectrum or evaluation at one or a few distinctive frequencies.

Figure 1 represents a wrist with pulsating artery under the skin and four electrodes placed on the top to register impedance change. Bioimpedance measurements on the wrist consist of invariable base impedance Z_0 and a variable part $Z(t)$ caused by the change in blood pressure inside the radial artery. Total impedance expresses then:

$$Z(t) = Z_0 + \Delta Z(t) \qquad (2)$$

Cardiac activity is represented by a minuscule variable $\Delta Z(t)$ that should reflect the physical volume change of the pulsating blood in arteries.
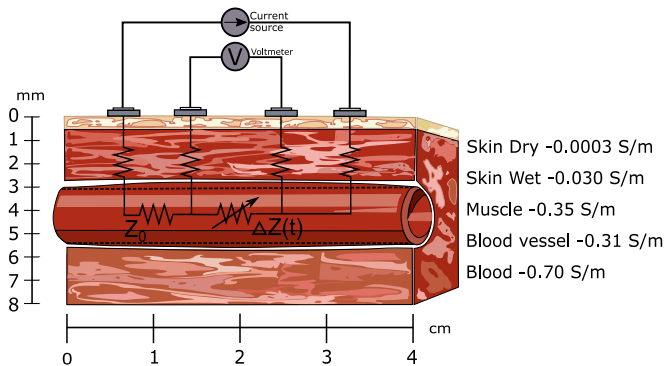

Figure 1. Tetrapolar setup to measure the time varying bioimpedance on radial artery to detect pulse waves. The whole impedance (Z) can be considered to consist of the basal impedance (Z_0) and the variable, $\Delta Z(t)$ caused by the pulse wave.

Our workgroup [48] is currently figuring out how to make this connection between impedance and pressure valuable and usable for accurate and continuous blood pressure monitoring. For example, the determination of systolic and diastolic pressures with a classical sphygmomanometer gives two discrete measurements. On the contrary, the continuous measurement with our application gives an accurate change of values over a long period of time, and it is possible to distinguish stochastic processes, disrupting the accurate measurement results.

Bioimpedance is a powerful tool as the method is fairly straightforward, measurements are noninvasive, and it is possible to extract a wide range of healthcare parameters. Also, equipment is usually low-powered and has a relatively low cost. However, due to many uncertainties and challenges, the bioimpedance technique is still overlooked in many tech companies and is not widely adopted in clinical practice. The medical area is extremely conservative - reaching the market with newly designed devices, or methods is a slow and excruciating process. It has to be extremely precise, reliable, easy to operate, and exceedingly harmless (the international safety standard IEC 60601), which means that all electromagnetic hazards must be considered. In addition, the bioimpedance change in the wrist at the radial artery is minuscule (approximately 0.1-1% of the base value), and the signal-to-noise-ratio is low, which means that the measurements on the human hand are prone to different artifacts. Fortunately, the intelligent design of electrodes can reduce the possibility of distorted signals, as electrodes are a crucial part of the measurement system in bioimpedance recordings.

2.3 Why do electrodes matter?

Electrodes constitute a significant source of errors in wearable technology due to stray capacitance and electrode polarization, high electrode-skin interface impedance, the noise of the interface, and contact uncertainties [47].

Since 1783 Luigi Galvani's experiment of electrical stimulation of a frog leg, electrodes have been used to transduce the biological body's ionic current to electron current and vice versa [49]. The definition of electrode taken from "Bioimpedance and bioelectricity" by Martinsen and Grimnes says: *the electrode is the site of the shift from electronic to ionic conduction* [44]. Therefore, an electrode is an electron-to-ion transducer.

Ionic conduction comes from the mobile ions - the ions from hydrogel or wet gel applied on the electrode or tissue. Also, tissue liquids like sweat and moisture classify as electrolytes and have ionic conduction, which means that the charge carriers are free **ions**. On the other hand, electronic conduction comes from the electrode itself, which is usually made of metal or carbon; the mobile charge carriers are **electrons**. The site where these two different conductions meet is the interface between the electrode and the tissue. **The interface discussed in this thesis consists of an electrode, electrolyte, and outer layer of the skin.** The interface functions as a transducer to complete an electric circuit with the electronic current in measurement electronics and ionic current in the skin.

2.3.1 Electrode-skin interface equivalent circuit

To better understand the importance of the electrode-skin interface, this chapter discusses the structure and equivalent circuit for skin layers, what is important for a good measurement site, and why it is so difficult to get a good bioimpedance signal.

Skin is made of multiple layers that cover and protect the body. Three main skin layers are the epidermis (Figure 2b), dermis, and subcutaneous layer. Cells within the innermost layers constantly multiply and push the older skin cells up toward the skin's surface. As these are pushed outwards, they undergo changes – dehydrate and die. These cells form a very thin (generally 10-15 μm) stratum corneum (SC), which is the most challenging skin layer regarding electrical measurements for impedance measurements. It is the outer and extremely dry layer of the skin that acts as a non-conductive isolation barrier. Sometimes SC is described as a "brick wall" – the corneocytes (mostly made up of keratin) that build up the layers are like bricks held together by lipids. This brick wall creates an effective barrier for water, toxins, and bacteria [50]. In contrast, the epidermis's underlying layers are a relatively hydrated environment. The transition from an essentially non-conductive lipophilic membrane (the SC) to an aqueous tissue (viable epidermis and dermis) gives rise to the skin's barrier properties [12]. Current between two highly conductive areas (electrode and skin layer under SC) couple capacitively, making the impedance of this interface frequency-dependent. Nonetheless, even at lower frequencies, current can pass through because of appendages in the layer; sweat glands, sebaceous glands, and hair follicles extend deep into the skin, providing a channel for the current to cross between the two highly conductive areas during measurements [51].

One possible model to represent electrodes on skin tissue was presented by M. R. Neuman [52]. Figure 2 is a representation of his model. Models with lumped components are, of course, too simple compared to the complex anatomy of human skin, but an approximate predictive model is needed to give some broad understanding and better insight. General electrical equivalent models of wet and dry electrodes on the skin are depicted in Figures 2a and 2c, respectively. When current is applied to the tissue through wet electrodes (Figure 2a), then the electrode material has some capacitance (C_{el}) and resistance (R_{el}) connected in parallel [53].
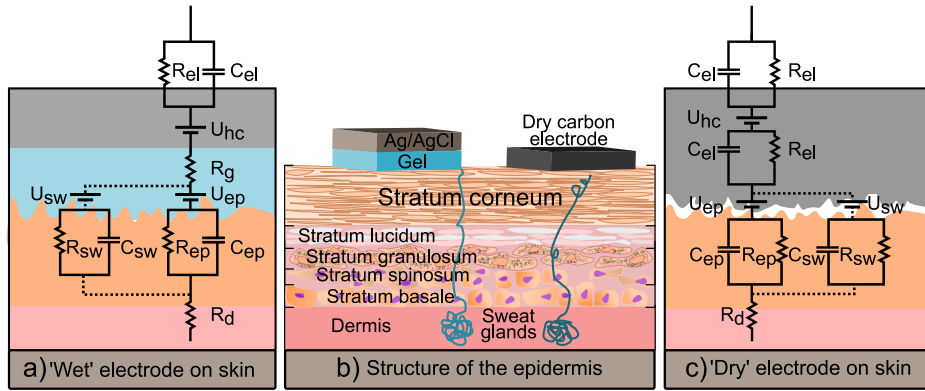
Figure 2. Electrical model of epidermis consisting of stratum corneum, lucidium, granulosum, spinosum, basale, and dermis with sweat glands (based on [52] and [53]). a - wet electrode is placed on the outer layer of the skin and its equivalent electrical model. b - skin layers named and sweat glands depicted together with two different types of electrodes on top. c – dry electrode is placed on the skin and its equivalent electrical model.

The resistive part of biological tissues represents mainly intracellular and extracellular fluid, and the capacitive element represents cellular membranes that hold the conductive intercellular fluid inside. The two membrane walls represent the capacitive plates, and nonconductive fluid is between them.

In Figure 2, U_{hc} represents half-cell potential, the voltage developed at the electrode-electrolyte interface. R_g is an electrolyte's resistance, which is usually relatively low. An ion gradient exists across the surface skin layers, and this creates a potential difference, a voltage source (U_{ep}), which is in series with a parallel circuit of resistor (R_{ep}) and capacitor (C_{ep}) again. If sweating occurs, which usually does, the sweat ducts produce an effective pathway through otherwise low-conductivity skin layers. This contributes to U_{sw} in series with R_{sw} and C_{sw} [53].

When dry electrodes (Figure 2c) are applied to the skin, the interface impedance is very high at first. In this case, the resistance of the electrolytic gel (R_g) is replaced by a resistor R_i in parallel with a capacitor C_i. When sweat starts accumulating, the air gaps between the electrode and the skin are filled with electrolytes, and the model is closer to the first one (Figure 2a) [53]. Therefore, even if we have a straightforward model of the electrical equivalent of the electrodes on the skin, including a double layer (lumped element model), determining the connections between the elements and component values is surprisingly challenging.

2.3.2 Electrical double layer

Electrodes can be classified as polarizable and non-polarizable depending on the charge transfer reaction at the interface under the given conditions. Ideally polarizable electrodes act as capacitors (capacitive electrodes) because only displacement current passes through the electrode-electrolyte interface. On the other hand, in the case of perfectly non-polarizable electrodes (non-capacitive electrodes), direct current can flow easily through the junction, and the electrode acts as a resistor.

In the real world, there are no ideally non-polarizable or polarizable electrodes; however, the Ag/AgCl electrode is considered the closest to a **non-polarizable** one. In this

case, the silver metal has a thin silver-chloride coat that acts as a buffer and allows current flow in both directions. When current is passed through the electrode, the silver electrode will leave an electron in the electrode and move into the silver-chloride layer as a cation. The chloride ion from the electrolyte solution travels into the AgCl layer as well to bind ionically with the silver cation. So it ends up depositing an insoluble layer buffer of AgCl on the electrode, which remains relatively stable [52].

In the case of **polarizable electrodes**, metal atoms (e.g., Pt being highly polarizable) cross the interface to become cations and meet anions in the charged solution while leaving behind electrons. Essentially, what happens in the interface is called a redox reaction (oxidation-reduction). As metal atoms go to the electrolyte solution, they create a half-cell potential – the electrolyte surrounding the metal electrode is at a different electrical potential from the rest of the solution. The important thing here is to note that this process is entirely reversible. This forms a charged double layer where a negative charge is accumulated at the electrode and a positive charge in the electrolyte.

Electrical double layers (EDL) form at the interface between dissimilar non-miscible phases, e.g., this happens with capacitive electrodes - when the metallic or carbon electrode comes in touch with the electrolyte (hydrogel or sweat, etc.). In 1879 Hermann von Helmholtz explained in his published paper [54] that two layers of opposite charges assemble at the junction between an electrode and electrolyte. Helmholtz layer can be defined as a one-molecule thick layer of positive and negative charges, which occurs at a surface where two different immiscible phases are in contact, e.g., a metal in electrolyte dissolved in a dissociating solvent [55].

Helmholtz simple double layer effect was later followed by the Gouy-Chapman diffuse model and succeeded by the dominant double layer Stern model, which combines the two [56]. Stern layer is the layer of ions to balance the charges over EDL. When the energetic barrier of the Stern layer is too high, the electron transfer between the electrode and electrolyte cannot occur, and it becomes like a barrier for the current flow – dielectric layer. Then the second layer, the diffusion layer, forms on the already formed Stern layer, consisting of a little bit looser negative and positive ions aligned to balance the EDL charge. The charge density increases towards the interface compared to the bulk electrolyte. The interface starts to behave as a capacitor where parallel plate capacitor formulas apply [57]. Low equivalent capacitance of the double layer results in high impedance. As the high impedance of the double layer is in series in the measurement path, it limits the low-frequency excitation current. Consequently, detecting tiny dynamic impedance changes in the wrist becomes problematic as measurement uncertainty increases remarkably.

2.3.3 Motion artifacts

Motion artifact occurs, as the name says, when a change in the contact area, contact force, or motion occurs between the electrode and the measurement site (skin). In this case, the charge distribution is disturbed at the interface when the electrode moves with respect to the skin—the measurements of electrode half-cell potential and interface impedance change. In turn, the differential voltage signal that appears between two sensing electrodes will lead to common-mode errors [57].

Since the electrolyte (sweat or moisture) under the dry electrode is extremely thin, even the slightest changes in the electrode location will cause significant disturbances in contact magnitude to the electrolyte in the interface. Interfaces of electrodes with gel are not affected by motion that much because thick conductive gel layers are stable against lateral and vertical movements. Because there are relative changes between the electrode-skin interface impedance and the motion artifact, one way to lower the motion

effect is to decrease the interface impedance [46]. Filtering the measurement signal is also a common way to reduce the artifacts; however, the artifacts often lie in frequencies similar to desired signal [17]. Because of this, careful analysis and filtering techniques must be used to separate the two signals in the desire to keep the original data.

There are also other biopotential signals (EMG, ECG), electrochemical noise (impurities adsorbed by the electrodes [58]), thermal noise (originating from very high interface impedance), coupling noise, and double layer phenomenon that disturb the desired signal significantly. Therefore, I have listed some possibilities to reduce the unwanted artifacts and lower the absolute impedance values at the interface:

- the optimal and balanced design of electrodes (e.g., material, size, shape);
- surface roughness of electrodes;
- conductive gel to reduce motion artifacts;
- constant contact pressure to minimize the interface impedance changes;
- stabilization time;
- abrasion/preparation of skin;
- homogenous measurement site;
- filtering the signal [17].

Another more customized approach is to pick electrodes that better fit the measurement's specific needs.

2.4 Electrodes for bioimpedance measurements

To design a wearable health monitor, the rules to follow are versatile, and it is important to meet design requirements based on technical and human factors. At the moment, there are no standard criteria for selecting and classifying the significant characteristics of wearables but from Francés-Morcillo et al. analysis [59] most frequently addressed human factors covered in literature are:

- comfortability;
- safety;
- biocompatibility;
- durability;
- aesthetics;
- intuitiveness;
- reliability.

In the case of physical ergonomics, "comfort" and "ease of use" were the most commonly referred to [59], which means that one significant challenge is to make the wearable device and direct contact sight – electrodes - convenient to ensure it offers a real value for the intended user. Furthermore, electrodes for wearables should be even more specific: suitable for continuous monitoring, possibly reusable, and still provide reliable contact between the skin and the electrode material. The electrode's material, size, shape, and disposition are still an open study area in the wearable noninvasive bioimpedance field [47].

The classical approach to measuring bioimpedance involves small rigid metal electrodes (10-200 mm^2) applied to the skin using a conductive electrolytic gel as an interface

[60]. More recent research has led to new electrode possibilities like textile electrodes, dry electrodes, electrodes with rough surfaces, tattooed electrodes, electrodes with adhesive, porous surfaces or covered by biolayers or tiny pins (0.2–0.4 mm long) penetrating the "stratum corneum" (see Table 2). Obviously, achieving all these good qualities is almost impossible without losing others in the process. Table 2 introduces some of the electrodes developed that can be used for bioimpedance registering.

Table 2. Different electrodes used for bioimpedance measurements introduced in the literature.

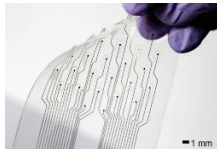| Type of electrode	Wet/dry	Flexible/ rigid	Advantages/disadvantages
Ag/AgCl with pre-applied gel [12] Application* Gold standard, ECG, EMG, EBI, EDA	wet	rigid	+ good contact with the skin + stable and low interface impedance + easy to apply + commercially available and widely used and studied + almost non-polarizable − irritating to the skin − strong adhesion is inconvenient − large gel and adhesive area − not reusable − short shelf-time
Metal electrodes [12] Application* ECG, EEG, EMG, EBI, EDA	dry	rigid	+ reusable + easy connection to electronics + widely available + not irritating − rigid − unstable contact − prone to high interface impedance

23

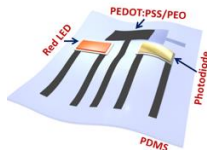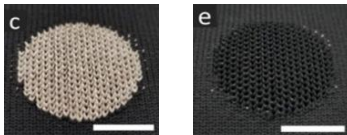|			
Flexible printed gold electrode [61]	dry	flexible	+ relatively cheap production (inkjet printing) + reusable + not irritating + flexible − fabrication challenges exist (high t° needed) − unstable contact − prone to high interface impedance
 Application* ECG, EEG, EMG, EBI			
Stretchable printed PEDOT:PSS electrode [13]	dry	flexible	+ stretchable + reusable + not irritating − fabricating issues (viscosity of polymer for printing) − prone to high interface impedance
 Application* ECG, EMG, EBI			
Textile electrodes (silver and carbon yarn) [62]	dry	flexible	+ comfortable for the wearer + not irritating + wide usability area (woven in multiple materials) + unnoticeable + reusable + stretchable − unstable contact with the skin − prone to high interface impedance
 Application* ECG, EMG, EBI			
Temporal tattooed electrode (metal thin film electrodes) [63]	dry	flexible	+ good contact with the skin + low aggression to the skin + unnoticeable design + stretchable (moves with the skin) − bulky connection to the electronics − not reusable − removing is difficult − careful applying procedure − thin material can break − not suitable for hairy sites
 Application* EDA, EMG, EBI			

Carbon-PDMS electrodes [64]	dry	flexible

+ good stretchability
+ comfortable for the wearer
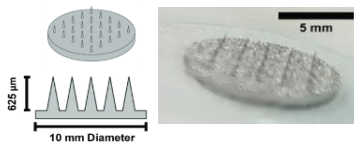+ reusable
+ not irritating

− prone to high interface impedance
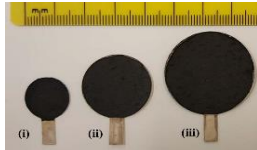
Application*
ECG, EMG, EBI

Obtrusive electrodes (micro-needle electrodes) [65]	dry	rigid

+ very good contact with the skin
+ reusable
+ easy connection to electronics

− inconvenient for long term use
− not suitable for sensitive skin
− tricky to fabricate

Application*
ECG, EEG, EMG, EBI

OMNI-WAVE™ adhesive carbon fiber electrode [66]	dry	flexible

+ good contact with the skin
+ easy to apply
+ low aggression to the skin
+ out-of-pack life 6 months
+ customizable
+ breathable non-woven cloth

− not reusable
− strong adhesion can be irritating
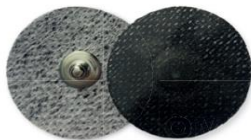
Application*
ECG, EEG, EMG, EBI

*ECG – electrocardiography, EMG – electromyography,
EEG – electroencephalography, EDA – electrodermal activity,
EBI – electrical bioimpedance

At broad, the electrodes can be classified as "wet", "dry", "semi-dry", and obtrusive.

"Wet" electrodes

Commercial production, low cost, and electrical stability of nonpolarizable Ag/AgCl have made these wet gel electrodes ubiquitous in the clinical environment for biological signal monitoring [67]. Electrodes with electrolyte gel effectively reduce the interface impedance and ensure good electrical contact with the skin. On the other hand, as wet gel or hydrogel electrodes have very high water and electrolyte levels, they are harsh to the skin and can cause skin irritation when used for long-term measurements [68]. In addition, conductive gels have hydrophilic properties. When sweat starts to accumulate under the electrode, the gel absorbs the water molecules causing the skin to dehydrate and interface impedance to increase again [69].

"Dry" electrodes are becoming essential with the development of wearable sensors. Recent research by Lee et al. [67] introduces methods for fabricating Ag/AgCl dry electrodes for wearable applications. They found the analyzed custom dry electrodes efficient compared with standard, commercial Ag/AgCl wet electrodes. However, moving artifacts and noise problems arose because of the minimal amount or lack of electrolytes at the interface. Luckily, when the electrode sits on the skin long enough, sweat glands start to produce sweat, which, in turn, acts as an electrolyte between the skin and the electrode. This means that the contact impedance decreases remarkably. Unfortunately, it takes time and can still be an unstable process that is difficult to control. In addition, rigid metal-type electrodes can be uncomfortable for the wearer and limit the usage possibilities in wearable technology.

For example, mechanically flexible and chemically inert dry electrodes are inkjet printed gold traces on plastic substrates [61]. However, processing inkjet-printed electrodes on plastic substrates is challenging. Gold nanoparticle ink requires high sintering temperatures in the range of 250°C, which is above the melting temperature of the most common plastics, such as polyethylene terephthalate (PET) and polyethylene naphthalate (PEN) [70]. Also, it seems that in addition to the flexibility, the on-skin electrodes are preferably required to have high stretchability (at least >15%) as the stretchability of human skin can be fairly large depending on the locations and conditions (failure strain of human arm ranges from 27% to 59% under dynamic load) [12].

A flexible plastic base can be replaced with a soft elastomer like PDMS substrate to fabricate stretchable flat film electrodes with inkjet printing. In this case, the conducting ink must be applied in serpentine or meander patterns or be itself stretchable. One possibility is to use poly(3,4-ethylenedioxythiophene) polystyrene sulfonate (PEDOT:PSS) conducting polymer blended with polyvinyl alcohol (PVA) [71]. Lo et al. work [13] demonstrates printed thin conductive films (sheet resistance 84 Ω/cm) on PDMS substrate that can resist up to 50% tensile strain and effectively measure ECG waveforms. Numerous other possible fabrication technologies are used to produce thin film electrodes, e.g., photolithography, spin-coating, etching, electroplating, and sputtering [14].

Mainly these same methods are used with temporary tattoo electrode arrays. Conductive arrays are usually printed on tattoo releasable film, and the electrode is laminated onto the skin by wetting the back side to dissolve the water-soluble sacrificial layer. These electrodes have excellent continuous contact with the skin, making them an attractive platform for wearable electronics. Still, numerous unsolved issues exist, the main one being the interconnection of soft and thin electrodes to rigid electronics - conductive traces are extremely thin and can break easily [72]. Textile electrodes, where conductive yarns (silver, carbon, gold) are woven (or knitted, embroidered) into base textile, are also stretchable, but the contact with the skin is usually unstable, high electrode-skin

impedance occurs, and the signal-to-noise ratio is low [55]. Nevertheless, these electrodes can be seamlessly integrated into fabrics and daily clothing, leading to "truly wearable" soft electronics in the future [73]. Numerous researchers have been developing carbon-based elastomer composite electrodes that can be used in the medical field to measure EMG, EEG, ECG, EDA [74]–[77]. Producing the composite material by mixing the electrically conductive carbon fillers with elastomers like PDMS is relatively straightforward, but dispersing the fillers homogeneously inside the PDMS can be challenging [12], [64]. However, the resulting conductive electrode material is versatile, reusable, soft, and stretchable – an excellent alternative to rigid metal electrodes.

"Semi-dry" electrodes are not well defined in the literature. However, a review article by Li et al. [78] describes semi-dry electrodes for EEG that release (preferably automatically) minimal amounts of electrolyte to yield reliable contact. At the same time, user comfort remains high. He emphasizes that the key strategy to improve the design of semi-dry electrodes is to establish a stable ionic conductive interface between the electrode and the skin.

Obtrusive electrodes Another interesting field of electrodes is obtrusive ones. Typically, microneedle electrodes with tiny (nano- or micrometer scale) spike- or needle-like surfaces are placed on the skin. These needles are carefully designed so that very dry and barrier-like stratum corneum is passed, but nerves are not touched, and the patient feels no pain. This way, the signal can be picked up easier because contact with the inner layer of skin is excellent. Most of these electrodes are rigid [15], [65], but recently flexible microneedle electrodes are also being developed. For example, Hou et al. [79] introduced Miura-ori (folding method) structured microneedle array electrodes for biosignal recording that effectively registered EMG and ECG. In addition to microneedle electrodes, where every spike is carefully designed and placed, textile electrodes with flocked surfaces introduced by Takeshita et al. [80] have similar properties – silver-plated fibers on the textile base material that remarkably reduce the interface impedance. However, obtrusive electrodes usually have complex properties and are expensive to manufacture. In addition, long-term use is limited as the obtrusiveness can cause inconvenience for the wearer. Also, a slight risk of contamination of the measurement site is possible when fragile spikes break off [14].

2.5 Carbon-PDMS composite

Composites are a combination of different materials that retain their distinctive properties to create a new material. Typically, these materials in stretchable electronics tend to be polymers with electrically conductive fillers inside.

Polymers are macromolecules formed by the chemical bonding of large numbers of smaller molecules or repeating units, called monomers [81]. *Polymer* comes from the Greek word and means "many parts", as *monomer* means "one part". There are vast areas of different polymers worldwide. For example, DNA, protein, and cellulose are natural polymers. Commonly used synthetic polymer substrates for stretchable and flexible electronics are polyethylene terephthalate (PET), polyimide (PI), poly(3,4-ethylenedioxythiophene), and polydimethylsiloxane (PDMS) [82].

Polydimethylsiloxane (PDMS), also called silicone rubber, boasts with its high elasticity (elastic modulus between 1.32 and 2.97 MPa [83]), high resistance to mechanical stress (tensile strength 3.51 to 5.13 MPa [84]), easy processing possibilities, reasonably low cost, and nontoxicity. Therefore it has become the primary polymer to be used in the production of wearable materials in the electronics field [85]. However, pure PDMS has limitations. For example, in sensor development, one restraint is that PDMS is an electrical

insulator (conductivity in the order of 10^{-12} S/m) which means that there are intrinsically large energy gaps inside the material, and the mobility of charge carriers is very low. Fortunately, adding different fillers, such as electrically highly conductive carbon and metal powder, can change the properties of otherwise insulating polymers and enhance electrical conductivity. Carbon nanofillers have a high surface area and electrical conductivity, so when carbon is incorporated into soft and elastic material like silicone, the resulting composite is potentially an excellent dry electrode material for bioimpedance measurements [86].

Consequently, the combination of PDMS with other materials allows optimization and expansion of its application possibilities. Fillers at specific concentration levels and degrees of dispersion create a three-dimensional network capable of promoting the electrical percolation of the composite [87]. This happens more effectively if conductive fillers have specific properties: excellent electrical conductivity, small size, and a high ratio between the width and length – high aspect ratio. These thin and long fillers are fibers and tubes, producing electrical conductivity at significantly low volume fractions [88].

A small filler diameter provides an optimal balance between polymer and carbon – the concentration of fillers can stay lower than with thicker particles, still ensuring electrical conductivity. Longer particles form pathways between neighboring fillers more efficiently since fewer contact junctions are required to create network structures. It is important to keep the filler concentration low as too much filler added to the elastomer causes an overall degradation of the mechanical performance (mechanical toughness or rigidness) [89]. Also, in the case of chemical crosslinking, an excessive amount of carbon nanofillers can absorb the platinum-containing catalyst of PDMS, lowering the crosslinking density and resulting in decreased stretchability [89].

When the particles are in contact or close enough to form tunnels for the moving electrons, more effective pathways will occur, and the material's conductivity will be higher [90]. This is called the tunnel effect. When the critical concentration of fillers has been achieved, and effective pathways have formed inside the composite, then the point where material turns abruptly from insulator to conductor is called the percolation threshold, Φ_C.
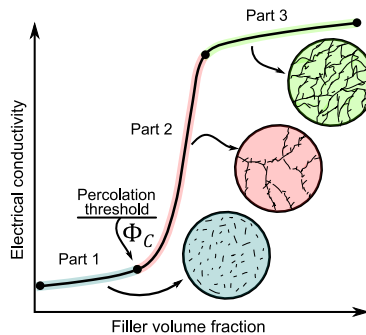

Figure 3. Figure 3 is redrawn from [90]. Electrical conductivity of composite material according to filler volume fraction. The percolation threshold (Φ_C) represents a point where the network of fillers forms and an insulating material becomes conductive. Part 1 represents a section where the concentration of fillers is low, and no effective pathways are formed. In part 2, the concentration of fillers is high enough to turn the composite into a conductor. Turing this part high rise in conductivity happens. Part 3 shows a case where the increase of filler concentration does not influence electrical conductivity so drastically anymore. Most of the effective pathways are formed.

Figure 3 depicts the line of percolation. The scaling law presented in Equation (3) describes the relationship between the composite electrical conductivity and the filler content [91]:

$$\sigma = \sigma_0 (\Phi - \Phi_C)^t \tag{3}$$

Where σ is the electrical conductivity of the composite, σ_0 and Φ are the conductivity and the volume fraction of conductive fillers, and t is a critical exponent related to the dimension of conductive networks in the polymer matrix. If the material is pressurized or stretched, the electrical pathways of fillers are very easily disturbed, but the homogeneous distribution of fillers inside polymers can reduce the risk of uncertainty.

2.5.1 Carbon nanomaterials as fillers

Materials with good charge-transport capabilities, electrical conductivity, inherent softness, and mechanical deformability are potentially suitable electronic fillers [89]. For example, carbon-based nanofillers have attracted significant attention for stretchable conductive composites because of their electrical conductivity, good chemical/thermal stability, and relatively low cost [92].

Carbon black is a highly popular filler used at the industrial level. It is relatively cheap, readily available, and widely researched. It has a high surface-to-volume ratio and three-dimensional branched structure, with some spherical particles being fused together unevenly, making it a rather agglomerated and unorganized filler [93], [94]. The aggregation of fillers significantly affects conductivity since the percolation threshold for longer fibers occurs at a considerably lower loading than for spherical particles [95]. This means that to improve the electrical conductivity and rubber matrix properties, a high content (nearly 60 per hundred parts of rubber (phr)) is required [93].

Graphite consists of graphene sheets layered and forming Van der Waals bonds between the layers. The overall structure is flaky and flat.

In carbon fibers, the carbon atoms are bonded in bundles that are more or less aligned parallel to the fiber's long axis. Fibers have a greater length-to-width ratio than the above-mentioned fillers. They are mechanically strong (tensile strength 3 to 7 GPa [96]), flexible (Young's modulus ranging from 200 to 500 GPa [96]), and electrically conductive. But it is still difficult to spread them inside base material due to their being quite thick particles (fiber diameter around 7 µm). Conical carbon nanofibers are much smaller in dimensions, and the aspect ratio is higher. This specific nanofiber structure consists of separate graphene layer cones stacked together, and one layered structure reduces the dimensions remarkably as the diameter is around 100 nm.

Graphene is a two-dimensional semimetal that has covalent bonds between carbon atoms. Graphene and its derivatives have been widely employed as conductive fillers to fabricate stretchable composite materials because of their excellent electrical properties, high surface area, and outstanding mechanical property [92]. Graphene layers can be rolled into three tube types: "zigzag", "armchair", and chiral tube type. These curvature differences of the tubes strongly influence electrical properties as electrons propagate only along the tube's axis [97].

Carbon nanotubes are long cylinders (2.5 to 20 µm) of covalently bonded carbon atoms. The use of carbon nanomaterials as fillers has grown markedly since the 20th century when Iijima published his paper about carbon nanotubes in 1991 [98]. Consequently, the first polymer composites using carbon nanotubes as fillers were reported by Ajayan et al. in 1994 [99]. CNTs are classified into two types: multi-walled carbon nanotubes (MWCNT) made of coaxial graphene cylinders and single-walled carbon nanotubes (SWCNT) consisting of one graphene layer that has been rolled into a tube. The average

thickness of one single-walled tube is around 0.8 nm [100].

Apart from those single-component conductive fillers mentioned above, composites with hybrid fillers have been reported to improve electrical and mechanical properties through synergistic effects between different nanofillers [74]. The structure and properties of hybrid fillers are usually dissimilar to each other. For example, dispersing a hybrid of plate-shaped graphene sheets and spherical carbon blacks increased electrical and thermal conductivity [101]. Or, even a small amount of carbon fiber and plate graphite powder fillers can effectively form a reinforcing network inside the composite material [102].

In general, careful consideration of the types of carbon fillers is needed for designing polymer nanocomposites for specific applications. For example, it has been reported that nano-size carbon fillers, especially carbon nanotubes, dramatically improve the mechanical properties of composites and provide higher electrical conductivity at relatively low (2 wt%) loading amounts compared to other types of carbon fillers [103]. On the other hand, the high cost reduces its usage areas, and usually, the choice of fillers comes down to the price, properties, and availability.

Table 3 briefly overviews different carbonaceous fillers, comparing their dimensions and price. Table information is taken from the supplier, Sigma-Aldrich, website [104].

Table 3. Comparison of different carbonaceous fillers by their size and approximate price.

Carbon filler	Size	Approx. price
Carbon black	10-500 nm in diameter	1 kg – 1.23 €
Graphite	50-800 µm in diameter	1 kg – 54.4 €
Carbon fiber	7 µm x 6 mm (diameter x length)	1 g – 0.1 €
Conical carbon nanofiber	100 nm x 20-200 µm (diameter x length)	1 g – 7.32 €
Carbon nanotube (multi-walled)	6-13 nm x 2.5-20 µm (diameter x length)	1 g – 161 €
Graphene	>500 m^2/g	1 g – 810 €
Carbon nanotube (single-walled)	0.78 nm avg. diameter	1 g – 1120 €

2.5.2 Filler dispersal methods

Usually, relatively large amounts of carbon fillers have to be well dispersed in the host polymer matrix of a viscoelastic solution to achieve the electric conductivity of the composite. Strong van der Waals forces between carbon fillers tend to agglomerate into large bundles very easily, which can cause uncontrolled electronic alterations and poor performance [105], [106]. Therefore, physical methods (mainly mixing techniques) and chemical ones (polymerization) are used to disperse the fillers inside the PDMS matrix. Depending on the type of materials, stretchable conductive composites can be fabricated using different processes or a combination of methods.

- **In-situ crosslinking/polymerization** - deals with carbon dispersion into the monomer matrix with solvent or without it. The main advantage of this technique is that it enables the grafting of polymer molecules on carbon fillers, leading to better interactions between fillers and the polymeric host matrix. Usually used

with polymers that are insoluble and thermally unstable and can't be processed by solution mixing and melt processing [107]. However, during the procedure, macromolecular chains of the polymer may become attached to the carbon nanofillers, which may interrupt the formation of an interconnecting network. Consequently, leading to lower electrical conductivity values [108].

- **Melt mixing** The method involves the dispersion of fillers in the elastomer matrix in the molten state by applying a shear force [108]. To delaminate nanosheets or split the aggregation of nanofillers, a two-roll mill, three-roll mill, internal mixer, ball milling, Haake torque rheometer, or extrusion and injection molding can be used [109]. The given method primarily suits thermoplastic polymers, i.e., polypropylene, polystyrene, etc., and it is widely popular in the polymer industry due to its simplicity, low cost, and speed [107], [110]. Despite the advantages, the elevated temperatures and high shear forces needed to incorporate fillers into the elastomer matrix make the materials prone to degradation [108].

- **Solution mixing.** The dry mixing of conductive nanofillers and elastomer matrix is an efficient method because it can be easily scaled up for mass production in the industry [92]. However, solution mixing is more commonly employed in academic studies to improve the dispersion quality. It usually involves dissolving a polymer and suspending the filler in a solvent [109]. When carbon fillers and polymer are mixed (high-speed shear mixing, ultrasonication, stirring), the solvent evaporates in a controlled manner. Solution-based methods are not so desirable at the industrial scale because of the necessity to handle large amounts of solvents [110].

During different dispersion steps, mechanical mixing is required for many of the methods described above. Standard methods for stirring the mixture to disperse the fillers are mechanical stirring, shear mixing, melt mixing, and ultrasonication [111]. Many mechanical mixing methods require high energy conditions – high speed, long mixing time, and high temperature to obtain a good dispersion. These destructive conditions, unfortunately, can lead to a decrease in fillers' aspect ratio due to fibers' breakage [112].

2.6 Semi-dry ionogel electrodes

In addition to dry-contact electrodes, semi-dry electrodes are being developed to help reduce high interface impedance between the electrode and the skin. In the current thesis, semi-dry electrodes are considered to have a solid-gel-like (ionogel) conductive electrolyte layer in contact with the skin. The hypothesis is that this layer can significantly lower interface impedance and reduce moving artifact problems. Moreover, these electrodes do not have adhesive tape and an excessive amount of "wet" electrolyte that conventional hydrogel ones have; thus, semi-dry electrodes should bridge the gap between wet and dry electrodes. Interestingly, except for EEG reservoir-type electrodes (mentioned in Chapter 2.4), there are not many other kinds defined as semi-dry electrodes in the literature.

Usually, the electrolyte of the wet and semi-dry electrodes will dehydrate gradually over time, making them unusable for long-term testing [98]. Shen et al. introduced in their work [99] semi-dry solid hydrogel EEG electrodes (based on N-acryloyl glycinamide monomer and glycerin). Developed electrodes were placed for 25 days in a ventilated environment, and after the shelf time, brain waves were still captured at an acceptable level. Also, the electrodes were tested for 8 h during EEG measurements, and contact impedance did not increase significantly over time. These findings show that semi-dry solid hydrogel electrodes will possibly improve biosignal detection.

Gelled electrolytes under conventional surface electrodes are usually hydrogels. Hydrogel is a polymeric material that can swell and retain a significant amount of water within its structure but typically will not dissolve in water [113]. As a result, hydrogels have a vast usage area, from energy storage applications to drug carriers in biomedical applications [114]. Also, different skin-mountable electrodes benefit from the hydrogels that fill the surface between the biological tissue and the electrode itself (e.g., Ag/AgCl pregelled electrodes). Unfortunately, the hydrogel electrolyte of the "wet" electrodes will dehydrate gradually over time, making them unusable for long-term testing [115]. Therefore, Shen et al. introduced in their work [116] semi-dry solid hydrogel EEG electrodes (based on N-acryloyl glycinamide monomer and glycerin). Developed electrodes were placed for 25 days in a ventilated environment, and after the shelf time, brain waves were still captured at an acceptable level. Also, the electrodes were tested for 8 h during EEG measurements, and contact impedance did not increase significantly over time. These findings show that semi-dry solid hydrogel electrodes may improve biosignal detection as they retain moisture very well without being uncomfortably sticky.

Effective semi-dry electrodes should provide sufficient electrolytic conductivity within changing conditions (repositioning, different skin conditions), have good contact with the measuring site, be resistant to dry-out, and be safe and comfortable for the wearer. For example, material groups like ionic liquids and hygroscopic salts retain moisture, have electrical conductivity, and are biocompatible and biodegradable. If we replace water with ionic liquids (or hygroscopic salts) in the gels, ionogels are formed.

Ionogels have attracted much attention due to their remarkable properties, such as nonvolatility, high ionic conductivity, and high electrochemical and thermal stability [117]–[120]. Furthermore, whereas hydrogels only form gels with water, many diverse ionic liquids exist that have various physical and chemical properties, broadening the possibilities to make excellent novel electrodes for bioimpedance measurements.

The following chapters introduce hygroscopic potassium salt (potassium acetate) and ionic liquids (choline acetate) that may be suitable for semi-dry ionogel electrodes .

2.6.1 Hygroscopic potassium salt

Potassium acetate (KAc) is a hygroscopic potassium salt of acetic acid (KCH_3CO_2). It is typically used as an acidity regulator, flavor agent, and preservative (E261(i)) in the food industry [121]. However, it also has a medical purpose as a substitute for potassium chloride to reduce potassium deficiency. This is because KAc is an important mineral for body organs to function correctly [122].

A saturated solution of KAc will form an equilibrium at a relative humidity of about 23% [123], which means that when environment humidity is higher than 23%, KAc absorbs water from the surrounding environment in a quantity that KAc completely dissolves in its own crystal water. Therefore, biological tissues and skin have higher humidity than previously stated, and KAc-based hydrogel, when in contact with the skin, for example, stays as a liquid. In addition, potassium acetate is a good base of the electrolyte because it is well-analyzed, has good electrical conductivity (4.86 wt% KAc in aqueous solution at 20°C has 37.59 mS·cm^{-1} [124]), is reasonably cheap, and the substance is readily biodegradable. Lei et al. discovered [125] that it is possible to harvest atmospheric water efficiently; 0.62 g/g water vapor sorption within 120 minutes with potassium acetate hydrogel. This suggests that KAc hydrogel can also hold its liquid form in contact with the skin for a long time.

2.6.2 Ionic liquids

Ionic liquids (ILs) are semi-organic salts that have a low melting point (melt at temperature below 100°C), and room-temperature ionic liquids (RTILs) have melting points at or even below room temperature. Ionic liquid's popularity started when green chemistry became a major scientific field, and ILs were used as suitable replacements for volatile organic solvents [126]. Ionic liquids have large structural diversity of ions, which can be either inorganic or organic, chiral or achiral, acid or base, simple to complex, etc., which makes the term "ionic liquid" very broad as there is no single comprehensive model that describes the entire family of ILs [127].

The more recognized IL cations are imidazolium, phosphonium, pyridinium, cholinium, etc. Anions can be inorganic (e.g., nitrate, sulfate, halide) or organic (e.g., triflate, acetate, benzoate, organic carboxylates) [128]. In this research, we used choline acetate ($C_7H_{17}NO_3$), which consists of cholinium cations and acetate anions. Choline acetate should be more biodegradable and biocompatible than recognized and widely used imidazolium ILs [129].

The main exceptional and desirable properties are ionic conductivity (ChAc electrolytic conductivity in carboxylic acid at 24°C is 9.93 mS·cm^{-1} [130]), negligible vapor pressure, high thermal and electrochemical stability, which reduces the risk of degradation into undesirable by-products, and low volatility [131]. Volatility is defined as the "readiness to vaporize or evaporate, the tendency to be readily diffused, or dissipated in the atmosphere, especially at ordinary temperatures" [132]. Ionic liquids have no effective vapor pressure, meaning they will not vaporize as the compound molecules bond well with each other. Therefore, ionic liquids have been used as "fixatives" with different highly volatile compositions to lower the evaporation rate or to impart increased stability of the component [133]. For example, it can be used to control fragrance release, e.g., in the detergent industry for household products [134]. The odor depends upon the concentration and nature of the fragrance molecules released into the air, and the design of an efficient delivery system has to control the release of these highly volatile components. The smart addition of ionic liquids can create better control over the scents evaporated within a given time frame so that highly volatile citrusy and fresh smells can also be mixed with poorly volatile sweet or musky ones [135].

This diverse group of salts is in liquid form at ambient temperatures, but they change their water content according to the environment [136]. The exploitation of ILs can be complicated because of their liquid state, namely the possible leakage or maintaining the liquid in a predefined physical shape [137]. Fortunately, combined with polymers, they can yield gels, which could be used as the electrolyte between the electrode and the skin – a quasi-solid-state electrolyte [138].

To our knowledge, only a few researchers have used ionic liquids as electrolytic gels in contact with the skin. For example, Leleux et al. [139] incorporated the IL gel onto electrodes made of Au and the conducting polymer poly(3,4-ethylenedioxythiophene) doped with poly(styrene sulfonate) (PEDOT:PSS). They showed that IL gel improves the electrodes' performance and helps maintain a low interface impedance over more extended periods (3 days) than commercially available Ag/AgCl pre-gelled electrodes (20 hours). Velasco-Bosom et al. [140] also used PEDOT:PSS electrodes coated with ionic gels (cholinium lactate) to form good electrical and mechanical contact to the skin for high-quality spatiotemporal recordings of EMG that allow identifying the motion of fingers. Isik et al. [141] prepared cholinium-based ion gels to be used as solid electrolytes for long-term cutaneous electrophysiology. The proposed solid gel was placed on PEDOT:PSS and gold layer. The ECG signals recorded during 72 hours did not display any degradation of

the signals indicating that the integrity of the gel was well preserved upon exposure to environmental and skin humidity [141].

2.6.3 Toxicity of choline-based salts

Ionic liquids are at low risk for aerial release, but removing them entirely from aqueous solutions is challenging, and toxicity can be problematic [131]. So, it is important to be mindful when used as electrodes in contact with living tissue.

The consensus is that the IL's toxicity depends on both - the specific anions and cations [142]. For example, choline (N,N,N-trimethylethanolammonium) cation can be classified as low toxic and biodegradable as it is also an essential nutrient for humans [143]. It is present in a lot of food (vitamin B) [144], active in essential key functions in the human body, like a precursor for phospholipids or building of neurotransmitters [145], etc. Also, there is a lot of research that has tested the toxicity of different choline-based salts (including choline acetate) towards:

- human tissue culture cells like human breast cancer cells (MCF-F)[130],
- melanoma cell (SK-MEL-28) [130], and cervix carcinoma cells (HeLa) [146];
- Filamentous fungi [147], [148], actinobacteria, yeast [148];
- Vibrio fischeri marine bacteria [149], [150];
- E.coli bacteria, hydra, garlic [151].

All these studies have described the choline-based ILs as "practically harmless" for tested systems. This gives confidence that choline acetate equals biocompatible liquid salt. Nevertheless, care must be taken as hazardous properties cannot be entirely excluded.

3 Fabricating carbon-PDMS composite

This chapter describes a simple and cost-effective carbon-PDMS material development, starting from the fabrication and finishing with analyzing the electrical properties of the material. In my work, the CNFs and CFs were employed to enhance the electrical properties of PDMS. The first part aims to characterize the electrical conductivity of the fabricated CNF and CF-based composites for potential sensing applications. The morphology of the composites was not investigated, but electrical conductivity and strain measurements were conducted. The objective was to find the optimized formulation to achieve electrical conductivity and obtain a flexible strain range. Also, having a reasonable viscosity for material processing and fabrication [152].

3.1 Materials and methods

For this study, polydimethylsiloxane (PDMS) was used, which is a chemical formula for silicone elastomer. Two-part platinum cure liquid silicone Dragon Skin™ 10 (shore hardness 10A) was purchased from, Smooth-on, Inc. It is durable, stretchable (0.15 MPa), fairly strong (tensile strength 3.3 MPa), and biocompatible. Carbon nanofibers (diameter 100 nm, length 20-200 μm, conical, >98% from Sigma-Aldrich, Germany) and carbon fibers (diameter 7 μm, length 6 mm, SIGRAFIL® C30, GRM Systems) were used as fillers to create an electrically conductive network through the PDMS polymer [153]. The CNF/CF-PDMS composite material was fabricated using mechanical stirring and a solvent-assisted ultrasonication method to ensure somewhat uniform dispersion of carbon particles within the polymer matrix. HMDSO (purity 98%, from Sigma-Aldrich, Germany) was used to reduce the mixture's viscosity for easier stirring. HMDSO is a low-viscosity solvent that evaporates quickly [154]. It is mainly used in organic synthesis and also acts well in silicone mixtures to thin the composite and simplify the vacuum degassing process [154].

Two process recipes for stretchable carbon-PDMS composites were applied. The first is depicted in Figure 4, and the other in Figure 5.

Recipe #1 for CNF/CF-PDMS composite (7.7 wt% CNF and 0.5 wt% CF) procedure steps were the following:

1. 0.25 g of CNF and 0.017 g of CF were added to silicone part A.
2. 7 mL of HMDSO solvent was added to reduce the viscosity.
3. The suspension was mixed in a closed vessel at room temperature for at least 2 hours using a magnetic stirrer.
4. The same procedure was repeated with silicone part B.
5. Mixtures A and B were poured into a third vessel and stirred for 1 hour.
6. The composite was vacuum degassed for 5 minutes to minimize air bubbles.
7. The mixture was left for 48 h at room temperature to complete the curing process.

In the first method, carbon fillers (CF and CNF), silicone, and hexamethyldisiloxane (HMDSO) were mixed (Figure 4a) (steps #1 to #3) by using magnetic stirring (Figure 4b) to disperse the agglomerated fillers inside the silicone matrix. The same steps were followed using silicone part B. Next, parts A and B were poured together (Figure 4c) and vacuum degassed (Figure 4d) (steps #5 and #6). Finally, the mixture cured for 48 hours at room temperature (Figure 4e) (step #7).
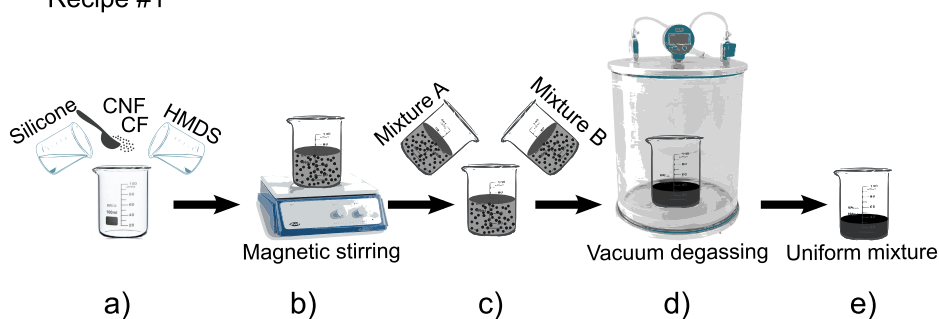
Recipe #1

Figure 4. Recipe #1 is depicted in picture form. Fabricating carbon-PDMS composites included mixing silicone, carbon fillers, and HMDSO (a-c), vacuum degassing the mixture (d) and curing it for 48 hours (e) to form stretchable conductive material.

Recipe #2: solution mixing for CNF/CF-PDMS composite (7.7 wt% CNF and 0.5 wt% CF) contains the following steps:

1. 10 mL of IPA surfactant was added to 0.25 g of CNF and 0.017 g of CF.
2. The suspension was mixed using a sonicator (at 40 kHz frequency, power of 30 W) for 15 minutes.
3. Silicone part A was added to the mixture.
4. Another 15 minutes of sonication of part A.
5. IPA was evaporated by placing the mixture on a hot plate (82°C) for 24 h.
6. The same procedure was repeated with silicone part B.
7. 7 mL of HMDSO was added to each mixture: A and B parts and mixed mechanically for a few minutes.
8. Mixtures A and B were poured together into a third vessel and magnetic stirred for 1 hour.
9. The composite was vacuum degassed for 5 minutes to minimize air bubbles.
10. The mixture was left for 48 h at room temperature to complete the curing process.

Numerous solvents help disperse the aggregates, i.e., hexane, toluene, acetone, chloroform, and isopropyl alcohol [155]. Articles [155]–[158] suggest IPA because it has relatively large surface tension and twice the vapor density of air, so the air bubbles are easily removed from the solvent. In addition, IPA has an amphiphilic structure comprising three hydrocarbon units and one hydroxyl group. The hydrophobic part is easily attached to the highly hydrophobic carbon nanofiber surfaces, forming IPA-coated CNFs with hydroxyl groups located on the outer layer of the carbonaceous nanofiber complexes [155].

In the current study, carbon fillers were mixed with isopropyl alcohol (IPA) (Figure 5a)(step #1), and these ingredients were ultrasonicated (step #2). The sonication time was kept short to reduce the risk of breaking the long carbon fibers inside the solvent. For that, 15 minutes of sonication was used, and 30 W of power at 40 kHz transferred to the mixture, separated the agglomerates of carbon. When CNFs and IPA were mixed and sonicated, strongly aggregated CNF bundles were temporarily separated by the physical force exerted by the ultrasound source. The separated CNF bundles were then coated with IPA solvent.
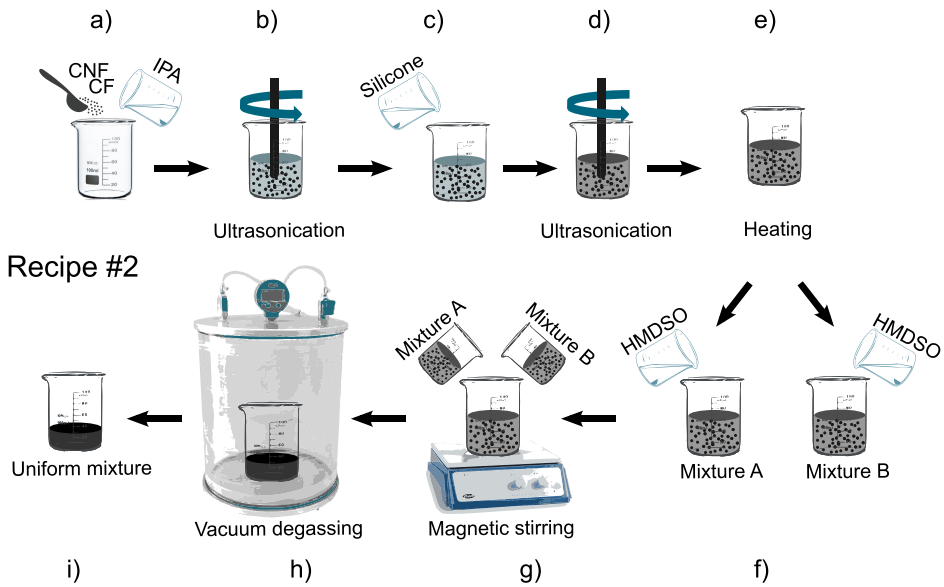
Figure 5. Recipe #2 to fabricate CNF/CF-PDMS composite. In addition to CNF and CF, the solvent was added to help disperse the aggregates (a). Before and after the addition of silicone (c), the mixture's ultrasonication (b and d) took place. The composite was heated (e) at 82°C to remove the solvent. Next, mixture parts A and B were stirred with a magnetic stirrer (f, g) and vacuum degassed (h). Finally, the uniform mixture cured 48 hours (i) before the measurements.

After adding silicone part A (step #3), another 15-minute set of sonication was required (step #4). The carbon fillers were successfully incorporated into a silicone matrix to produce a uniform composite. Next, IPA had to be removed from the mixture by heating it (Figure 5e). The evaporation temperature was around 82°C. The mixture was placed on a hot plate and dried there for 24 hours (step #5). All these procedures were repeated for the silicone part B. After the heating, two silicone mixtures remained: carbon fillers with silicone part A and carbon fillers with silicone part B. At this point, both mixtures were very dry and viscous, so HMDSO was added (step #7) to make the blend easily mixable with a magnetic stirrer. After 1 hour of stirring (step #8), vacuum degassing took place to remove air bubbles that were trapped inside the composite (Figure 5h)(step #9). Finally, the mixture was uniform (Figure 5i). 48 hours of drying at room temperature (step #10) led to the testing part, as the material was dry and stretchy enough to be measured.

Recipe #1 is far simpler and less time-consuming, and due to this, most of the fabrication in the current research was made following the instructions in Figure 4. Therefore, the design criteria were cost-effectiveness, sufficient electrical conductivity, and an easy fabrication process to achieve the best possible homogeneity of fillers inside a polymer.

3.2 Experimental setup

3.2.1 Sample preparation

Carbon-PDMS composite materials prepared were characterized by measuring electric resistance under compressive cyclic loading/unloading and cyclic stretching/releasing.

For this purpose, samples were cut with a scalpel into two different sizes:

a) 2x2 cm square with a thickness of 2 mm;
b) 2x5 cm rectangle with a thickness of 2 mm.

Sample (a) was used for pressure loading/unloading (Figure 6a) and sample (b) for stretching/releasing (Figure 6b).
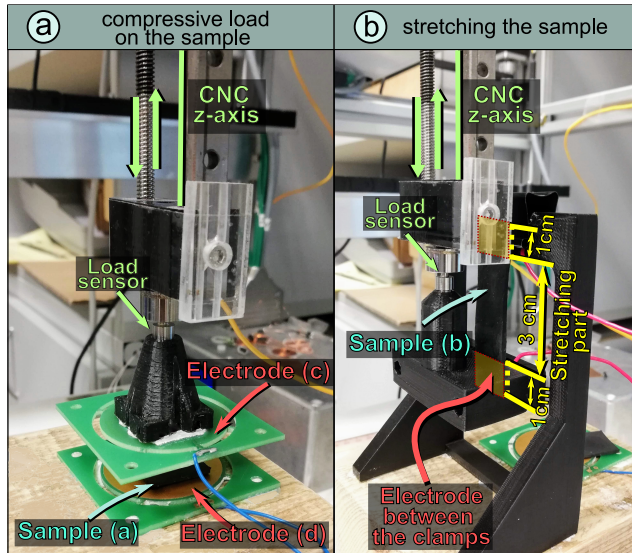

Figure 6. CNC device is used for loading/unloading to make (a) compressive tests on the sample and (b) tensile stress sensitivity measurements (stretch the sample).

3.2.2 CNC device

A three-coordinate custom-made CNC device enabled prolonged and reliable movement of the mechanical z-axis with a minimum rate of 5 μm per second. One gold-coated metal plate electrode was attached to the CNC device's up-and-down moving axis (in Figure 6 marked (c)), and the other electrode was fixed on an immobile rigid base (Figure 6(d)). Electrodes were connected to the impedance analyzer, and a pressure sensor (parameter) was attached to the z-axis of the CNC device to register the load applied on the sample material between the electrodes.

3.2.3 Impedance measurement setup

The electrical impedance values of each composite sample were registered using Impedance Analyzer 6500B series (Wayne Kerr Electronics), and the load values (provided by the CNC load sensor) were recorded simultaneously through the LabVIEW 2014 program. Measurement frequency (10 kHz) was picked so the response would be purely resistive (phase angle approximately 0 degrees).

3.2.4 Pressure loading and unloading

Sample (a), depicted in Figure 6a, was placed between the two electrodes, and the moving plate pressed and released the material at the rate of 5 μm per second. At the same time, impedance change was registered as a function of varying load from 0 g to 1200 g, approximately 0-30 kPa. This kind of measurement gave a cyclic graph that showed

how the resistance changed with changing pressure (Figure 8 in Chapter 3.3.1). The contact between the electrodes and the sample under the test was continuous during the measurements.

3.2.5 Tensile strain sensitivity

Tensile strain measurements were conducted on several samples. For this, both ends of the sample in Figure 6b were fixed between two electrodes, leaving 3 cm between the clamps free to stretch. Carbon-PDMS material samples were tested under cyclic tensile loading/unloading. This means the sample was extended to 100% strain with the rate of 0.1 mm per second and released with the same step. The gauge factor was calculated to describe the sensitivity of the material with Equation (4):

$$K = \frac{\Delta R/R_0}{\varepsilon} \tag{4}$$

with

$$\varepsilon = \frac{l_T - l_0}{l_0} \tag{5}$$

K is the gauge factor, $\Delta R/R_0$ is the relative resistance change, and ε is the amplitude strain, where l_T is its elongation at the moment T, and l_0 represents the initial sensor's length.

3.2.6 Strain dependent resistivity

An average of 100 loading/unloading cycles were applied to each sample to evaluate the resistivity of the composite materials. Volume resistivity was calculated from the measured resistance with the formula:

$$\rho = \frac{R \cdot A}{l} \tag{6}$$

where ρ is volume resistivity, R is the measured resistance, A is the area of the sample, and l is the thickness.

3.3 Results

An effective conductive network is formed when a sufficient amount of carbon fillers are dispersed inside the PDMS substrate. Rigorous mechanical stirring will decrease the number of clustered fillers to some extent. However, agglomerates can not be entirely spread without numerous extra time-consuming steps (e.g., longer mixing time, drying the carbon fillers before use, and surface functionalization [159]). Nonetheless, after 2 hours of mixing, the blend of PDMS and carbon fillers seemed uniform and homogenous to the unaided eye. Also, electrical conductivity was achieved after vacuum degassing and drying the sample material at room temperature (23°C) for 48 hours.

Figure 7 shows how resistivity decreases with a growing number of conductive fillers. At low CNF content (2 wt%), the resistivity is high, around 15 kΩ·m, and a sparse conductive network is formed. When the carbon concentration is increased, resistivity rapidly decreases by several orders in magnitude, which suggests that the critical volume of fillers to form electrical connectivity is over 2 wt% and under 4 wt%. The exact percolation threshold was not identified in the scope of this work.
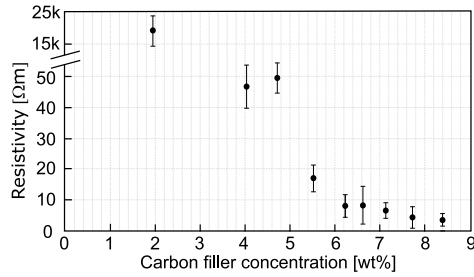
Figure 7. Different carbon nanofiber concentrations and resistivity response. When the concentration of carbon fillers was low (2 wt%), the resistivity was very high (over 15 kOhm·m). However, increasing the concentration to 4 wt% lowered the resistivity remarkably (to approx. 50 Ohm·m), suggesting that the percolation threshold is between 2-4 wt%.

3.3.1 Number of loading cycles' influence on impedance

Figure 8 depicts a sample of fabricated carbon-PDMS material under compressive loading/unloading and its impedance change. At first, the contact between the electrode and the sample is light, and the impedance is high, but with every step closer, the contact improves. Understandably, with stronger compression, more fillers are pushed together, forming numerous extra conductive pathways inside the composite material. If unloading takes place, the pressure on the sample decreases, and the impedance increases again. During loading/unloading, the measuring electrodes had constant contact with the samples even at the end of the cycle when pressure decreased to a minimum.
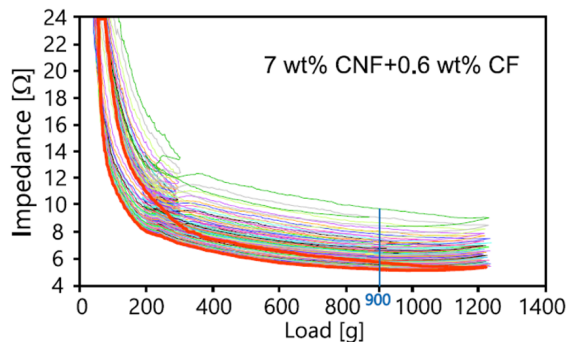

Figure 8. One composite sample with 7 wt% of carbon nanofibers and 0.6 wt% of carbon fibers under 50 compressive loading/unloading cycles and its impedance response. With every consecutive cycle, impedance decreased. The pressure sensor of the CNC machine displays strong linearity at around 200 g of load, but the interest region for my measurements is unaffected.

Tests revealed the presence of hysteresis (Figure 8) because the unloading part of the cycle shows a slight delay in recovering into its original state, forming noticeable impedance loops. This is because a soft and stretchable sample is trying to reach its original condition, but it takes a longer time than it has – the next cycle is already loading. That is why the impedance is lower with each consecutive pressure load cycle. With around 200 g of load, the pressure sensor of the CNC machine displays strong nonlinearity. However, this device defect can be overlooked because the interest region is unaffected.

3.3.2 CF vs. CNF dispersal

Carbon nanofibers (CNFs) were used in favor of carbon nanotubes as the cost is significantly lower – single-walled CNTs can typically have an 80% higher price than CNF-s. So, CNFs are an effective, low-cost replacement for carbon nanotubes. Also, in my setup, dispersing the fillers as homogeneously as needed to see the advantage of CNT-s superior length-to-diameter ratio was hardly possible. In addition, to lower the production cost and produce more effective conductive pathways, I used CNF and CF fillers simultaneously. Hybrid conductive fillers have been reported to increase electrical conductivity as the fillers complement each other by bridging the gaps more easily due to different geometries [91].

Figure 9 represents samples with the same carbon filler concentrations (7.7 wt%) using recipe #1 (Chapter 3.1). The following results were registered when a 900 g (23 kPa) load was on the composite material. The blue line shows the CNF-PDMS samples' average, and the red line CNF/CF-PDMS samples' average over 1000 cycles. Standard deviation is depicted as bars on either side of the mean to represent the variation of the measurements of samples with the same concentrations. When CNF and CF fillers were combined inside the PDMS matrix, it was possible to achieve very low resistivities (1 Ohm·m) at the 10th cycle. Still, on average, the resistivities did not differ enormously (CNF-PDMS samples having approximately 16% higher resistivity).
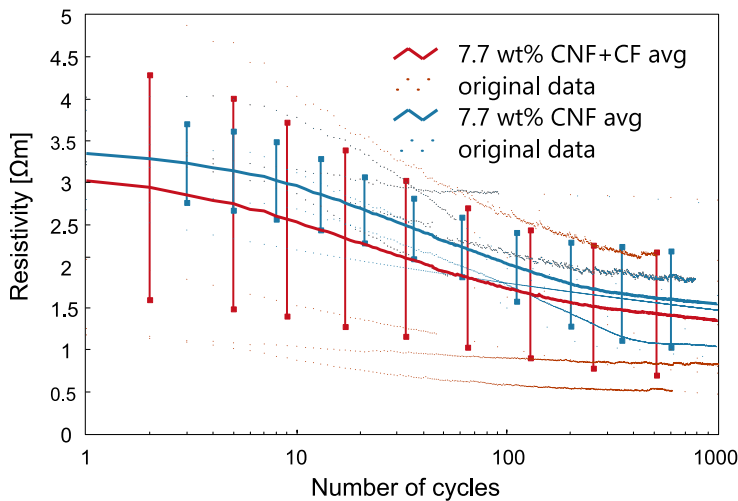

Figure 9. CNF/CF-PDMS and CNF-PDMS samples have the same filler concentrations and preparation methods (recipe #1). CNF-PDMS samples had an average of 16% higher resistivity. In the case of hybrid fillers, the resistivity values varied more between the samples (red vertical bars on either side of the mean).

On the other hand, in Figure 9, vertical bars show clearly that the data varies a lot more when hybrid fillers are used. CNF-PDMS samples' resistivity varies approximately 60% less than CNF/CF-PDMS same concentration composites' on the 10th cycle. This is because CFs have significantly bigger dimensions than CNF particles. Therefore, it is more difficult to disperse them inside the PDMS matrix uniformly, which means that fewer conductive pathways form, resulting in higher resistivity. On the other hand, CNF particles are smaller but tend to get agglomerated into bundles. Adding CFs can connect the bundles and form

co-supporting conductive pathways making the sample less resistive. Therefore, a good probability is that improving the fabrication process to disperse the hybrid carbon fillers inside the PDMS matrix more homogeneously decreases the standard deviation between the samples.

3.3.3 IPA effect

In recipe #2, IPA (isopropylalcohol) is used as a solvent for carbon filler dispersion. Articles [130]–[133] suggest IPA because it has relatively large surface tension and twice the vapor density of air, so the air bubbles are easily removed from the solvent. In addition, IPA has an amphiphilic structure comprising three hydrocarbon units and one hydroxyl group. The hydrophobic part is easily attached to the highly hydrophobic carbon nanofiber surfaces, forming IPA-coated CNFs with hydroxyl groups located on the outer layer of the carbonaceous nanofiber complexes [131]. Thus, IPA, together with the ultrasonication mixing method, helps to separate the carbon nanofibers and carbon fibers more homogeneously.

Figure 10 shows 4 samples with the same carbon filler concentrations – 7.7 wt%.

- CNF/CF-PDMS – 7.2 wt% carbon nanofibers and 0.5 wt% carbon fibers, fabrication recipe #1 is used;
- CNF-PDMS – 7.7 wt% of carbon nanofibers, fabrication recipe #1 is used;
- CNF-PDMS IPA – 7.7 wt% of carbon nanofibers, fabrication recipe #2 with IPA solvent is used;
- CNF/CF-PDMS IPA – 7.2 wt% carbon nanofibers and 0.5 wt% carbon fibers, fabrication recipe #2 with IPA solvent is used.

Even though all the samples have the same concentration of carbon fillers, the resistivity values on the 10th cycle vary from 1 to 4 $\Omega \cdot$m. This contrast can be partly explained by the different fabrication methods (recipes #1 and #2) and different filler types (CNF and CF) used. Analysis reveals that the relation "resistivity versus the number of compressive load cycles" is best described by the three-parameter power function:

$$y = a \cdot x^b + c, \tag{7}$$

where a is amplitude, b is power, and c is offset. Figure 10 presents a set of original data and the corresponding power fit formulas and curves. The samples' resistivity decay rates, as a ratio of the resistivity values at cycles 1 and 50, are calculated from the smoothed (by power fit function) data.

It is interesting to note from the data comparison of the two methods that the CNF-PDMS IPA and CNF/CF-PDMS IPA samples' resistivity change with compressive cycles was significantly less than with the other two composites. For example, recipe #2 samples give lower factor values – 1.20 and 1.17 (Figure 10, blue and green line) compared to recipe #1 samples - 1.71 and 1.46 (Figure 10, red and yellow line). This lets to speculate that the samples with IPA are more stable over consecutive pressing cycles and fabrication process #2 disperses fillers more effectively than process #1. Thus, IPA, together with the ultrasonication mixing method, probably helps to separate the carbon nanofibers and carbon fibers more homogeneously.
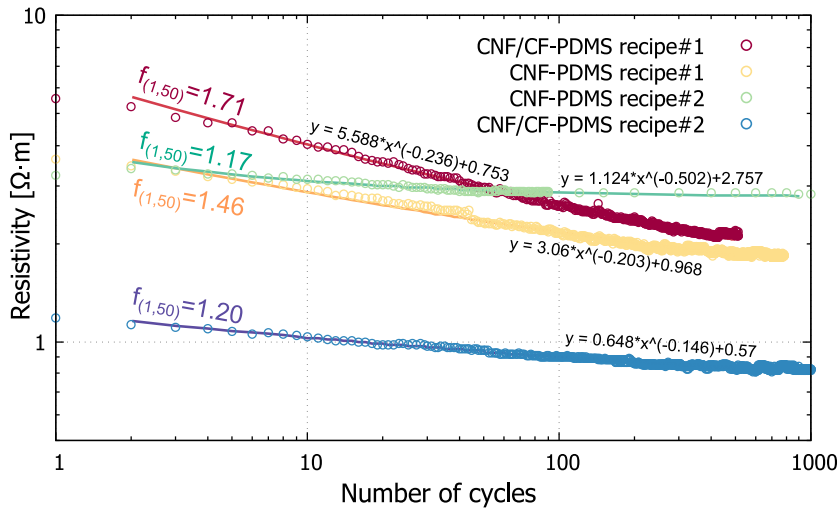
Figure 10. Four different samples with the same carbon filler concentration (7.7 wt% - CNF+CF, CNF IPA, CNF, and CNF+IPA). Factor values on each line ($f_{(1,50)}$) represent the ratio of the resistivity values decay at cycles 1 to 50—samples with IPA using recipe #2 show lower decay rates than recipe #1 samples.

3.3.4 Concentration influence

Figure 11 shows CNF/CF-PDMS with different concentrations (5.3 wt%, 6.8wt%, 7.7 wt%, 8.3 wt%) of carbon fillers inside silicone when recipe #1 is used. Depicted lines result from averaging at least 10 samples' resistivity changes with consecutive cycles.

Most samples were registered until the 100th cycle, and few were measured until the 1000th cycle. Using extrapolation and linear fitting, the prediction of resistivity change with regression of cycles showed a slowing resistivity decrease. Nevertheless, the decline continued indefinitely. The average resistances of these cycles with error bars were calculated to illustrate how filler concentration influences the resistivity and how much the resistivity varies between samples of the same concentration.

Four different concentrations are depicted, and the overall trend is the same – with each cycle, the resistivity declines. When the concentration is lower, the resistivity is higher, as expected. The more filler particles are inside the polymer, the stiffer and less elastic it is. With every pressure cycle on the sample, the material does not have time to return to its original state, which means that more pathways stay connected when the new cycle begins – conductivity is also higher. Analysis showed that samples with filler concentrations of 5.3 wt% and 6.8 wt% have resistivity rates slightly higher (1.58 and 1.65, accordingly) than the other two (7.7 wt% and 8.3 wt%) that have 1.46 and 1.37, which means that the evolution of the sample is slightly different according to filler concentrations. More conductive sample materials' resistivity decreases less with pressure load cycles.

For this material's goal application, reasonably low (1-5 Ω·m) resistivity at 8.3 wt% is sufficient. Some researchers [160] have gotten resistivity as low as 0.02 Ω·m by using carbon nanotubes inside PDMS. Still, when the material is used as electrodes on the skin, the electrode-skin interface impedance overpowers the electrode material's good conductivity anyway. For comparison, a conventional Ag/AgCl electrode's electrolytic gel has resistivity around 100 Ω·m [161].
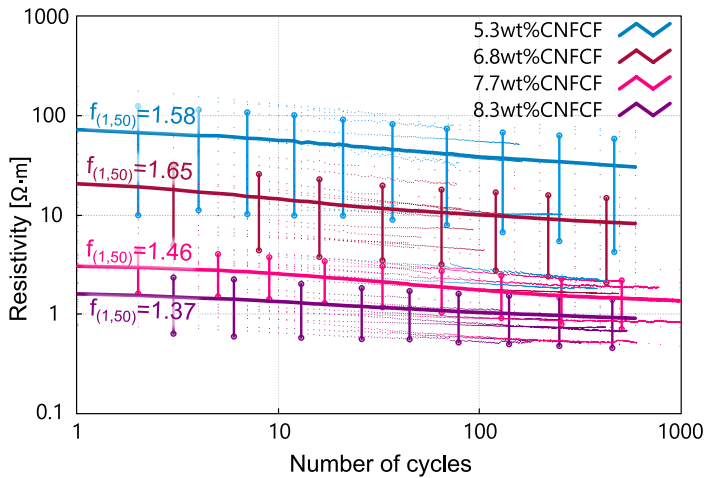
Figure 11. Average resistivity change of different CNF/CF-PDMS samples over 1000 cycles. Concentrations of fillers differ from 5.3 wt% to 8.3 wt%

3.3.5 Aging

Compressive loading/unloading test of the samples showed that when pressing on the material, the resistivity decreased, and during unloading, resistivity increased but did not get to its original level. After the first measurement of pressure loading and unloading of the carbon-PDMS sample, it stayed in the rest position for 10 days in the open air. When the same sample was measured again, the resistivity was an average of 100% higher. This phenomenon is defined in this work as the aging of the sample material. The aging definition is not covered in most articles researching carbon-silicone polymers, only considered unstable or unpredictable materials.

In addition, another curious aspect appeared: the more loading/unloading cycles were made on the sample before leaving it on the shelf, the less resistivity increased with time. In other words, the more a sample is under the loading cycles in the first stage of the experiment, the closer it is to the first measurements made on the first days. Also, the more conductive the sample was in the beginning, the less aging affected the material.

Figure 12 shows how samples with 7.7 wt% and 8.3 wt% carbon filler concentrations increase resistivity on average 5 times when the pieces were left untouched for weeks (175 days). In the case of 360 days on the shelf (8.3 wt% sample), the resistivity was 34 times more than on the first days (Figure 12, yellow line).
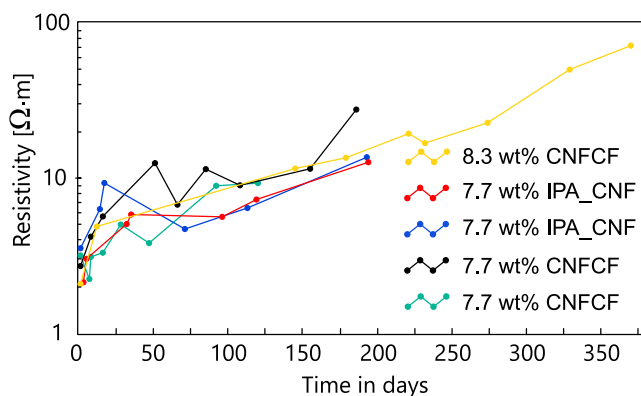
Figure 12. Five samples with similar carbon concentrations and aging depicted over 120 to 360 days. The resistivity of the samples increases with time.

During purposeful physical impact (compressive cyclic loading) on the sample material under the test, some internal changes start to happen simultaneously. Analyzing these physical modifications was not in the scope of this thesis, but some hypothetical scenarios that can influence the aging effect are:

- nanofibers and fibers changing their placement;
- CNF and CF dispersion level and alignment;
- CNF and CF breaking or bending;
- evaporation of solvent residue;
- ambient humidity change.

3.3.6 Retention of a sample under compressive load

The sample (CNF/CF-PDMS with 8.3 wt% of fillers) was exposed to a long (19 days) cyclic pressure loading between approximately 0 to 30 kPa (0 to 1200 g of load) to investigate its retention. The results are depicted in Figure 13, which shows the impedance change as a function of time. Firstly, the impedance decreased by about 17%, and from the 3rd to the 6th day, it stayed steadily near 4 Ohms. After the 6th day, a consistent increase lasted until the end of the testing, 19 days later, when impedance had grown from the lowest point near 4 Ohms to 5.4 Ohms (35%). Consequently, the seeming stabilization after the 3rd day of testing can be misleading. Given that this finding was based on one sample, the results from such analysis should be treated with considerable caution.

In Figure 13, black dots represent the original measurement data, and the first peaks during days 1 to 6 seem pretty random. These abrupt changes in impedance can come from the internal changes inside the sample material due to external forces: some minuscule air bubbles popping or carbon fibers breaking. However, the peaks from day 12 until 19 are very regular. Analyzing the data showed that at noon every day since the 12th day, impedance increased ca 0.5 Ohms and slowly decreased as the day went by. Looking back at the weather information on the days these peaks appeared, it showed sunshine without clouds. Sun shining probably increased the temperature and changed the ambient humidity, which consequently increased the impedance. After analysis of the results, these peaks were recognized as unwanted weather influences and regarded.
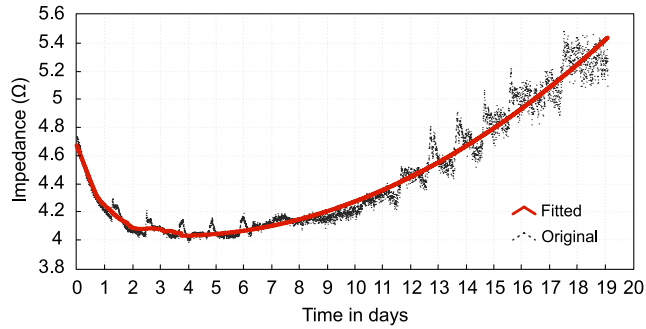
Figure 13. 19 days of testing a CNF/CF-PDMS fiber sample under compressive loading/unloading cycles.

3.3.7 Tensile strain sensitivity

In CNF/polymer composites, several topics were investigated in a limited manner, for example, strain. Strain measurements are well covered in literature [162]–[164] as carbon-PDMS material is often used as strain sensors. When a carbon-PDMS sensor is stretched, its resistivity changes; the more it changes, the better sensor is, as even the slightest movement is registered in resistivity numbers.

In the current work, the tensile strain sensitivity results were similar and did not depend much on the concentration of the carbon fillers when it was above the percolation threshold. However, by stretching the sample to 100% strain, the relative resistance increased 75% with the linear response (see Figure 14). The gauge factors of all tested samples were approximately 0.7. This value is lower than reported by other researchers, Wu et al. [158] and Wang et al. [165], where the gauge factor is almost 24. The main reason for smaller strain sensitivity is the rigidness due to higher filler concentration and probably poor homogeneity of the particles inside PDMS. As tensile strain had a minor influence on resistance in my work, the material is less sensitive to moving artifacts when used as bioimpedance electrodes. I consider this an advantage in this specific work.
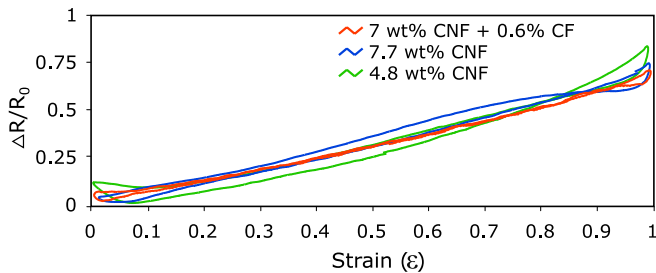

Figure 14. All tested samples have a similar responses to stretching and releasing cycles.

3.4 Conclusion

The goal was to create a carbon-PDMS composite material that is electrically conductive and elastic using a simple and cost-effective fabrication recipe. For this, two recipes were presented. Recipe #1 had a straightforward 5-step procedure, including magnetic stirring

as mixing preference. Recipe #2 required IPA as a solvent to disperse the carbon fillers more effectively inside the polymer matrix. In addition, ultrasonication was used as a mixer. Samples with two different fillers (CNF and CNF+CF) and concentrations were studied and experimentally characterized under compressive load cycles.

Impedance measurements showed that carbon fillers inside silicone rubber increase the electrical conductivity (0.7 S/m at 8wt%), but due to the fillers' poor distribution, the material's stability is low. In addition, the concentration of carbon fillers had to be at least 2-4 wt%. This means the percolation threshold using the introduced technique is over 2 wt% and under 4 wt%.

The evidence from this study suggests that using hybrid conductive fillers (CNF and CF) is an effective way to make a low-cost conductive composite material. The 'bridge effect' between carbon fillers and different geometries is beneficial for forming co-supporting conductive pathways. Furthermore, by comparison with single filler systems, using hybrid carbon nanofiller at certain mass ratios benefits both filler dispersion, which results in the formation of bridged conductive paths with higher efficiency [91]. In my research, the strain was not focused on, but some simple experiments were conducted to investigate the strain sensing capability of the composed material: tensile loading tests - stretching and releasing the sample and measuring impedance change during these cycles. The results showed that the strain sensitivity of composite material is low – gauge factor 0.7.

Cyclic shifts and resistivity measurements showed that the carbon-PDMS material is not easily understandable. In addition, many aspects (decreasing resistivity with pressure loading, hysteresis, aging [140]) were not considered prior to this research and needed to be acknowledged for further experiments.

Main outcomes:

1. Carbon-PDMS composite fabrication recipe #1 proved to be sufficient to make electrically conductive material with a percolative threshold between 2-4 wt%;

2. Carbon-PDMS fabrication recipe #2 showed a more stable cyclic decline of resistivity, which is associated with potentially more efficient filler dispersion inside the polymer matrix;

3. CNF samples' resistivities are variating less than with CNF-CF samples';

4. The gauge factor of different samples was similar – around 0.7.

The next chapter investigates electrodes that are fabricated using the developed carbon-PDMS composite.

4 Eletrodes made of carbon-PDMS composite

This chapter explains the importance of the electrode-skin interface measurement and describes a very convenient measurement setup developed for our specific needs. The construction of carbon-PDMS material into electrodes is introduced, and different electrodes are tested and their interface impedance compared.

4.1 Electrode quality assessment

The quality of the electrode is challenging to assess comparatively. Specific measurements need specific electrodes, and there is no universal and ideal electrode for bioimpedance measurements. The properties are affected by the electrode material, size of the area, electrolyte between the skin, electrode build-up, temperature, current density, the frequency of the current used in the measurement, etc. All this means that the analysis of the interface impedance and quality of the electrodes depends on numerous variables, and in real life, it is nearly impossible to find only one value or factor that characterizes the quality of the electrodes on the skin. A thorough analysis of the system and numerous exceptions is needed to fully understand the interface impedance measurement results.

4.1.1 Two-electrode and four-electrode measurement

Typically, two methods are used for bioimpedance measurements: a two-electrode system and a four-electrode system.

In the **two-electrode technique**, two electrodes are used, and the contact impedances of both electrodes are measured along with the desired tissue impedance – which means that the same electrode pair is used to apply the current and to measure the resultant voltage. This method is, therefore, very susceptible to problems due to the magnitude mismatch, or drift of contact impedances. Nonetheless, the procedure is straightforward, leading to widespread use for body composition measurements, where large electrodes can be used, and high contact impedance does not play a serious role. Also, measurements that use high frequencies (MHz range) can use the two-electrode method without problems [166].

In a **four-electrode technique**, one electrode pair is current carrying and the other, a different pair, picks up the corresponding potential difference in the tissue [44]. This way, the contact impedances do not influence the voltage measurement and hence should be insensitive to problems arising from electrode contact. Although the four-electrode technique is less sensitive to contact impedance problems, issues still occur. In particular, significant mismatches in the resistive and/or capacitive properties of the voltage detection electrode can result in an error in both the real and reactive parts of the measured impedance [60]. Tetra-polar systems are commonly used to detect bioimpedance at lower frequencies (under MHz) with skin surface electrodes or probes meant for different body cavities [44]. Tetra-polar configuration is used to minimize the influence of the electrodes in the bioimpedance measurement process, but still, electrodes remain a major issue.

4.1.2 Impedance measurements of the interface on the human forearm

The anatomy of the forearm includes skeletal bones (radius and ulna), arteries, veins, nerves, muscles, adipose, skin, and interstitial fluids. Individual differences at the wrist include size, skin thickness, skin water content, bone anatomy, vascular branch size and locations, sub-dermal water content, and adipose/muscle/bone/vasculature content with the sensing region. All of these parameters will impact the actual impedance measured at the wrist. This leads to person-specific conductivity [45].

The impedance of the electrode-electrolyte interface affects the biosignal to be measured. Knowing the real impedance values allows us to avoid numerous inconveniences and act accordingly to prevent them. Interface impedance evaluation can help to:

- avoid signal distortion, attenuation, and noise to ensure correct amplifier matching [167];
- continuous interface impedance measurements can be used to estimate motion artifacts [168];
- avoid common mode rejection ratio (CMRR) reduction. CMRR of the amplifier reduces with high interface impedance, leading to excessive powerline interference [169].

Therefore, too high impedance in the interface will pose many problems with the measurements. But how high is "too high impedance"? It is difficult to answer as the results can vary with each specific measurement method, electrode size and amount, skin type and preparation method, etc. For example, interface impedance measurements are frequency dependent, and the choice of bandwidth changes the ohm values strongly. Also, using dry electrodes can show much higher interface impedance than using wet electrodes, and high temperature in the room can affect the sweat accumulation under the electrode and influence the interface results as well. Most of the measurement methods of interface impedance in numerous studies are designed for specific needs. For this reason, it is complicated to compare the actual values of interface impedance, but we can analyze the time and force dependency, frequency response, stabilization time, or skin preparation effect. Therefore, it is important to understand the factors influencing contact impedance to reduce its undesirable contributions to impedance measurements.

Widely used interface impedance techniques described in the literature are bipolar and three-electrode measurements. When using the bipolar method, two electrodes are placed on the skin, a known current is injected into one electrode, and the voltage drop between those two electrodes is measured. In this configuration, skin-electrode impedance, electrodes' own impedance, and body impedance between the electrodes are registered. However, the body impedance is usually many times smaller than the interface impedance, meaning that it is reasonable to assume the body impedance is negligible. The resultant impedance is divided by two to obtain the impedance for one electrode [170]–[173]. The downside of this technique is that we cannot know the actual interface impedance of both electrodes, but relatively serious assumptions are made by thinking the electrodes have the same values. There is no way of knowing if one or the other is poorly placed on the skin or if contact is loose.

The other method uses a 3-electrode configuration, consisting of one working electrode and two as a counter electrode and reference electrode. In this case, the system consists of electrode impedances, skin and body tissue impedance, and the skin-electrode interface. The measured impedance is the combination of those individual impedances altogether [174]–[177].

Figure 15 shows how to calculate the skin-electrode impedance on B. For this, two other electrodes (A and C) are used. A high-impedance buffer prevents the current flow between B and C. A known sine wave current is passed through electrode B, and when the voltage between electrodes B and C are measured, the absolute magnitude of the impedance of the skin-electrode interface B is the peak voltage divided by the peak current [170]. In this way, only one electrode interface impedance is determined. For another electrode, the impedance measurement setup has to be reorganized, so the electrode stabilization starts again.
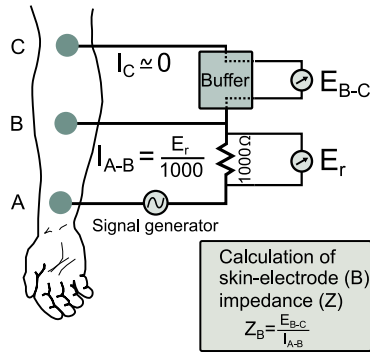
Figure 15. Redrawn from Degen and Loeliger [169], where three electrode interface impedance measurement is introduced. Skin-electrode interface impedance of electrode B is calculated using two other electrodes placed on the skin (A and C).

4.2 Interfacial impedance measurement methodology

4.2.1 System description

An efficient measurement setup was worked out in the scope of this research to compare the electrodes. With this setup, it is possible to test three (optimal number on the forearm of the test subject) different sets of electrodes placed on the human forearm and register the electrode-skin interface impedance almost simultaneously, to be more precise – sequentially. This means there is no need to change the system or the placement of the electrodes on the skin at the testing time. Toggling quickly between the electrode sets gives a more reliable result than replacing the electrodes and starting the measurements from the start again. When the sets under the study have similar exterior properties and stabilization time on the skin, it reduces the number of uncertainties. It gives more solid proof of the experiments conducted.

4.2.2 Practical considerations for measurement setup

If electrodes are moved between the measurements, some extra considerations must be made: waiting for the same stabilization time, different placement concerns, skin condition changes, etc. As electrode-skin interface impedance is dependent on a considerable number of parameters, our utmost goal was to reduce the variables by guaranteeing the same circumstances during these three sets of electrodes' comparison. Therefore, all the electrodes stayed on the forearm during the registration of interface impedance. In addition to interface impedance measurements, the body tissue impedance between the two sensing electrodes can be registered during the same measuring setup. The possibility of getting information about the electrode-skin interface and body tissue without the setup change is a great advantage.

During the first measurement series, one set of four electrodes was connected to the instrument with a four-pin connection, and the measuring time was around 20 seconds. It took three seconds to register and calculate four electrodes' interface impedance, which means that during these 20 seconds, each electrode's interface impedance was registered 6-7 times. After registering, the first set was disconnected, the second set of electrodes was connected to the instrument, and measuring took place similar to the first set. The same procedure was repeated with the third set. A series of tests took place until the electrodes had been on the hand for approximately two hours.

The measurements were performed mainly with the step of 5 minutes and after 30 minutes with the step of 10 minutes. During the 2 hours, I registered the interface impedance change and the potential difference between the two sensing electrodes (body tissue impedance). Keeping the excitation voltage constant made it possible to check which electrode set and even which electrode provides the best contact with the skin. Accordingly, it was possible to make changes in case an electrode showed unreasonably high impedance due to inefficient contact, cable disconnection, or some defect of the electrode material.

An MFLI Lock-in Amplifier by Zürich Instruments was used to sense and amplify the differential signal from the electrodes. The device was configured as a four-electrode system which registers the total current through the setup and the potential difference between the two sensing electrodes - U_{HIGH} and U_{LOW} shown in Figure 16. Figure 16 depicts the configuration proposed – three rows of electrodes (3 different sets of electrodes consisting of 4 electrodes each) on the forearm, cables connected to the MFLI analyzer, and computer with LabVIEW software for registering. Current through the current electrodes is depicted as I_{HIGH} and I_{LOW}. The excitation voltage was $1\,V_{pk}$, and the instrument was configured to operate with a 100 Hz sixth-order low-pass filter; 100 Hz measurement bandwidth was enough to assess the resulting signals and measure cardiac pulse. All the measurements were performed at two frequencies, 10 kHz and 70 kHz. Measurement depth (penetration depth) strongly depends on measurement frequency, so the frequencies chosen were fairly low. The outer layer of skin, stratum corneum (SC), gives large impedance in series with the viable skin, and at frequencies, under 10 kHz, SC dominates the measurement result [178].
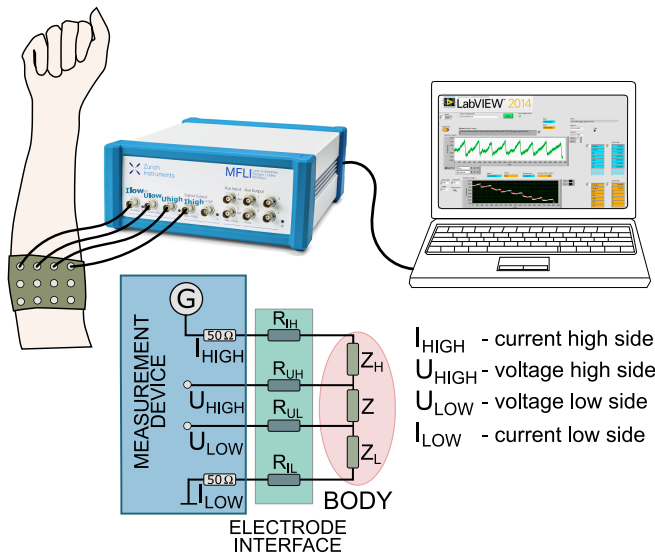

Figure 16. Measurement setup consisting of MFLI lock-in amplifier, electrode sets on the forearm (3 different sets of 4 electrodes on the hand), and a computer for LabVIEW software.

4.2.3 Electrode-skin interface calculation

The specific measurement setup and calculations described next apply to all four-electrode measurement systems where:

- voltage is being measured differentially from the two middle terminals;
- current is being measured with a voltage shunt or transimpedance amplifier (in this case, the value of the shunt must be zero in the calculations),

  and:
- it is possible to read out both voltage and current values from the measurement device.

Figure 17 shows the setup to measure the interface impedance of all four electrodes. It consists of a measurement device, electrode interface, body tissue under the test, and relays controlled by the measurement device's user-programmable GPIO (general purpose input output) pins. The goal is to calculate separate electrode interfaces by excluding body impedance values. For this, numerous sequential measurement and corresponding calculation steps must be followed, described thoroughly in the next few pages.
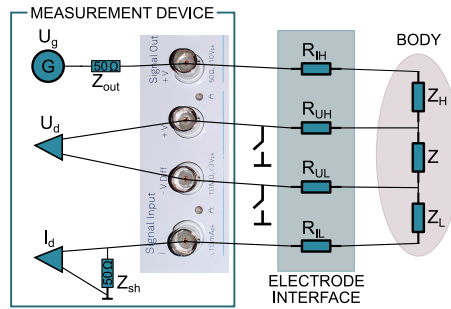
Figure 17. Measurement setup consisting of the measurement device, electrode interface, and body.

Zürich Instruments MFLI Lock-in Amplifier provides three measurement values by default, and these are:

- $\mathbf{U_g}$: Generator output voltage
- $\mathbf{U_d}$: Voltage Demodulator output
- $\mathbf{I_d}$: Current Demodulator output

In addition, known values from the data sheet of the measurement device are $\mathbf{Z_{out}}$, which is a 50 Ω series resistor at the output of the generator, and $\mathbf{Z_{sh}}$, which is a 50 Ω resistor as the current shunt.

Figure 18 depicts how to start the calculation process by finding the value of the body impedance $\mathbf{Z}$. The red line shows how the current flows during the first step – the current is measured as a voltage drop across the shunt resistor $\mathbf{Z_{sh}}$. The blue line illustrates the voltage measurement path. To calculate body impedance $\mathbf{Z}$, measured voltage, $\mathbf{U_{d1}}$, is divided by the whole current, $\mathbf{I_{d1}}$, through the setup shown in Equation (8).

$$Z = \frac{U_{d1}}{I_{d1}} \tag{8}$$

$$r_{total} = \frac{U_g}{I_{d1}} \tag{9}$$

Where $\mathbf{r_{total}}$ (Equation (9)) is the impedance of 7 components ($Z_{out}, R_{IH}, Z_H, Z, Z_L, R_{IL}$, and Z_{sh}) on the current path from $\mathbf{U_g}$ to the ground.
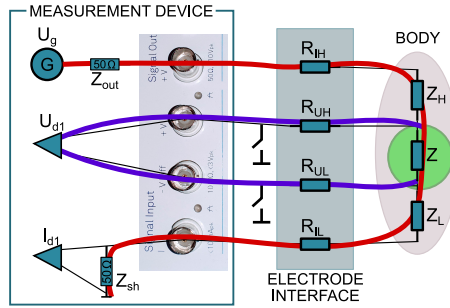
Figure 18. Calculation of the body impedance Z. The red line shows how the current flows through the body. The blue line illustrates the voltage measurement path.

The assumption is that the distance between 4 electrodes on the body is the same and the tissue under the measurement site is relatively similar, so we can write Equation (10), which says that the impedances Z_H, Z_L, and Z are the same. For this, it is important to pick a measurement place on the body that is more or less homogenous – the inner side of the forearms is a good example used in my experiments.

$$Z_H = Z_L = Z \tag{10}$$

$$RI_{total} = r_{total} - Z_H - Z - Z_L - Z_{out} - Z_{sh} \tag{11}$$

When solving Equation (11), we have the total electrode-skin impedance of the two current electrodes, **RI_{total}**. The next step involves calculating the first three electrode-skin impedances – **R_{IH}**, **R_{UH}**, and **R_{IL}** and for that, +V input is shorted to the ground.

In Figure 19, the yellow line represents the total current, and the purple shows the current through the **R_{UH}**. The red line is the current flowing through the components **Z**, **Z_L**, **R_{IL}**, and **Z_{sh}**. After the subsequent measurement, the measured voltage, **U_{d2}**, indicates the potential on **U_{LOW}**, and the measured current, **I_{d2}**, displays the current through the components **Z**, **Z_L**, **R_{IL}**, and **Z_{sh}**.
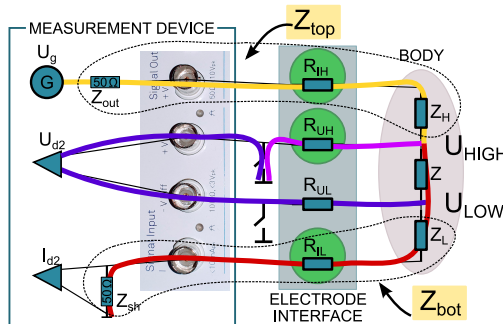

Figure 19. Calculation of the electrode-skin impedances of R_{IH}, R_{UH}, and R_{IL}.

Equation (12) shows the total impedance (Z_{bot}) of the path from U_{LOW} to the ground. And when Z_{bot} is known, it is easy to calculate the first two electrodes' interface impedances with Equations (13) and (14).

$$Z_{bot} = \frac{U_{d2}}{I_{d2}} \tag{12}$$

$$\mathbf{R_{IL}} = Z_{bot} - Z_L - Z_{sh} \tag{13}$$

$$\mathbf{R_{IH}} = RI_{total} - R_{IL} \tag{14}$$

Z_{top} is the total impedance of the path from U_g to U_{HIGH}, which leads to Equation (15). Potential U_{HIGH} is calculated using Equation (16).

$$Z_{top} = Z_{out} + R_{IH} + Z_H \tag{15}$$

$$U_{HIGH} = (Z_{bot} + Z) \cdot I_{d2} \tag{16}$$

$$U_{TOP2} = U_g - U_{HIGH} \tag{17}$$

Equation (17) calculates U_{TOP2}, which is a voltage drop across Z_{top}.

$$I_{total2} = \frac{U_{top2}}{Z_{top}} \tag{18}$$

With Equation (18), I_{total2} is calculated. Current through the electrode, R_{UH} is marked as I_{RUH}, calculated by Equation (19). Finally, Equation (20) gives us the third electrode's, R_{UH}, interface impedance.

$$I_{RUH} = I_{total2} - I_{d2} \tag{19}$$

$$\mathbf{R_{UH}} = \frac{U_{HIGH}}{I_{RUH}} \tag{20}$$

The final step is to calculate the electrode-skin impedance of the fourth electrode, R_{UL}. Now, V_{diff} input must be shorted to the ground.
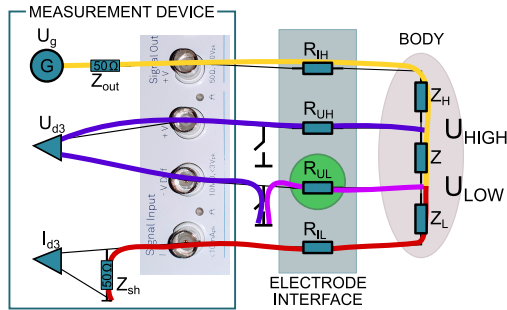

Figure 20. Calculation of the electrode-skin impedance R_{UL}.

In Figure 20, the yellow line shows the total current, the purple line depicts the current flowing through the R_{UL}, and the red line shows the current through Z_L, R_{IL}, and Z_{sh}. Here the measured voltage U_{d3} indicates the potential on U_{HIGH}, and the measured current I_{d3} demonstrates current through the components Z_L, R_{IL}, and Z_{sh}. U_{top3} is a voltage drop across Z_{top} calculated by Equation (21). Finally, Equations (22), (23), (24), and (25) are all sequentially calculated to get the last electrode's (R_{UL}) interface impedance.

$$U_{TOP3} = U_g - U_{d3} \tag{21}$$

$$I_{total3} = \frac{U_{top3}}{Z_{top}} \tag{22}$$

$$I_{RUL} = I_{total3} - I_{d3} \tag{23}$$

$$U_{LOW} = Z_{bot} \cdot I_{d3} \tag{24}$$

$$\mathbf{R_{UL}} = \frac{U_{LOW}}{I_{RUL}} \tag{25}$$

To emphasize, with the proposed method, it is possible firstly to measure each electrode's interface impedance (sequentially, in 3 steps) without moving the electrodes and secondly also to get a valuable reading of body tissue impedance under the tested electrodes. This gives a great advantage over other similar measurement systems. All the important information can be obtained within a short time and, most importantly, without tweaking the setup. It is possible to measure interface impedance and switch to body tissue response by retaining all the valuable information.

4.2.4 A pool of test specimens/electrodes to compare

Comparing electrodes placed on the skin is tricky as the skin impedance can vary between the days and even during the day. Consequently, simultaneous measurements of different electrode sets are the most accurate way to analyze interface impedance. For example, I can place three different types of electrodes on the forearm and have a proper parallel comparison. However, as the number of electrode sets that fit on the subject's forearm was limited, I had to examine and compare samples measured on separate days. Fortunately, the insight I get from the three-set assessment is valuable for making assumptions for additional sets.

Five different electrode sets were compared to see which kind of electrodes we could use to improve bioimpedance measurements on the skin:

- Ag/AgCl pre-gelled electrodes (Comepa Industries, France);
- Ag/AgCl dry electrodes (Comepa Industries, France);
- CNF/CF-PDMS smooth electrodes (custom-made);
- CNF/CF-PDMS microneedle-like fiber electrodes (custom-made);
- OMNI-WAVE™ carbon fiber sticker electrode (OMNI-WAVE™ by FLEXcon Company Inc., US).

Pregelled Ag/AgCl electrodes (see Figure 21g) are conventionally used to monitor ECG, EEG, EMG, and other measurements in the medical field daily. The dry Ag/AgCl electrode, depicted in Figure 21c, is a silver snap coated with Ag/AgCl but without adding hydrogel.

CNF/CF-PDMS smooth electrodes (see Figures 21a and 21b) and CNF/CF-PDMS fiber electrodes (Figures 21e and 21f).

Developed carbon-PDMS material was glued with conductive silver coating paste on a snap connection similar to conventional Ag/AgCl stud connectors. The difference between my fabricated "smooth" and "fiber" carbon electrodes is that, for CNF/CF-PDMS fiber electrodes, the fabricated material (introduced in Chapter 3) was rolled into a cylinder, and round electrodes were cut with a sharp scalpel from the cylinder. This revealed the fibers sticking from the base material shown in Figure 21e. In contrast, as the name suggests, CNF/CF-PDMS smooth electrode surface is smooth (see Figure 21a). It does not have fibers sticking from the surface as there is no cutting edge, but round electrodes are constructed using a die-cut press. Finally, OMNI-WAVE™ carbon fiber and salt adhesive sticker electrodes by FLEXcon were tested. From Figure 21d, the long carbon fiber strands inside the adhesive can be seen clearly.
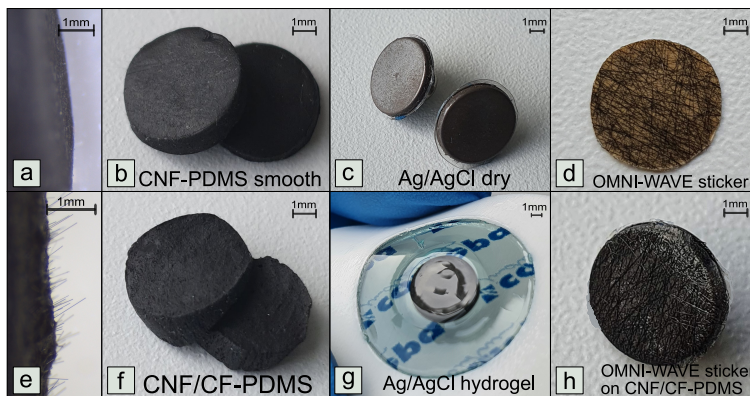
Figure 21. (a) Close-up of CNF-PDMS smooth electrode from the side. (b) CNF-PDMS smooth electrodes from the top. (c) Ag/AgCl dry electrodes without hydrogel. (d) OMNI-WAVE™ carbon fiber sticker. (e) CNF/CF-PDMS electrode from the side when CF strands are sticking out from the base material. (f) CNF/CF-PDMS electrodes from the top. (g) Ag/AgCl pre-gelled electrodes. (h) OMNI-WAVE™ CF sticker on CNF/CF-PDMS electrode.

The novel adhesive electrodes that FLEXcon produces seem promising and interesting for patient monitoring in the healthcare industry. The main advantage in front of Ag/AgCl hydrogel is their consistently low impedance, and as these electrodes are not moisture dependent, the shelf life is longer [179]. The material is not commercially available just yet but has passed ISO 10993 standard for biocompatibility and AAMI EC-12 – standard for disposable ECG electrodes [66]. As I got a few samples of the OMNI-WAVE™ material, I had an opportunity to compare state-of-the-art carbon electrodes with my fabricated electrode material.

4.3 Results

4.3.1 Considerations for assessment of electrodes

In addition to comparing impedance values, several parameters that influence the interface impedance are discussed: frequency, stabilization time, preparation of the skin, and pressure on the electrodes. The main goal was to analyze the interface impedance stability over time using numerous different electrodes. The measurements that were published in [180] by the author were conducted at room temperature (approximately 23°C) by using a

four-electrode setup to minimize the effect of electrodes' polarization during determining the base impedance (Z_0). For the measurement site, a forearm of a healthy female (body mass index 21) was cleaned with an alcohol prep pad, and informed signed consent was obtained from the volunteer on whom the impedance was measured.

4.3.2 Frequency response

Bioimpedance spectroscopy (frequency sweep) can be used to study the frequency response when a low-amplitude electrical signal is injected into the tissue under the test. In my study, the main focus was on interface impedance under the electrode but comparing how each electrode measures body impedance on a wide range of frequencies gives confidence that no major missteps are happening when using custom-made materials and setups.

The bioimpedance parameter is strongly frequency dependent – the current penetration depth and conduction paths vary with the changing frequency of the applied signal. Custom-made electrodes - CNF/CF-PDMS fiber, CNF/CF-PDMS smooth, carbon textile (Zorflex FM101L100 – 0.4 mm) were compared with Ag/AgCl hydrogel and Ag/AgCl dry electrodes, likewise with OMNI-WAVE™ sticker electrode. In addition, a frequency sweep was conducted with ChAc chitosan/gelatin and KAc chitosan/gelatin electrodes introduced in Chapter 5. All of the electrodes except the textile roll gave a similar frequency response.

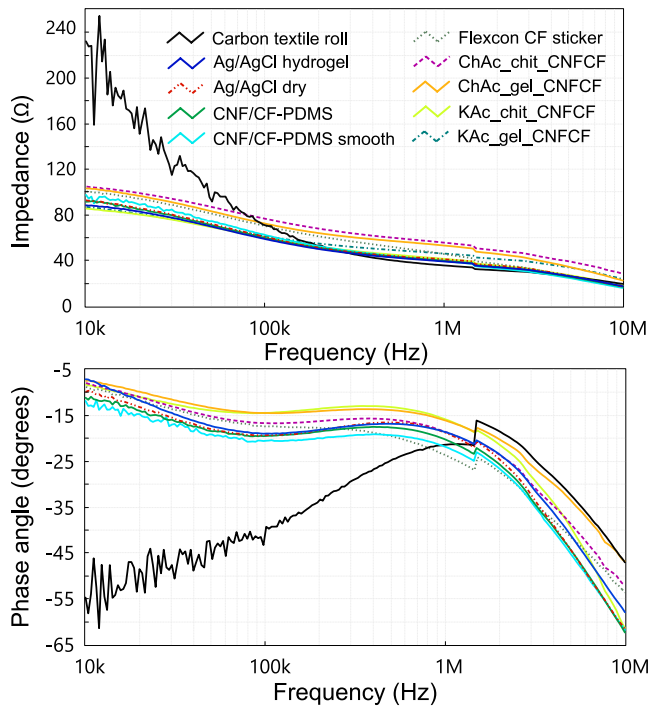The impedance spectrum of the whole electrode-body system is characterized in Figure 22.

Figure 22. Frequency-dependent measurements of 10 different electrode sets. Most of the electrodes showed similar frequency response, except textile roll, which had higher impedance and lower phase angle.

The results depict the impedance (base impedance Z_0) of body tissue (Figure 22, upper graph) under the sensing electrodes (U_{LOW} and U_{HIGH}) and phase angle (Figure 22, lower graph) to show how capacitance influences the resistance measurements. At 10 kHz, the base impedance is around 100 Ω and starts to decrease until it reaches 20-30 Ω at 10 MHz – the higher the frequency, the lower the impedance of tissue, as with higher energy, more current can flow through the intracellular liquid. Phase angle stays around -5° to -20° during the frequency spectrum from 10 kHz to 1 MHz. At 1.5 MHz, the strong observable discontinuity of the phase angle is caused by the Keysight E4990A auto-ranging function and can be ignored in our experiments.

The textile electrode set showed a different response than others (see Figure 22 - black line). Until 100 kHz, the base impedance (Z_0) is much higher (at 10 kHz, twice as much) compared with other electrodes, even though all the measurement conditions were the same. In addition, the phase angle displayed more significant capacitive behavior (starts from 60° at 10 kHz). Presumably, the capacitive behavior is explained by the fact that unreliable contact with the skin is formed because the air is present between the threads of the textile roll. Carbon is hydrophilic, i.e., it absorbs moisture into its yarns without leaving enough electrolytes (sweat) on the skin's surface. This effect is not desired from a practical point of view, but in theory, the interface impedance between two hydrophilic environments (skin and textile) is lower. Moisture absorption in the carbon textile increases the conductive ionic components in the material, and already existing ions become more mobile, making contact with the biological tissue better. This is addressed below, in Chapter 5, where carbon textile is infused with experimental electrolytes like ChAc chitosan/gelatin and KAc chitosan/gelatin.

Biological tissues typically display extremely high dielectric constants at low frequencies, under 10 kHz, which are not discussed in the current work. The higher the frequency, the less capacitive the response [39]. From the conducted frequency sweep, the distinctive moment (phase angle of Z_0 reaches saturation) of the base impedance (Z_0) is at 70 kHz. Therefore, two frequencies were applied for interface impedance measurements - 10 kHz and 70 kHz.
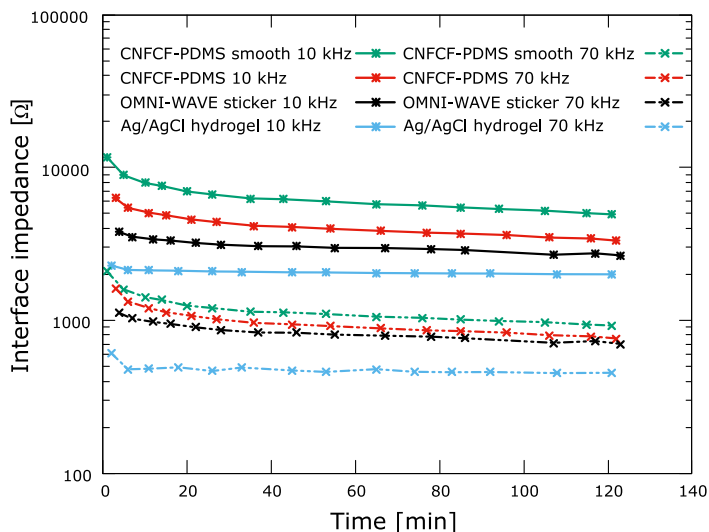

Figure 23. Electrode-skin interface impedance changes in time on two frequencies – 10 kHz and 70 kHz.

Measurements were conducted using a setup described in Chapter 4.2. Figure 23 shows how the interface impedance of 4 electrode sets decreases with time. The green and red lines represent custom-made CNF/CF-PDMS smooth, and fiber electrodes (respectively) interface impedance change. The black line shows OMNI-WAVE adhesive electrodes, and the blue line indicates the conventional Ag/AgCl pre-gelled electrode's response. All four electrode sets have approximately 75-80% lower interface impedance when the applied current is 70 kHz compared to the 10 kHz signal, as impedance measurements are frequency-dependent. All interface measurements were performed on two frequencies, but most of the graphs depicted in this work are at 10 kHz as the charts are virtually similar with the difference in absolute impedance values.

4.3.3 Time dependency and contact retention

Figure 24 shows five main electrode sets analyzed in this work: two custom-made carbon-PDMS electrodes, conventional Ag/AgCl electrodes with and without hydrogel, and a state-of-the-art adhesive OMNI-WAVE™ sticker. Electrodes were measured on separate days, and even though it may be exaggerated to compare the interface impedances on the same graph, there were at least 5 interface impedance measurements made to each electrode set, among which a notable trend could be seen. For every new measurement, a new electrode was taken – reusing the electrodes typically showed higher impedance due to residue from the skin (OMNI-WAVE™ adhesive electrode) or aging of the material itself (custom-made electrodes and Ag/AgCl hydrogel electrodes). The mean value of all the measurements is depicted with a connected line, while the small circles show the actual values registered. Error bars represent variation between different measurements.
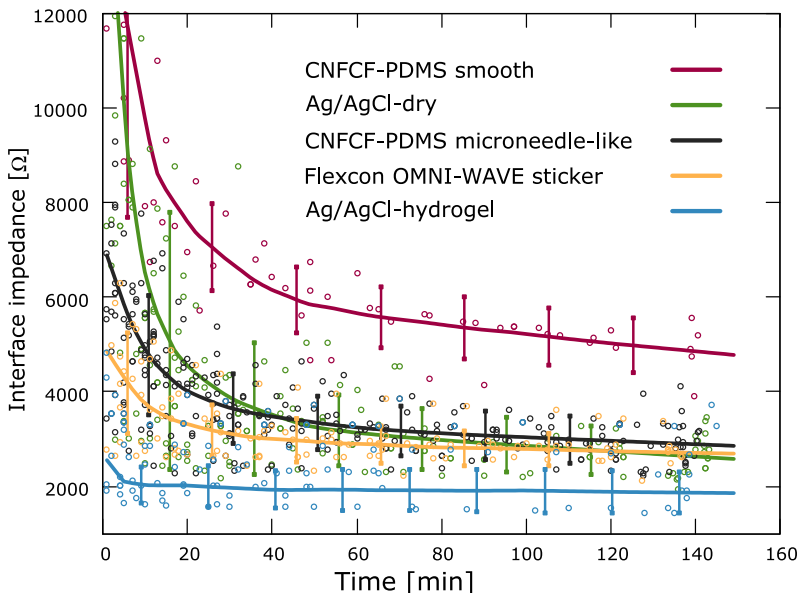

Figure 24. Five electrode sets and their mean interface impedances change with time. Dots represent the real measurements, and error bars show variation between different measurements.

Figure 24 shows CNF/CF-PDMS smooth electrodes have the highest mean interface impedance, around 6-7 kOhms at 10 kHz. CNF/CF-PDMS fiber electrodes, with the fiber strands sticking from the base material, show lower impedance, around 4 kOhms. Ag/AgCl

dry electrodes and OMNI-WAVE™ stickers show similar responses to carbon-PDMS electrodes. Still, the Ag/AgCl dry electrode error bars are bigger, suggesting that the difference between measurements varies more.

Dry and rigid Ag/AgCl metal snap electrodes are more affected by the environment, such as sweat accumulation and skin condition. The electrodes themselves are relatively unchangeable compared to custom-made carbon material, showing better stability over time. When sweat accumulates under the electrodes, it fills the gaps between the electrode and the skin layer, making more effective electrolyte area. This reduces the electrode–skin impedance and is strongly dependent on time. Within the first 30 minutes since the electrodes are placed on the hand, electrode–skin impedance reduces remarkably. After that, it starts to reach its saturation point.

This behavior is evident for four dry electrode variants (CNF/CF-PDMS smooth, CNF/CF-PDMS microneedle-like fiber, Ag/AgCl dry, and OMNI-WAVE™ sticker). Ag/AgCl hydrogel electrodes had a slightly different response which is understandable as we are dealing with a "wet" electrode. The amount of electrolyte is vast compared to dry electrode sweat accumulation. Firstly, the hydrogel electrode had low interface impedance, around 2 kOhms at 10 kHz, and secondly, the signal was reasonably stable over 150 minutes depicted. In addition, the stabilization time was around 5 minutes. It is important to note that when a motion artifact occurs, the stabilization process of the interface starts all over again.

During the experiments, the forearm was kept as stable as possible. The differences between dry and wet electrodes were expected, but the CNF/CF-PDMS fiber electrode's stability over time and comparability with OMNI-WAVE™ adhesive sticker electrode was positively surprising.

4.3.4 Skin preparation effect on interface impedance

30 minutes before all of the measurements conducted in this research, the subject's skin was prepared by cleaning it with an alcohol prep pad to remove any dirt, moisture, or grease piled up. Cleaning the skin does not influence the interface impedance noticeably, but abrasion of the skin before the measurement affects it remarkably. Stratum corneum thickness varies from 10 µm on the legs to 600 µm on the palm, but the mean thickness on the human forearm is around 20 µm [181]. This means it is quite easy to deliberately damage the skin surface to remove a large portion of the epidermal impedance. Abrading the skin with sandpaper-like textiles or stripping the stratum corneum layers with adhesive tape is a common practice before applying conventional Ag/AgCl hydrogel electrodes in healthcare facilities.

The current study used light abrading with rough textiles on somewhat sensitive forearm skin. The results were similar: interface impedance decreased after abrading the skin (see Figure 25). More effect was seen when dry electrodes were used (approximately 25-30% decrease). The hydrogel electrode interface improved by under 10%. Although the light removal of the stratum corneum gave significant results, the decision to use this kind of intrusive technique must come through careful consideration. The outer layer of the skin protects the body from adhesives and electrolyte gels that can be irritating due to additives and high salt concentrations. Abrading or stripping can be beneficial for short-term measurements, but continuous long-term (over 20 minutes) measurements are not desirable for the patient's comfort.
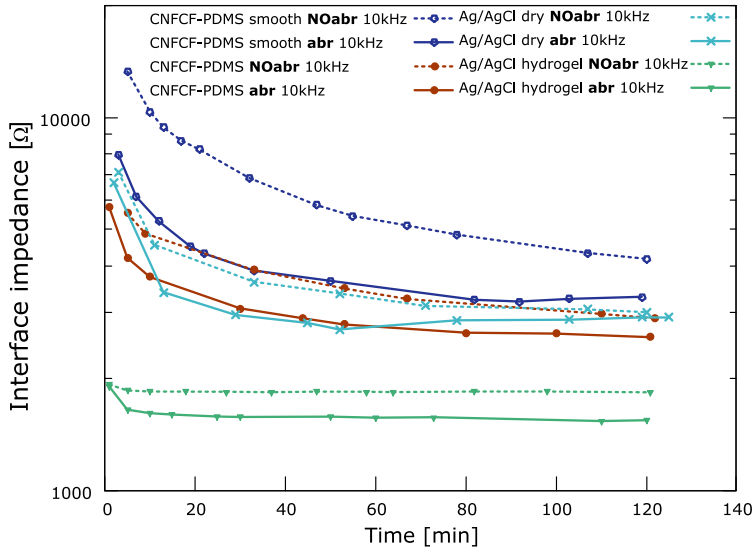
Figure 25. Abrasion effect on interface impedance of four different electrodes – CNF/CF-PDMS smooth and fiber, Ag/AgCl dry, and pre-gelled.

4.3.5 Effect of pressure on interface impedance

Skin-electrode interface impedance can be affected by applying pressure on the measurement electrodes. Studies have concluded that the pressure on the electrodes improves the effective contact area and can reduce the interface impedance [174], [177].

Five different sets of electrodes were tested by applying the "no pressure" and extra pressure. When no additional pressure was used, the force measured on the electrodes was approximately 2 kPa, which was considered "no pressure". With extra pressure, 10.6 kPa was applied to the tested electrodes.

The pressure effect was most prominent on dry electrodes, especially with soft PDMS electrodes – CNF/CF-PDMS smooth and CNF/CF-PDMS fiber (see Figure 26 purple and pink line). Almost 45% lower interface impedance was achieved with smooth electrodes and 60% lower impedance with fiber electrodes. OMNI-WAVE™ adhesive sticker, rigid Ag/AgCl dry, and Ag/AgCl hydrogel electrodes showed negligible change with 10 kPa pressure applied. The findings correlate with other research [177], [182] rigid metal electrodes and wet hydrogel electrodes have less effect because of pressure change. This is understandable as the effective contact area usually does not change with wet and rigid metal electrodes. However, soft and elastic dry electrodes possibly have more air pockets due to pores and surface roughness (carbon fiber strands, for example) between the skin and the sensing area. Now, when more pressure is applied, air pockets are filled with skin surface irregularities; the electrode's size can also increase. All this leads to more space for electrons and ions to move around and carry charge from one site to another, decreasing interface impedance.

It is difficult to accept that no standard values define a particular interface impedance as being too high, and we should change the electrodes, abrade the skin or apply pressure. Most studies are made for specific needs with varying and incomparable results, so working out the common values has proven challenging, if not impossible.
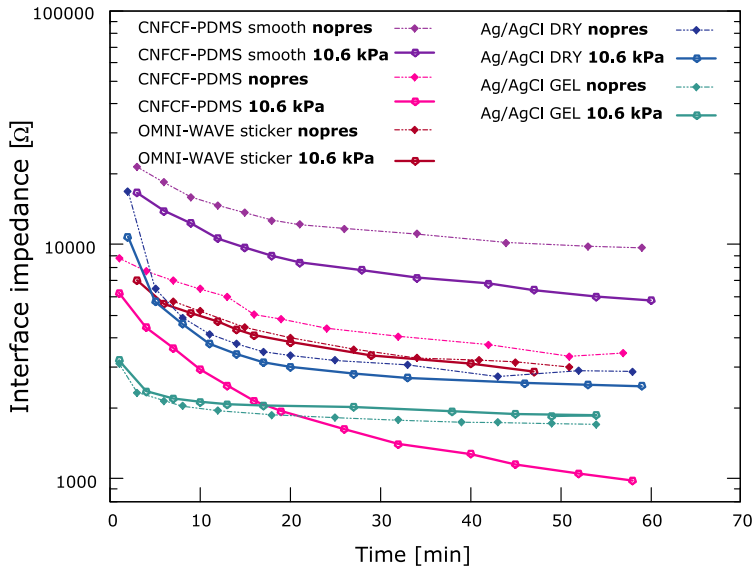
Figure 26. Pressure effect on 5 different electrode sets – custom-made carbon-PDMS electrodes, Ag/AgCl dry and hydrogel electrodes, and OMNI-WAVE™ sticker electrode.

4.3.6 Verification of dry-contact electrodes by biopotential measurements on the wrist

One specific goal of this research was to find some correlation between the electrode's interface impedance and body tissue impedance under the test. The novelty and specificity here are that I can measure these two values sequentially without changing anything after placing the electrodes on the skin with the proposed measurement setup.

Measurements on the radial artery were conducted with previously tested four electrode sets (CNF/CF-PDMS smooth, OMNI-WAVE™ carbon sticker, CNF/CF-PDMS fiber, Ag/AgCl hydrogel) to visualize the cardiac cycle in impedance form. The same four-electrode system used for interface impedance measurements on the forearm (introduced in Chapter 4.2) had to be placed now on the radial artery on the wrist. The more precisely the electrodes are arranged on the desirable artery, the easier it is to get an excellent cardiac pulse. The impedance signal is reciprocal to pressure change inside the arteries. When pressure arises, impedance decreases. This is because when more blood is under the sensing electrodes, the tissue under the sensing electrodes is more conductive - impedance decreases. And the other way around—lowering the pressure results in less blood under the electrodes, and impedance increases. The waveform of impedance pulse and pressure pulse are, in fact, not that different, but it is difficult to register impedance change mainly due to moving artifacts. Figure 27 shows four cardiac cycles measured on the radial artery with different electrodes. There is a 0.1% change in impedance with blood pressure variations. Figure 27A shows the cardiac cycle measured with CNF/CF-PDMS smooth electrodes. The signal is noticeably noisy, and the signal-to-noise ratio (SNR) is 7, indicating that the ratio between the valid measured signal and noise is low. Also, the average interface impedance of four electrodes on the wrist is 6.5 kOhms at 10 kHz, which is considerably higher than Ag/AgCl hydrogel interface impedance (1 kOhm) shown in Figure 27D. The cardiac signal of Ag/AgCl hydrogel (yellow line) is very clear, and the signal SNR is as high as 96, suggesting there is almost no noise picked up. Visualization of cardiac waveform with different electrodes clearly

shows a distinctive link between the electrode-skin interface impedance and noisy signal. Electrodes must have excellent contact with the skin to avoid problems arising from low SNR values.
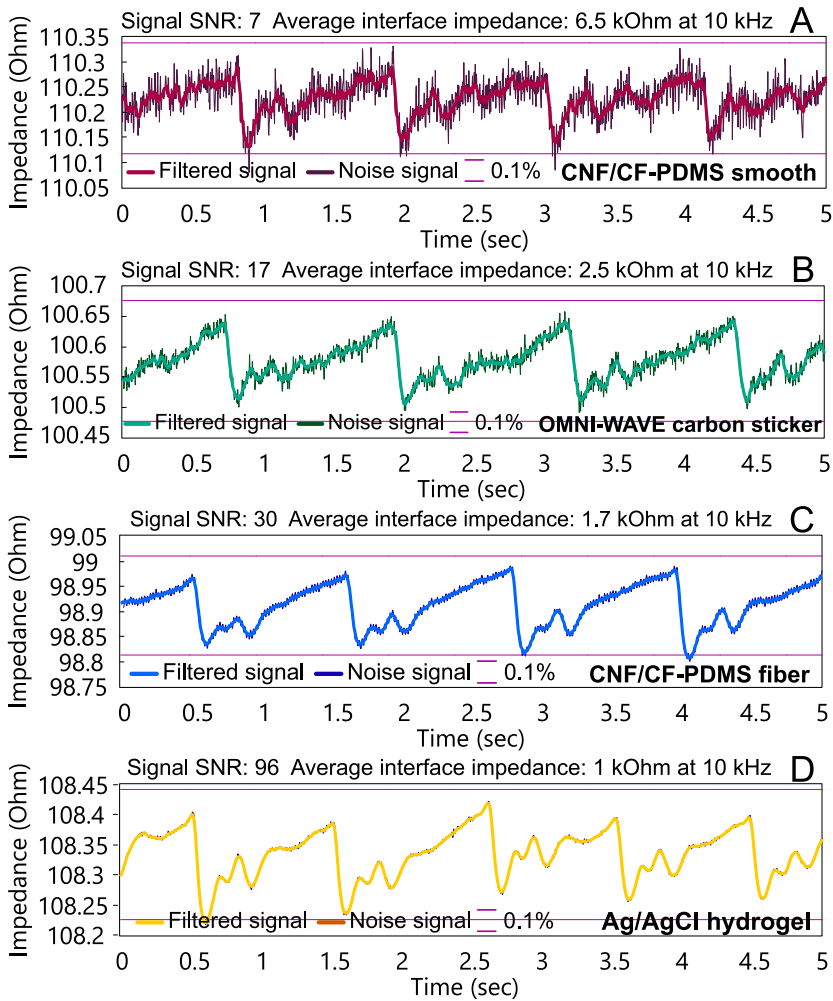

Figure 27. CNF/CF-PDMS fiber and smooth, OMNI-WAVE™ sticker, Ag/AgCl hydrogel shows cardiac pulse wave when placed on the wrist. Some conclusions from noise calculations can be made – the lower the interface impedance; the cleaner the body tissue signal.

4.4 Conclusion

The accurate measurement of underlying tissue impedance is often rendered difficult by the presence of enormous electrode-skin interface impedance. This chapter introduced testing multiple electrodes' interface impedance with a highly effective measurement system. The system's novelty lies in the fact that it is possible to assess the interface impedance of four separate electrodes of three different sets in a short period without repositioning the electrodes. Furthermore, as an extra feature, it is possible to

measure body tissue impedance between two sensing electrodes with the same setup and have a correct correlation between the interface impedance and its influence on the bioimpedance signal measured from the body. This is very important because artifacts introduced by the electrodes could lead to incorrect diagnostic assessments, but with the proposed setup, the deviations are noticeable from the beginning.

This study found that the choice of electrodes for bioelectrical measurements will heavily influence the measured signals, and it is important to find the best-suited electrode for the intended use. Stretchable and soft carbon material electrodes with fibers on the surface have been studied, compared, and reported. The interface properties of the skin-electrode impedance have also been researched experimentally. Produced and tested carbon-silicone material was applied as electrodes to measure bioimpedance change on the human forearm and electrode-skin interface impedance. As a reference, Ag/AgCl electrodes' impedance with gel and without gel was measured simultaneously.

The electrode–skin impedance of all the tested materials depends on the pressure on the electrodes, contact duration, preparation of the skin beforehand (abrasion), and frequency. For example, the measurements showed that Ag/AgCl pre-gelled electrodes have the lowest interface impedance. This is because the hydrogel on top of the electrode plate fills spaces between the tissue and the base, making contact more stable in time. On the other hand, dry electrodes, such as CNF/CF-PDMS, do not have the extra layer of electrolyte or hydrogel added to the base material, and contact problems can occur. Moreover, this results in higher electrode–skin interface impedance. Fortunately, the tissue tends to produce sweat, creating a natural electrolyte between the electrode and the skin, which reduces interface impedance and improves the signal quality to some extent.

In addition, CNF/CF-PDMS fiber electrodes' interface impedance was very similar to OMNI-WAVE™ dry adhesion sticker electrodes and had a lower average contact impedance than smooth carbon electrodes. Long carbon fibers poking out from the base material improve the contact between the skin and electrode, lowering the interface impedance. Also, registering the heart pulse from the radial artery showed less noise than with smooth carbon electrodes (Chapter 4.3.6). Reusing smooth, fiber, and Ag/AgCl electrodes proved more or less ineffective as electrodes were not so well in contact with the skin due to the residue.

The most effective dry electrodes were:

- OMNI-WAVE™ adhesion sticker;
- Carbon nanofiber + carbon fiber electrodes (CNF/CF-PDMS microneedle-like fiber electrodes).

and optimal guidelines to follow are:

- 30 min stabilization time;
- abrading the skin lightly;
- the constant pressure of approximately 10 kPa.

5 Ionogel electrodes

The materials and designs used for electrodes must support the natural motions and processes of the underlying tissues. Non-invasive, comfortable, and non-constraining measuring of human vitals, in addition to accuracy and stability, is a goal worth pursuing. The last chapter introduced carbon-PDMS dry electrodes with carbon fibers as a possible alternative for conventional Ag/AgCl hydrogel and dry electrodes. However, new electrolytic gels were analyzed and tested as dry electrodes are unpredictable and give high interface impedance results due to the contact with the skin being unstable and susceptible to environmental noise. Consequently, semi-dry ionogel electrodes were produced, and interface impedance was measured on the test phantom, pork skin, and human forearm. Hygroscopic salt potassium acetate and ionic liquid choline acetate were used together with polymers (gelatin and chitosan). Specific test phantom material was produced with PVA (polyvinyl alcohol) tube for possible future testing purposes.

5.1 Preparation of ionogel electrodes

We prepared four combinations of different electrolytes to be tested as ionogels between the electrode and the skin. Two of these were based on choline acetate (ChAc) (purchased from Iolitec, Germany), and two were based on hygroscopic salt potassium acetate (KAc) (purchased from Sigma-Aldrich, Germany):

a) Choline acetate + gelatin (ChAc_gelatin);

b) Choline acetate + chitosan (ChAc_chitosan);

c) Potassium acetate + gelatin (KAc_gelatin);

d) Potassium acetate + chitosan (KAc_chitosan).

Firstly, water was added to ChAc or KAc. Then the mixtures were combined with polymers - gelatin or chitosan to form an ionogel. Chitosan is chitin derivative (shellfish, squid, and oyster content is about 2% to 12%), which can be defined as a semicrystalline heteropolymer in a solid state [183]. Gelatin is a protein made from the skins and bones of porcine, bovine, or fish [184]. Both materials are primarily used as gelling agents and thickeners in the food and medical industries. The purpose of gelatin and chitosan was to make the ionic liquid more solid gel-like for easier dosing on the electrode. Also, for reusability purposes, the mixture had to be thicker and stickier for more extended durability and to achieve better contact with the skin.

Next, the preparation of choline acetate and potassium acetate electrolytes and electrodes is described. To form ionogels, two basic recipes were used – A and B. In the case of recipe option A, the polymer substrate was gelatin, and in recipe option B, chitosan.

Recipe A1: Electrolyte choline acetate + gelatin (ChAc_gelatin) or potassium acetate + gelatin (KAc_gelatin).

1. Choline/potassium acetate and gelatin were weighed (ratio 1:1, 2:1, 3:1, 4:1) and mixed.

2. Water was added to the mixture where the gelatin swelled.

3. The whole mixture was placed on a heating (60°C) magnetic stirrer and stirred overnight.

Recipe B1: Electrolyte choline acetate + chitosan (ChAc_chitosan) or potassium acetate + chitosan (KAc_chitosan).

1. Choline/potassium acetate and chitosan were weighed (ratio 1:1, 2:1, 3:1, 4:1) and mixed.
2. 10% acetic acid (HAc) was added to the mixture.
3. The whole mixture was heated at 60°C on a magnetic stirrer overnight.

   Options A and B instructions were followed the same way when choline acetate or potassium acetate was used. The other two options were the different base materials on which the electrolytes were applied. The carbon textile electrode base was used for measurements on pork skin and PVA-gelatin measurement phantom. In addition, CNF/CF-PDMS electrode was tested on the human forearm.

Recipe A2: Using carbon textile (Zorflex FM101L100 – 0.4 mm) as the base material for the electrolyte.

1. The textile was cut into a 1x2 cm piece using scissors.
2. A conductive silver coating paste was applied on the shorter side of the textile with a 2 mm wide stripe.
3. 0.5 mm thickness of metal wire was placed on the silver paste. Paste dried, and wire stuck to the base making an effective contact between the wire and the carbon textile.
4. The connection was secured by applying silicone to the silver paste and wire.
5. The textile was folded twice and glued to the silicone base for a more comfortable measuring setup.
6. ChAc_gelatin/chitosan or KAc_gelatin/chitosan was dropped on the carbon textile using a pipette while ensuring that the whole textile area was covered with the electrolyte.

Recipe B2: Using carbon nanofiber/fiber-PDMS as the base material for the electrolyte.

1. Fabrication of CNF/CF-PDMS electrode material was introduced in Chapter 3.
2. ChAc_gelatin or KAc_gelatin was pipetted on the CNF/CF-PDMS electrode and ensured that the whole electrode was covered.

   Chitosan ionogel (with choline acetate or potassium acetate) turned out to be less dense than gelatin ionogel (with both choline acetate and potassium acetate). Therefore, applying the chitosan gels was easy on the base material, but it was too runny, so the carbon textile absorbed most of the gel. On the contrary, gelatin-based ionogel needed heating to make it pourable and to apply to the electrode base material. Hence, since it gelled on the base material, leaving the surface soft and smooth, it could be categorized as a semi-dry electrode. Also defined here as an electrode with an electrically conductive liquid component in a continuous solid state inside the soft matrix (solid-state ionogel).

   For experiments, the IL choline acetate ionogels (ChAc_gelatin and ChAc_chitosan) and potassium acetate ionogels (KAc_gelatin and KAc_chitosan) were combined with carbon textile (Zorflex FM101L100 – 0.4 mm). First, the carbon textile electrode surface was covered with gel using a pipette (Figure 28A, choosing base material section). Composed

electrodes were then dried for 24 hours in the open air before measurements were conducted. The next day, electrodes were placed on the pork skin or PVA-gelatin phantom for an hour to register electrode interface impedance.

Figure 28 illustrates the general procedure from ionogel preparation to choosing a test object.
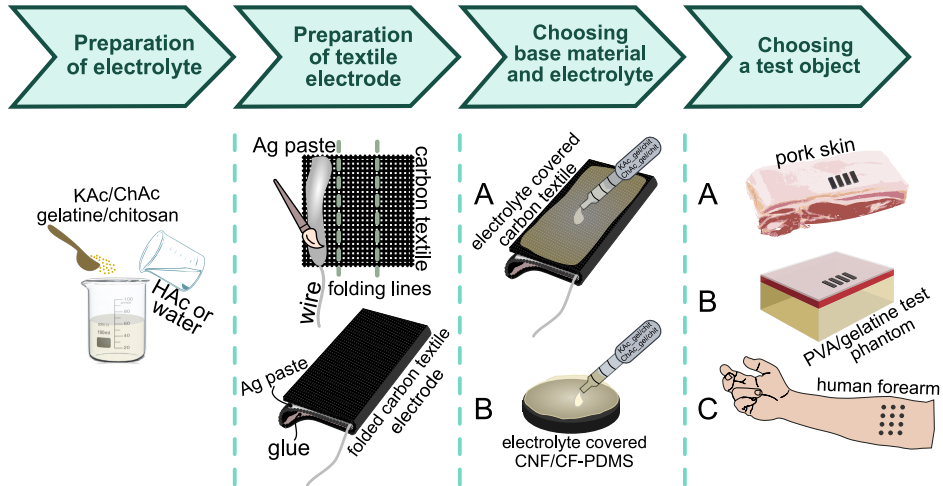

Figure 28. Preparation of electrolytic ionogels and combining them with different base materials. The first section shows the materials that are mixed to form gels. The next part introduces constructing the carbon textile electrode. The third part illustrates the addition of ionogels on the formed textile base (A) and custom-made CNF/CF-PDMS fiber material (B). Finally, the last section depicts three test subjects: A - pork skin, B - a PVA-gelatin test phantom, and C - a human forearm.

5.2 Test phantom

As the establishment of general design rules for choline acetate's biocompatibility is still in the focus of ongoing work, this chapter aims to design and fabricate an electrically conductive simple test phantom with polyvinyl alcohol (PVA) artery to evaluate the feasibility of ionic liquid electrodes.

The human body is composed of bones, fat, and aqueous tissues. Understandably, body fat and bones have poor electrical conductivity, whereas the aqueous tissues, rich in electrolytes, are more electrically conductive. Phantoms are objects that mimic living tissues and are often used in medical diagnostics fields like optical spectroscopy, ultrasound, radiology, and magnetic resonance imaging, to name a few. Noticeable reports of phantoms that are developed mainly for impedance tomography (EIT) are typically representing skin [185], [186], head [187], or thorax [188], [189].

Unfortunately, mimicking actual tissue's electrical response is problematic over a wide frequency range. Namely, biological tissue is very heterogeneous because of its intricate micro- and macrostructure: it consists of extracellular fluid and cells containing the intracellular medium separated by the cell membrane, leading to a complex electrical circuit with lipid bilayers inducing distributed capacitance [190]. At low frequencies, the current flows through the extracellular fluid, and charges accumulate on the membrane (polarizable interface). As frequency increases, the cell membrane capacitor charges and discharges the current at the frequency rate. Thus the charge displacement in the cell

membrane becomes significant and passes through the cells themselves. This behavior reflects in the varying relative permittivity and bioimpedance [166].

To conclude, there is probably little use in mimicking a complex biological environment in a phantom, as the primary challenge is to achieve a similar magnitude of electrical response. In addition to frequency dependence, each individual, each physiological condition, and contrasting degrees of anisotropy in muscle, fat, or other tissue types can exhibit a different value [191]. However, as long as the test phantom is designed for a specific use case, it is valuable for calibrating, testing, and controlling new devices or electrodes primarily because the tissue-similar material is easy to fabricate and has stable, long-lasting, and reproducible well-controlled parameters (electrical conductivity, σ or relative permittivity, ε_r).

5.2.1 PVA-gelatin tissue phantom with pulsatile artery

The base material for a tissue-mimicking phantom is often polyvinyl alcohol, gelatin, agar, polysaccharide gels, alginate, and superabsorbent polymers [192]. In the current research, gelatin was picked to mimic the matrix material as it is cheap, hydrophilic, biodegradable, and easy to handle, allowing simple modeling of the phantom's shape [193]. Also, gelatin is a polymer made of collagen obtained from cattle bones, pig skin, or fish scales, making the material very natural [184]. As the linear relation of electrical conductivity between NaCl concentration and water is well known and studied, the gelatin-based phantom material's electrical conductivity was manipulated using this salt. In addition, it was tested how conductivity changes with the manipulation of gelatin concentration – a lower concentration of gelatin results in higher conductivity [194]. The recipe for used gelatin base material is covered in the author's III article [195]. In addition to the gelatin base, a polyvinyl alcohol layer was included to imitate the skin surface and pulsatile artery.

Polyvinyl alcohol (PVA) is a water-soluble synthetic polymer prepared by partial or complete hydrolysis of polyvinyl acetate. Because of its solubility pattern and easy degradability, PVA is also known as a 'green polymer' and is often used in various pharmaceutical and biomedical applications in the form of hydrogels, including phantom materials [187], [196]–[198]. For example, the US-based company, SynDaver, which manufactures the world's most sophisticated synthetic human and animal tissue analogs, body parts, and task trainers, uses water, salt, PVA, and proprietary blends of fibers as their primary tissue-mimicking material [199].

A physical or chemical cross-linking procedure is needed to form PVA-based hydrogels. The gelation of PVA solution (60% to 90% of water) by physical cross-linking consists of numerous successive freezing and thawing cycles – the more cycles, the more stable and stronger the gel becomes [200]. For chemical cross-linking, various reagents (such as carboxylic acids [201]) can be used to join molecules by a covalent bond and form PVA hydrogels. For biomedical applications, physical cross-linking is more beneficial as it does not leave any residual toxic cross-linking agents in the mixture [202]. However, it can take several days to prepare a properly cross-linked cryogel as freezing and thawing happen very slowly.

Therefore, quick and straightforward chemical cross-linking was used in our application, where PVA gel does not have to be as pure of chemicals as implantable vascular grafts. The method is adapted from [203], [204] and illustrated in Figure 29.

First, PVA powder (Mowiol™ 10-98, Sigma-Aldrich, Germany) was added to the heated (90℃) distilled water and stirred until complete dissolution. When the solution cooled down to room temperature, cross-linker 15 wt% sodium trimetaphosphate (STMP) and alkaline content of 30 wt% sodium hydroxide were added to the mixture. For the PVA
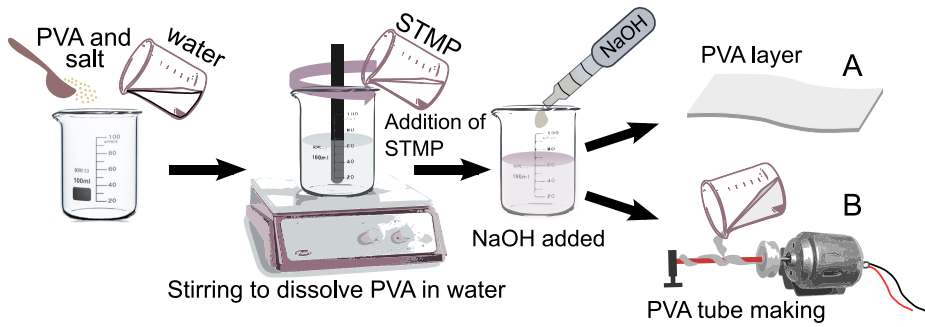
Figure 29. Preparation of PVA skin layer and PVA tube for stretchable artery mimicking. NaCl was used for electrical conductivity manipulation, sodium trimetaphosphate (STMP) was added as a cross-linker, and sodium hydroxide was for. For the PVA tube, a small motor turned a paper straw, and the PVA composite was spread on the straw until the mixture dried.

layer (Figure 29A), the mixture was poured into a low glass container for uniform thin layer production. Then, the PVA tube was made by pouring the solution onto a rotating straw and spreading the mixture back and forth with a spatula until it dried and did not drip anymore (Figure 29B).

The tube was rotated for 24 hours for equal spreading across the tube. The cross-linked PVA hydrogel layer and tube were retained in distilled water inside a closed box as the moisture level decreased rapidly in the open air. Fortunately, even if the material dries out, it restores its properties after placing it into the water. The flexibility and biocompatibility of cross-linked PVA gel make it an excellent material that can be used for various broader artery-mimicking applications in future research.

Figure 30 shows the fabricated PVA-gelatin phantom assembled with a PVA artery-mimicking tube, PVA "skin" layer on top, and two different gelatin layers with varying electrical conductivities. In addition, KAc_gelatin carbon textile electrodes were placed on the outer layer, and pressure was applied with uniform weights (10 kPa).
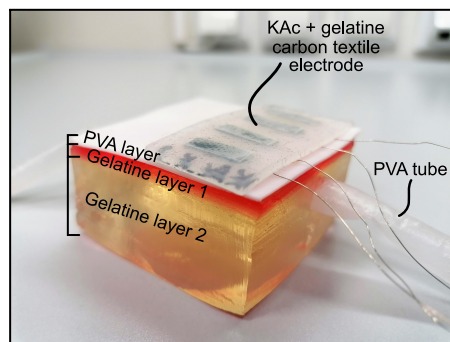
Figure 30. Prepared PVA/gelatine test phantom for ionic liquid electrode testing. In addition, the PVA tube is depicted inside the phantom material to mimic the blood artery.

5.2.2 Validation of PVA-gelatin phantom

Pressure change inside the 'artery' and impedance variations from the top layer of the phantom (PVA layer) was registered simultaneously to validate the PVA hydrogel tube as a mock artery. The mock artery inside the PVA-gelatin phantom was connected to a roller pump (Stöckert SIII Heart Lung System). An electrolyte solution was pumped through it to simulate the pulsating artery. Figure 31 shows a test phantom, where four stainless steel electrodes are placed on the surface to detect impedance variations. A plate was used to apply pressure and hold the electrodes while measuring.
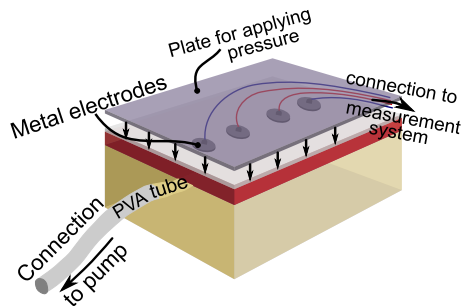
Figure 31. Setup showing four electrodes placed on the test phantom with mock artery to detect impedance variations when electrolyte solution was pumped through the mock artery inside the test phantom.

The first two measurements (Figure 32A and 32B) were made without a PVA tube and depict simultaneous pressure and impedance change measured from the top of the PVA-gelatin phantom surface with a tetra-polar impedance measurement system.

Figure 32A shows that when a silicone tube is used as an artery, the pressure is in phase with impedance change. Contrary to the silicone 'artery', the gelatin around the silicone tube has good electrical conductivity. When pressure increases, impedance increases, suggesting that when the geometry of the non-conductive silicone artery expands under the sensing electrodes, the impedance also increases – there is more material with high impedance than before.

The second experiment was conducted with a tube-shaped cavity inside the phantom. Again, saltwater was pumped through it, and the results (Figure 32B) show that the pressure and impedance change are in opposite phases. Unfortunately, the fragile cavity inside the gelatin split after approximately one minute of pressure applied. Nevertheless, these comparisons showed clearly that a more efficient and tissue-like tube was needed.

Figure 33A shows the fabricated PVA-gelatin phantom's impedance change to pulsating pressure applied to the PVA tube inside the phantom. When the pressure increased, the impedance decreased, implying the similar phenomenon as it is with real arterial pressure and impedance relation. Increasing the pressure decreases impedance because the artery under the sensing electrodes expands, and electrically conductive saltwater is detected through measurements. Figure 33B shows the real bioimpedance measurement situation, where impedance change is registered from the human wrist, and brachial pressure is simultaneously measured using an invasive method. Results depict that the impedance also decreased with growing pressure. The resemblance between these two graphs validated the use of a PVA tube as a simple, flexible, and effective artery to be used with bioimpedance measurements to detect pressure changes.
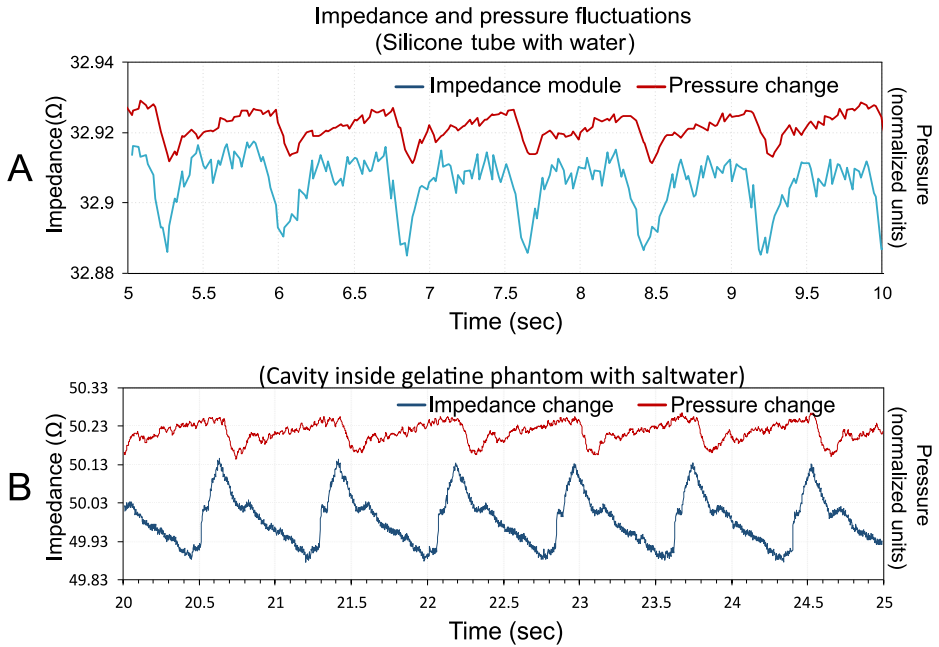
Figure 32. First experiments with silicone tube (A) and cavity (B) inside the PVA-gelatin phantom. The pressure (red) and Impedance (blue) change were registered simultaneously.
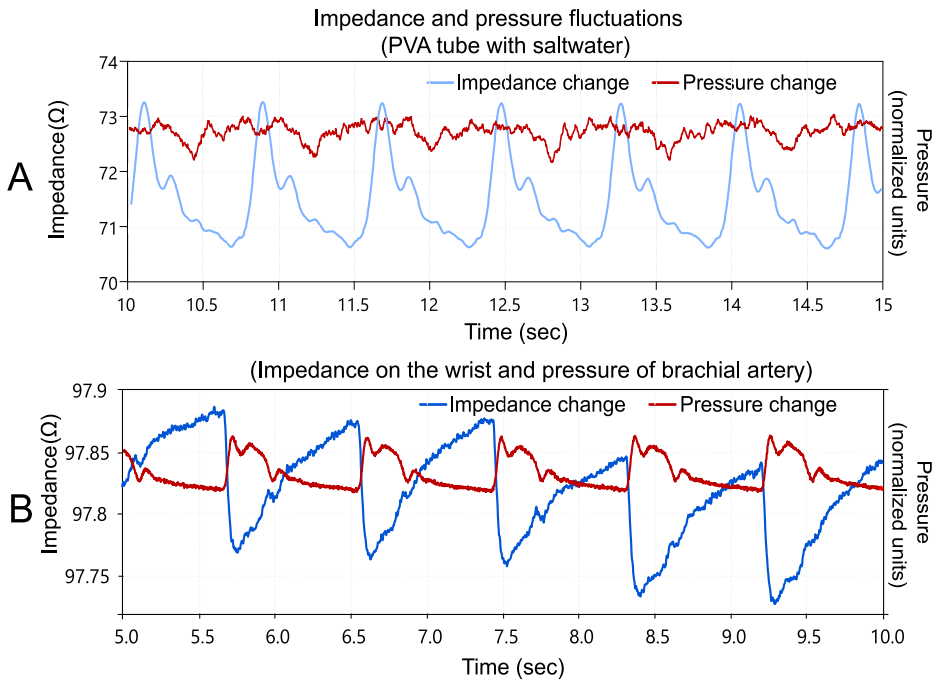

Figure 33. Impedance and pressure fluctuations with custom-made PVA tube and saltwater (A) and real bioimpedance measurements on human wrist and pressure inside the brachial artery (B).

5.2.3 Pork skin as test phantom

Measuring interfacial impedance on a PVA-gelatin test-phantom with the same electrodes differs from using natural pork skin for measurements. As pork skin is biological tissue without any preservatives, it starts to degrade within a few hours depending on room temperature. Between the experiments, it was necessary to keep the pork skin refrigerated (+4…6°C) to slow the gradual degradation. Still, for comparable measurements, it was warmed up again to room temperature. Based on my experience, the maximum time the sample can be used is 24 hours. Even if it was kept in the fridge overnight, the first signs of natural degradation could be observed already on the next day. In addition to the degradation of the sample, it was also difficult to get similar pieces of pork skin.

The samples were obtained from the local meat market on separate days, and unfortunately, they varied: different thicknesses of fat, muscle, and skin layer. Additionally, the texture of the skin was also irregular. That is why the PVA-gelatin phantom was used as an alternative.

PVA-gelatin material was stable for at least one month, with preservatives added to prevent bacterial growth in gelatin. The PVA "skin" layer was stored in a closed container with water between measurements to retain moisture. As a result, it could be used repeatedly (limited time at once to prevent water evaporation from the material) without any problems or changes in its structure and impedance values. But the "skin" PVA layer on the top of the phantom was slightly wet (wet skin profile), and when electrodes were placed on the surface, the interface impedance absolute values were significantly lower than with pork skin.

5.3 Results

5.3.1 Testing the ionogel electrodes

Chapter 5.1 proposed choline acetate and potassium acetate electrolytic ionogels as a layer between the carbon electrode and skin. Figure 34 shows two-combinations as follows:

- Figure 34 left: A shows an ionic liquid ionogel electrode with carbon textile base material, and B depicts a dry-contact microneedle-like carbon-PDMS electrode on the skin.

- Figure 34 right: C shows microneedle-like carbon –PDMS electrode with ionic liquid ionogel, and D shows the conventional Ag/AgCl hydrogel electrode on the skin.
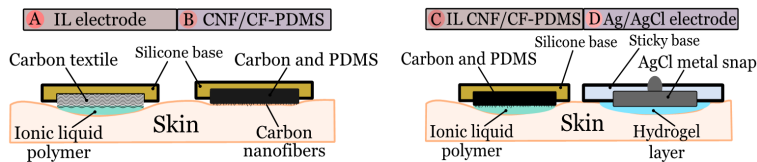

Figure 34. A – Ionic liquid electrode where carbon textile is the base material and IL polymer is the gel between the skin and the electrode. B – our developed soft and stretchable carbon electrode with fibers slightly sticking into the skin. C – CNF/CF-PDMS electrode as the base material and IL as the extra layer for better contact. D – commercially available Ag/AgCl gel electrode.

Electrode-skin interface change was registered, and results can be seen in Figure 35. Ionogel electrode with gelatin as the gelation agent shows lower interface impedance on pork skin than chitosan ionogel electrode (Figure 35 – darker blue and pink lines show the impedance of ChAc_gelatin and KAc_gelatin, respectively, and light blue and dark purple

show ChAc_chitosan and KAc_chitosan electrodes). The gelatin-based gel attached to the pork skin's surface more effectively due to its stickier nature. Also, the contact with the skin was probably better due to more electrolytic gel present. On the other hand, carbon textile quickly absorbed the chitosan ionogel after application, leaving the surface dry and resulting in higher interface impedance.
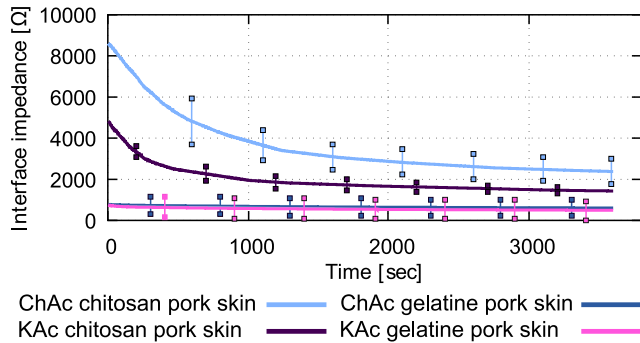

Figure 35. The graph shows the interface impedance change over one hour. Four different electrolytes are compared on the pork skin. Chitosan electrodes show higher interface impedance than gelatin ones.

ChAc_gelatin and KAc_gelatin electrode interface impedances differed minimally, but with chitosan electrodes, the potassium acetate ionogel (KAc_chitosan, dark purple line in Figure 35) had, on average, 35% lower interface impedance than choline acetate ionogel electrodes (ChAc_chitosan, light blue line in Figure 35). Probably the reason is that the potassium acetate is electrically more conductive than the choline acetate.

Figure 36 shows KAc and ChAc electrode interface impedance measured on the PVA-gelatin test sample. Unfortunately, the top layer of the phantom was too wet, and consequently, the interface impedance was very low (100-200 Ohms). In addition, the values were almost the same with different electrode types suggesting that it is impossible to make any far-reaching conclusions when analyzing the interface impedance of proposed new semi-dry ionogel electrodes on PVA-gelatin phantom material. The developed phantom proved to be more stable in time and more convenient to use than pork skin but still different from the real dry skin, and future research is needed to improve the top layer.
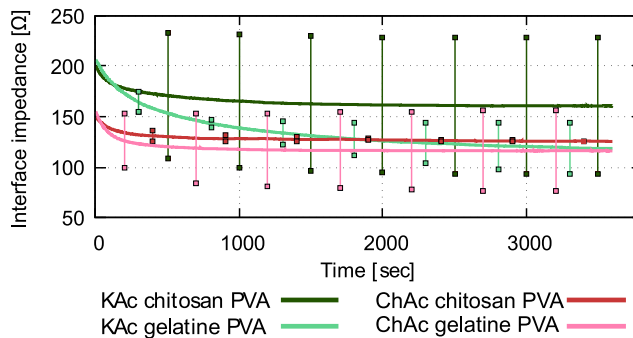

Figure 36. Four different electrolytes are compared on PVA-gelatin test phantom. The interface impedance values did not differ much with different electrode types.

Further experiments were conducted on the human forearm to get an insight,

compare the composed choline and potassium acetate gelatin ionogels with commercial Ag/AgCl hydrogel, and estimate the feasibility in real-life applications. CNF/CF-PDMS fiber electrode was covered with ChAc_gelatin or KAc_gelatin (Figure 34C) and placed on a cleaned forearm of our volunteer (all consents obtained). Even though no official data is available on the toxicity of choline acetate used in electrolytes, there is a strong belief that the compound is harmless and biocompatible. Therefore, there are few other similar studies where the electrolyte is tested on human skin [139], [140], [205]. Our measurement setup was identical to what was introduced in Chapter 4.2.2. Figure 37 and 38 show impressively how similar commercial Ag/AgCl hydrogel and my developed ChAc_gelatin and KAc_gelatin electrodes' interface impedance is. Two measurements were conducted. During the first measurement, the interface impedance was registered for 2 hours at frequencies 10 and 70 kHz (Figures 37 and 38, connected lines).
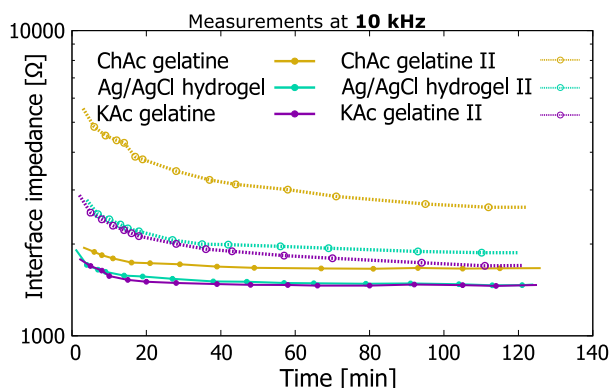
Figure 37. Electrode-skin interface impedance measurements on the human forearm with novel ChAc_gelatin and KAc_gelatin carbon electrodes. For reference, commercial Ag/AgCl pre-gelled electrodes were taken. All three electrodes give virtually similar interface impedance values. ChAc_gelatin electrode's interface impedance module is higher, but the overall trend is still very similar.
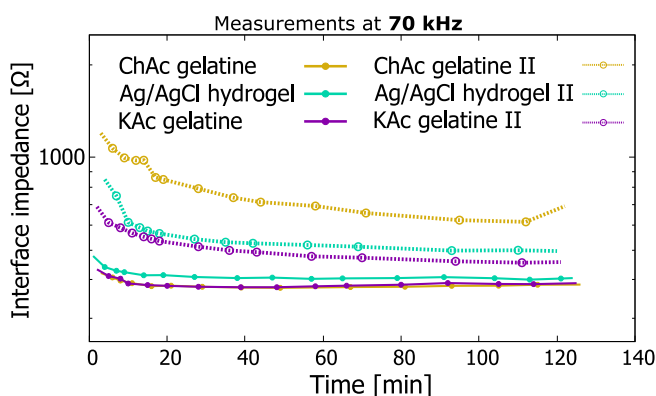

Figure 38. At 70 kHz, the interface impedance value is lower than at 10 kHz, but the 3 different electrode sets act very similarly.

The electrodes were removed from the hand after the first measurement and left to dry in the open air. The second measurement took place 24 hours later, and dotted lines in Figure 37 and 38 represents the interface impedance registered with the same electrodes on the same test subject. Surprisingly, the potassium acetate gel electrode had a matching response to the conventional wet electrodes. As commercial Ag/AgCl hydrogel contains a significant amount of potassium salts, the conductivity of both gels is understandably similar. The choline acetate ionogel impedance module was about 40% higher with repeated measurements, but the overall trend is still the same.

5.3.2 Reusability of ionic liquid electrodes

Figure 39 depicts electrodes (carbon textile base and CNF/CF-PDMS fiber base) with chitosan and gelatin electrolytes before and after a single measurement on the skin surface. The dry carbon textile surface (Figures 39A and B) showed no difference before and after. It was a different case with chitosan and gelatin ionogels on the textile. After measurements, the electrolyte dried out and fully clogged the yarns (Figure 39C before and 39D after). Gelatin-based electrolyte texture was more viscous and gluey before the measurements (Figure 39E) - perfect for electrode contact. After the measures, again, the electrolyte lost its moisture and seemed dry and dense (Figure 39F). The reusability improved if gelatin ionogel was applied to CNF/CF-PDMS fiber electrode. After the first measurement, the surface was in a similar semi-dry condition (Figure 39G before and 39H after).
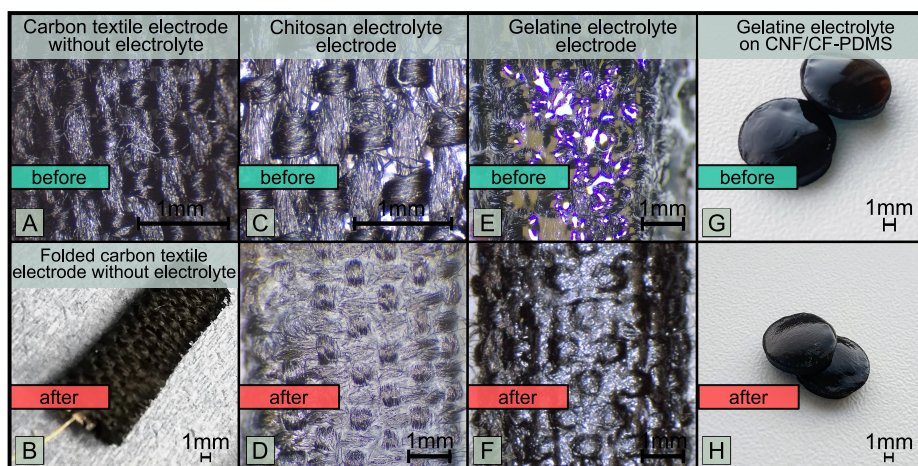

Figure 39. Carbon textile base electrodes with added electrolytes - chitosan electrolyte and gelatine electrolyte before and after the measurements. G and H represent gelatine and chitosan electrolytes on CNF/CF-PDMS soft electrodes. A and B show how the carbon textile electrode looks without the electrolyte addition.

5.4 Conclusion

To conclude, in the current chapter, choline acetate ionogels (ChAc_chitosan and ChAc_gelatin) were composed to complement dry carbon textile and CNF/CF-PDMS fiber electrodes. In addition, hygroscopic salt; potassium acetate based ionogels (KAc_chitosan and KAc_gelatin) were prepared. The main goal of these fabricated materials was to have

a comparable interface impedance with Ag/AgCl hydrogel electrodes (around 2 kOhms at 10 kHz) and improve the contact with the skin. In addition, reusability was addressed.

As choline acetate has uncertain toxicity levels, most measurements were made on pork skin and designed PVA-gelatin test phantom. To improve the phantom, a PVA tube was developed to mimic a pulsating artery inside the gelatin base material. Results showed that every test object (pork skin, PVA-gelatin phantom, human forearm) has advantages and disadvantages – rapid degradation of pork skin, underperforming phantom material, and safety concerns with a human forearm. Still, for our specific case, the natural human forearm proved to be the most useful. Nevertheless, the PVA-gelatin sample may allow simplified measurement of the interface impedance of electrodes if the skin layer on top of the test sample is further developed to mimic dry skin more accurately. Moreover, the developed PVA "artery" tube inside the test phantom can open up new possibilities to look into the more problematic areas which go hand-in-hand with bioimpedance measurement of a cardiac pulse. For example, how are pressure and impedance correlating, and what influences the impedance curve?

Developed semi-dry ionogel electrodes' reusability was analyzed visually and by comparing interface impedances. Results showed that interface impedance (electrodes on human forearm) was, on average, 25% higher for potassium acetate and Ag/AgCl hydrogel electrodes and even 75% higher for ionic liquid choline acetate electrodes after the first measurement. Given that these results are based on a limited number of experiments, the analysis outcome should be treated with considerable caution. Even though the ionogels proved very efficient in reducing the interface impedance of developed dry electrodes, they were not reusable. The contact with the skin provoked moisture diffusion between the ionogel and the skin, which means that the gel lost its beneficial properties (moisture level decrease). However, it is a step forward in producing semi-dry, reliable, comfortable, and reusable electrodes for bioimpedance measurements.

In future research, we have to optimize the gel preparation so that developed semi-dry ionogel electrodes will keep the moisture level unchanged for an extended period after placing them on the biological tissue.

6 Conclusion

6.1 Summary of the thesis

The first part of the thesis concentrated on fabricating a carbon-PDMS composite that has electrical conductivity, is soft, stretchable, and easy to produce. Microneedle-like electrode material was developed using IPA as a solvent, ultrasonication and magnetic stirring for mixing, and carbon nanofibers and carbon fibers as hybrid fillers inside the silicone rubber. In addition, my work describes thorough testing of the carbon samples' impedance response to compressive loading/unloading cycles, strain sensibility, and the aging phenomenon.

The second part of the research focused on a comparative study between novel micro-needle-like carbon-PDMS electrodes, sticker (OMNI-WAVE™), rigid metal, and commercial hydrogel electrodes showing the feasibility of dry carbon fiber electrodes as a possible flexible alternative to rigid metal electrodes. The interface impedance of CNF/CF-PDMS fiber was lower than smooth carbon-based electrodes' and averagely similar to metal and OMNI-WAVE™ carbon sticker electrodes' impedance. The most significant novelty in this work is the electrode-skin interface impedance measurement setup. The proposed method enables electrode contact quality checks simultaneously with tissue characterization. This gives a valuable extra feature to the setup developed (no need to reposition the electrodes on the skin between the measurements).

The last part of the work introduces novel ionic liquid (ChAc_gelatin) and potassium acetate-based (KAc_gelatin) ionogels infused with carbon-based electrodes. As a result, these semi-dry electrodes had interface impedance comparable to commercial Ag/AgCl hydrogel ones. However, the reusability of the electrolyte was not proved as contact with the skin changed the water content and imbalanced the material. Therefore, future development of the gel is needed. In addition, a simple PVA-gelatin phantom with a mock artery was developed. It was used as a test bench for multiple bioimpedance-based measurements that need ionic conduction and changing pulsating impedance.

With this work, the following research questions have been answered:

1. *How to cost-effectively produce a carbon-polydimethylsiloxane (PDMS) composite with a good distribution of carbon fillers inside the PDMS matrix for electrical conductivity?*

   Two recipes were proposed, and combining magnetic stirring and ultrasonication to mix the carbon fillers inside the PDMS matrix proved efficient if the composite's viscosity was low. For thinning the composite, HMDSO was used, and distributing the carbon fillers more homogeneously required a solvent (IPA).

2. *How to improve the contact between the skin and the (dry) electrode?*

   Preparing the skin beforehand by abrading is a valuable technique to lower the interface impedance when dealing with dry electrodes. Still, the method is time-dependent because the skin starts regenerating the stratum corneum during the long-time measurements.

   Natural electrolytes (sweat) appearing between the dry electrode and the skin lowers the interface impedance making the measurements also time-dependent.

   External pressure applied to the electrodes is limited to preserve the convenience of the subject under the test. The pressure effect was evident with dry soft electrodes like CNF/CF-PDMS microneedle-like and smooth but not remarkably with hydrogel, metal, or OMNI-WAVE™ sticker electrodes.

<u>Microneedle-like carbon fiber strands</u> of a carbon-based soft and stretchable electrode surface proved to be an effective way to reduce the interface impedance. Soft and flexible fibers are strong enough to slightly scrape the outer layer of dry skin and provide a more effective contact.

Applying <u>novel ionogel</u> based on choline acetate and potassium acetate on the carbon-based electrodes reduced the interface impedance to the level of Ag/AgCl hydrogel electrodes.

3. *How to combine carbon-PDMS electrodes with ionic liquid ionogel to prepare semi-dry electrodes?*

Choline and potassium acetate based ionogel electrodes are a fascinating field to develop further as the research area is still relatively new. ChAc_gelatin and KAc_gelatin electrolytes proved to help reduce the interface impedance of the electrode and skin effectively by making contact more stable on the skin. These electrodes gave very similar results to commercial Ag/AgCl hydrogel ones.

    3.1 *Explore the trade-off between contact impedance and repositioning in ionic gel semi-dry ionogel electrodes.*

    When the electrolytic gel was applied to the carbon base (carbon textile, CNF/CF-PDMS electrode), the initial interface measurements were very similar to conventional electrodes (Ag/AgCl). Unfortunately, second measurements with the same gel electrodes showed a significant increase in interface impedance. Especially poor results were with carbon textile electrodes; electrolytes (ChAc_gelatin and KAc_gelatin) quickly absorbed and dried out when left in the open air. However, carbon-PDMS electrodes combined with ChAc_gelatin and KAc_gelatin showed a prospect as semi-dry electrodes with a low contact interface impedance when used on the forearm.

4. *How to develop appropriate and applicable metrics to evaluate the quality of dry and semi-dry electrodes?*

A highly effective and novel interface impedance measurement setup was designed to evaluate each electrode's interface impedance separately. By doing that, we can quickly assess if the electrode placement on the test subject is acceptable. In addition, it is possible to get information about the bioimpedance of the tissue under the same sensing electrodes without repositioning them on the skin. Assessing interface impedance gives valuable feedback about the electrodes used. For example, low and stable electrode-skin interface impedance typically ensures capturing of a signal with acceptable quality. In addition, multiple electrode interfaces were successfully registered continuously with the new measurement method, which is hardly possible with other popular methods.

5. *Choice of representative test bodies. Specifically, is PVA-gelatin phantom sufficient in interface impedance comparative study?*

PVA-gelatin phantom has much better stability and preservation possibilities than pork skin. However, the test phantom at the current build-up is not entirely satisfactory to be used for an interface impedance comparative study. The skin layer on the top mimics wet skin making the contact impedance too low, and it is hard to differentiate between electrodes' performances. Nevertheless, if the top layer is developed more skin-like, the test phantom will successfully imitate the wrist with

pressure pulse and bioimpedance change accordingly. The PVA-gelatin test phantom with a mock artery was validated and responded similarly to a natural artery with blood pressure.

6. *Are developed CNF/CF-PDMS electrodes usable in bioimpedance measurements on the wrist to detect heart rate?*

    All of the carbon electrodes developed (CNF/CF-PDMS fiber and smooth), sticker electrodes, metal, and hydrogel electrodes showed cardiac pulse when placed on the radial artery on the wrist. The signal quality depended on the moving artifacts, interface impedance (contact with the skin), placement on the radial artery, and subject under the test. Figure 27 depicts how noisy the signal can be with high interface impedance (CNF/CF-PDMS smooth) compared to conventional Ag/AgCl hydrogel electrodes with much lower interface impedance.

    6.1 *Are the results comparable to commercially available electrodes?*

    Developed CNF/CF-PDMS fiber electrodes showed lower interface impedance than CNF/CF-PDMS smooth electrodes, and cardiac cycle measurements were less noisy. OMNI-WAVE™ carbon sticker electrodes proved to have a similar response to microneedle-like carbon electrodes, except that they are not so prone to movement artifacts due to their adhesive properties. However, in reusability matter, dry carbon-PDMS electrodes have an advantage. To sum up, developed dry electrodes are comparable to commercially available ones, but certain advantages and disadvantages to each alternative must be considered.

6.2 Limitations

This thesis focused on fabricating a simple recipe for CNF/CF-PDMS electrode material. Still, hundreds of possibilities are presented in the literature to improve the homogeneity of the fillers inside the silicone matrix. Therefore, the aim of the current work was shifted to the interface impedance measurements on the human skin with dry carbon electrodes. In light of this, the developed carbon material itself did not have to be perfectly homogeneous, have very high conductivity, and have a low percolation threshold.

Interface impedance measurements and electrodes comparison study was conducted by using only one subject under the test. However, as the results could remarkably variate between the subjects, a better generalization of the quality of the electrodes could be given if a more significant number and more varied samples (old, young, different race, sex, healthy, ill) of test subjects were compared.

As the choline acetate toxicity issue is still undergoing work, the measurements on the human hand are limited in current research. Therefore, no long-lasting and repeated measurement sets were depicted; only insightful results based on five different interface impedance registering sets are available.

The PVA-gelatin phantom model is prepared by keeping electrical conductivity and mechanical strength in mind. Another essential feature of natural tissues is permittivity, which is not covered in this thesis.

6.3 Further work

The author acknowledges that this thesis only covered some aspects needed for good electrode development and quality assessment, but it successfully lays the groundwork for further research. A few potential study topics are described as follows:

- Implementing OMNI-WAVE™ carbon fiber-based electrodes in bioimpedance measurements for cardiac pressure registering. The sticker electrodes are excellent for one-time measurements of bioimpedance. The motion artifacts are minor and comparable to conventional hydrogel electrodes as the sticker holds the electrode intact to the skin. The electrically conductive adhesive under the electrode connects the effective pathways between the carbon fibers; hence, the material is thin and light because the amount of fillers is meager. Interface impedance is stable and variation similar to metal electrodes' interface. Comprehensive experiments must be conducted to see if the cardiac signals from actual patients are as easily discoverable as it is with hydrogel electrodes.

- Completing the PVA-gelatin test phantom with mock artery by developing a more advanced skin layer on top to be used as a proper skin-tissue mimicking phantom. Also, to put the PVA artery into use by preparing a complete test setup to discover insightful results on how pressure and bioimpedance change are connected. In addition, validating the test phantom by comparing the electrical conductivity and mechanical properties with real tissues and manipulating the phantom's electrical permittivity to be used in radar sensor technology applications.

- Developing ionic liquid (choline acetate) ionogels further to achieve no diffusion between the electrolyte and the skin could result in reusable semi-dry electrodes - ideal for bioimpedance measurements with wearable devices to detect cardiac pressure change.

The bioimpedance measurement technique is simple methodology-wise but very powerful. It can detect various useful information the body is giving us; we just have to look for the right place with the right equipment at the right time.

List of Figures

List of Tables

References

[1] Department of Biomedical Engineering Linköping University, Linköping, Sweden and L. Rattfält, Smartware electrodes for ECG measurements: Design, evaluation and signal processing. Linköping University Electronic Press, 2013. doi: 10.3384diss.diva-100134.

[2] "Programm: Horizon Europe - Cluster 1 - Destination 1: Staying healthy in a rapidly changing society | EuroAccess Macro-Regions." https://www.euro-access.eu/programm/horizon_europe_-_cluster_1_-_destination_1_staying_healthy_in_a_rapidly_changing_society (accessed Jul. 05, 2022).

[3] J. E. Mück, B. Ünal, H. Butt, and A. K. Yetisen, "Market and Patent Analyses of Wearables in Medicine," Trends Biotechnol., vol. 37, no. 6, pp. 563–566, Jun. 2019, doi: 10.1016/j.tibtech.2019.02.001.

[4] "Global Wearable Technology Market Trends & Analysis Report 2021-2028: Adoption of Fitness Trackers and Health-based Wearables is Anticipated to Propel Growth - ResearchAndMarkets.com," Jan. 04, 2022. https://www.businesswire.com/news/-home/20220104005806/en/Global-Wearable-Technology-Market-Trends-Analysis-Report-2021-2028-Adoption-of-Fitness-Trackers-and-Health-based-Wearables-is-Anticipated-to-Propel-Growth—ResearchAndMarkets.com (accessed May 19, 2022).

[5] "The emerging clinical role of wearables: factors for successful implementation in healthcare | npj Digital Medicine." https://www.nature.com/articles/s41746-021-00418-3 (accessed May 19, 2022).

[6] T. Arakawa, "Recent Research and Developing Trends of Wearable Sensors for Detecting Blood Pressure," Sensors, vol. 18, no. 9, p. 2772, Aug. 2018, doi: 10.3390/s18092772.

[7] Valencell, "Valencell Ear PPG Blood Pressure Estimation Validation Study," Jan. 2020.

[8] "Blood Pressure Watch | OMRON HeartGuide Wrist BP Monitor," OMRON Healthcare. https://omronhealthcare.com/products/heartguide-wearable-blood-pressure-monitor-bp8000m/ (accessed May 19, 2022).

[9] N. Galm, R. G. Mayster, and M. F. Fehler, "Drowsiness detection," US10966647B2, Apr. 06, 2021 Accessed: May 19, 2022. [Online]. Available: https://patents.google.com/patent/US10966647B2/en

[10] "Hypertension." https://www.who.int/news-room/fact-sheets/detail/hypertension (accessed May 19, 2022).

[11] E. Huigen, A. Peper, and C. A. Grimbergen, "Investigation into the origin of the noise of surface electrodes," Med. Biol. Eng. Comput., vol. 40, no. 3, pp. 332–338, May 2002, doi: 10.1007/BF02344216.

[12] H. Wu et al., "Materials, Devices, and Systems of On-Skin Electrodes for Electrophysiological Monitoring and Human–Machine Interfaces," Adv. Sci., vol. 8, no. 2, p. 2001938, 2021, doi: 10.1002/advs.202001938.

[13] L.-W. Lo, J. Zhao, H. Wan, Y. Wang, S. Chakrabartty, and C. Wang, "An Inkjet-Printed PEDOT:PSS-Based Stretchable Conductor for Wearable Health Monitoring Device Applications," ACS Appl. Mater. Interfaces, vol. 13, no. 18, pp. 21693–21702, May 2021, doi: 10.1021/acsami.1c00537.

[14] X. Niu, X. Gao, Y. Liu, and L. Hao, "Surface Bioelectric Dry Electrodes: A Review," Measurement, vol. 183, p. 109774, Jun. 2021, doi: 10.1016/j.measurement.2021.109774.

[15] C. O'Mahony, F. Pini, A. Blake, C. Webster, J. O'Brien, and K. G. McCarthy, "Microneedle-based electrodes with integrated through-silicon via for biopo-tential recording," Sens. Actuators Phys., vol. 186, pp. 130–136, Oct. 2012, doi: 10.1016/j.sna.2012.04.037.

[16] Y. Fu, J. Zhao, Y. Dong, and X. Wang, "Dry Electrodes for Human Bioelectri-cal Signal Monitoring," Sensors, vol. 20, no. 13, Art. no. 13, Jan. 2020, doi: 10.3390/s20133651.

[17] J. Riistama, Characterisation of wearable and implantable physiological measure-ment devices. Tampere University of Technology, 2010. Accessed: May 19, 2022. [Online]. Available: https://researchportal.tuni.fi/en/publications/characterisation-of-wearable-and-implantable-physiological-measur

[18] R. Kusche, S. Kaufmann, and M. Ryschka, "Dry electrodes for bioimpedance mea-surements—design, characterization and comparison," Biomed. Phys. Ampmath-semicolon Eng. Express, vol. 5, no. 1, p. 015001, Nov. 2018, doi: 10.1088/2057-1976/aaea59.

[19] B. M. J. P. Group, "In praise of mercury sphygmomanometers," BMJ, vol. 322, no. 7296, p. 1248, May 2001, doi: 10.1136/bmj.322.7296.1248.

[20] R. Fitz, "A History of Medicine. By Douglas Guthrie, M.D. With an Introduction by Samuel C. Harvey, M.D., Wm. H. Carmalt Professor of Surgery," Am. Hist. Rev., vol. 52, no. 3, pp. 492–493, Apr. 1947, doi: 10.1086/ahr/52.3.492.

[21] W. H. Lewis, "The Evolution of Clinical Sphygmomanometry," Bull. N. Y. Acad. Med., vol. 17, no. 11, pp. 871–881, Nov. 1941.

[22] "Wireless Blood Pressure Monitor - QardioArm," Qardio. https://www.qardio.com/qardioarm-blood-pressure-monitor-iphone-android/ (accessed Oct. 21, 2022).

[23] "Samsung Galaxy Watch5," The Official Samsung Galaxy Site. https://www.samsung.com/global/galaxy/galaxy-watch5/ (accessed Oct. 21, 2022).

[24] Garmin and G. L. or its subsidiaries, "Garmin IndexTM BPM Smart Blood Pressure Monitor," Garmin. https://www.garmin.com/en-US/p/716808 (accessed Oct. 21, 2022).

[25] "Evidence | Clinically Validated Blood Pressure Monitoring," Aktiia. https://aktiia.com/uk/evidence (accessed Oct. 21, 2022).

[26] "PPG blood pressure research collaboration for high BP subjects," Valencell. https://valencell.com/blood-pressure-data-collection/ (accessed Oct. 21, 2022).

[27] M. Kuwabara, K. Harada, Y. Hishiki, and K. Kario, "Validation of two watch-type wearable blood pressure monitors according to the ANSI/AAMI/ISO81060-2:2013 guidelines: Omron HEM-6410T-ZM and HEM-6410T-ZL," J. Clin. Hypertens., vol. 21, no. 6, pp. 853–858, 2019, doi: 10.1111/jch.13499.

[28] "Akern® - Science in Body Composition," Akern.
https://www.akern.com/en/ (accessed May 19, 2022).

[29] "Impedimed's bioimpedance spectroscopy."
https://www.impedimed.com/ (accessed Aug. 16, 2022).

[30] "Bodystat," Bodystat.
https://www.bodystat.com/products/ (accessed May 19, 2022).

[31] "The new generation of body composition analysis."
https://www.seca.com/en_us/554.html (accessed May 19, 2022).

[32] "MELANOMA - Scibase." https://scibase.com/uk/the-nevisense-product/
(accessed May 19, 2022).

[33] "Injeq IQ-Tip® spinal needle | Precision. Care. Confidence.," Injeq.
https://injeq.com/ (accessed May 19, 2022).

[34] "Impedance Spectroscopy," Eliko, Jun. 29, 2021.
https://eliko.tech/quadra-impedance-spectroscopy/ (accessed May 19, 2022).

[35] "Dräger PulmoVista® 500."
https://www.draeger.com/en_uk/Products/PulmoVista-500
(accessed May 19, 2022).

[36] "toSenseTM." https://www.tosense.com/ (accessed May 19, 2022).

[37] "Philips-Biosensor-BX100-respiration-rate-computation-and-validation-summary_
Whitepaper.pdf." https://www.convenzis.co.uk/wp-content/uploads/2021/04/
Philips-Biosensor-BX100-respiration-rate-computation-and-validation-summary_
Whitepaper.pdf (accessed May 19, 2022).

[38] "AURA Strap." https://auradevices.io/strap.html (accessed May 19, 2022).

[39] L. Ward, "Electrical Bioimpedance: From the Past to the Future," J. Electr. Bioimpedance, vol. 12, pp. 1–2, Mar. 2021, doi: 10.2478/joeb-2021-0001.

[40] D. BK, N. Novas, J. Gazquez Parra, and F. Manzano-Agugliaro, "Dielectric and Bioimpedance Research Studies: A Scientometric Approach Using the Scopus Database," Publications, vol. 6, p. 6, Jan. 2018, doi: 10.3390/publications6010006.

[41] G. A. Cohn and R. Kusche, "Bioimpedance based pulse waveform sensing," US20180078148A1, Mar. 22, 2018 Accessed: Aug. 16, 2022. [Online]. Available: https://patents.google.com/patent/US20180078148A1/en

[42] V. P. Rachim and W.-Y. Chung, "Multimodal Wrist Biosensor for Wearable Cuff-less Blood Pressure Monitoring System," Sci. Rep., vol. 9, no. 1, Art. no. 1, May 2019, doi: 10.1038/s41598-019-44348-3.

[43] T.-W. Wang et al., "Intelligent Bio-Impedance System for Personalized Continuous Blood Pressure Measurement," Biosensors, vol. 12, no. 3, p. 150, Feb. 2022, doi: 10.3390/bios12030150.

[44] S. Grimnes and Ø. G. Martinsen, "Chapter 5 - Excitable Tissue and Bioelectric Signals," in Bioimpedance and Bioelectricity Basics (Third Edition), S. Grimnes and Ø. G. Martinsen, Eds. Oxford: Academic Press, 2015, pp. 119–139. doi: 10.1016/B978-0-12-411470-8.00005-2.

[45] "Who Wears Me? Bioimpedance as a Passive Biometric," presented at the 3rd USENIX Workshop on Health Security and Privacy (HealthSec 12), 2012. Accessed: May 19, 2022. [Online]. Available: https://www.usenix.org/conference/healthsec12/workshop-program/presentation/cornelius

[46] C. Gabriel, S. Gabriel, and E. Corthout, "The dielectric properties of biological tissues: I. Literature survey," Phys. Med. Biol., vol. 41, no. 11, pp. 2231–2249, Nov. 1996, doi: 10.1088/0031-9155/41/11/001.

[47] D. Naranjo, J. Reina-Tosina, and M. Min, "Fundamentals, Recent Advances, and Future Challenges in Bioimpedance Devices for Healthcare Applications," J. Sens., vol. 2019, pp. 1–42, Jul. 2019, doi: 10.1155/2019/9210258.

[48] M. Min, H. Kõiv, E. Priidel, K. Pesti, and P. Annus, Noninvasive Acquisition of the Aortic Blood Pressure Waveform. IntechOpen, 2019. doi: 10.5772/intechopen.86065.

[49] J. G. Webster, Medical Instrumentation Application and Design, 4th Edition. John Wiley & Sons, Incorporated, 2009.

[50] "What Is the Stratum Corneum?," Healthline, Sep. 27, 2018. https://www.healthline.com/health/stratum-corneum (accessed Sep. 06, 2022).

[51] "Why Electrodes Matter: Electrode-Electrolyte Interface," PulseAI. https://www.pulseai.io/blog/why-electrodes-matter-electrode-electrolyte-interface (accessed Oct. 18, 2022).

[52] M. R. Neuman, "Biopotential electrodes," in The Biomedical Engineering Handbook: Second Edition, 2nd ed., vol. 3, CRC Press, 2000, pp. 745–757. Accessed: May 19, 2022. [Online]. Available: http://www.fis.uc.pt/data/20062007/apontamentos/apnt_134_5.pdf

[53] A. Cömert, M. Honkala, and J. Hyttinen, "Effect of pressure and padding on motion artifact of textile electrodes," Biomed. Eng. OnLine, vol. 12, no. 1, p. 26, Apr. 2013, doi: 10.1186/1475-925X-12-26.

[54] H. Helmholtz, "Studien über electrische Grenzschichten," Ann. Phys., vol. 243, no. 7, pp. 337–382, 1879, doi: 10.1002/andp.18792430702.

[55] "Helmholtz double layer," TheFreeDictionary.com. https://encyclopedia2.thefreedictionary.com/Helmholtz+double+layer (accessed May 19, 2022).

[56] S. Srinivasan, "Electrode/Electrolyte interfaces: Structure and kinetics of charge transfer," Fuel Cells, Jan. 2006, doi: 10.1007/0-387-35402-6_2.

[57] P. Kassanos, "Bioimpedance Sensors: A Tutorial," IEEE Sens. J., vol. 21, no. 20, pp. 22190–22219, Oct. 2021, doi: 10.1109/JSEN.2021.3110283.

[58] S. Aronson and L. A. Geddes, "Electrode potential stability," IEEE Trans. Biomed. Eng., vol. 32, no. 11, pp. 987–988, Nov. 1985, doi: 10.1109/TBME.1985.325650.

[59] L. Francés-Morcillo, P. Morer-Camo, M. I. Rodríguez-Ferradas, and A. Cazón-Martín, "Wearable Design Requirements Identification and Evaluation," Sensors, vol. 20, no. 9, Art. no. 9, Jan. 2020, doi: 10.3390/s20092599.

[60] E. T. McAdams, J. Jossinet, A. Lackermeier, and F. Risacher, "Factors affecting electrode-gel-skin interface impedance in electrical impedance tomography," Med. Biol. Eng. Comput., vol. 34, no. 6, pp. 397–408, Nov. 1996, doi: 10.1007/BF02523842.

[61] Y. Khan et al., "Inkjet-Printed Flexible Gold Electrode Arrays for Bioelectronic Interfaces," Adv. Funct. Mater., vol. 26, no. 7, pp. 1004–1013, Feb. 2016, doi: 10.1002/adfm.201503316.

[62] M. Alizadeh-Meghrazi et al., "Evaluation of dry textile electrodes for long-term electrocardiographic monitoring," Biomed. Eng. OnLine, vol. 20, p. 68, Jul. 2021, doi: 10.1186/s12938-021-00905-4.

[63] S. Taccola et al., "Toward the Use of Temporary Tattoo Electrodes for Impedance-metric Respiration Monitoring and Other Electrophysiological Recordings on Skin," Sensors, vol. 21, no. 4, Art. no. 4, Jan. 2021, doi: 10.3390/s21041197.

[64] A. A. Chlaihawi, B. B. Narakathu, S. Emamian, B. J. Bazuin, and M. Z. Atashbar, "Development of printed and flexible dry ECG electrodes," Sens. Bio-Sens. Res., vol. 20, pp. 9–15, Sep. 2018, doi: 10.1016/j.sbsr.2018.05.001.

[65] K. J. Krieger, J. Liegey, E. M. Cahill, N. Bertollo, M. M. Lowery, and E. D. O'Cearbhaill, "Development and Evaluation of 3D-Printed Dry Microneedle Electrodes for Surface Electromyography," Adv. Mater. Technol., vol. 5, no. 10, p. 2000518, 2020, doi: 10.1002/admt.202000518.

[66] "OMNI Wave Signal Receptive Media - FLEXcon."
https://www.flexcon.com/products/spotlight/health-care/omni-wave-signal-receptive-media
(accessed May 19, 2022).

[67] M. Lee, A. Paul, Y. Xu, W. Hairston, and G. Cauwenberghs, "Characterization of Ag/AgCl Dry Electrodes for Wearable Electrophysiological Sensing," Front. Electron., vol. 2, Jan. 2022, doi: 10.3389/felec.2021.700363.

[68] M. Connolly and D. Buckley, "Contact dermatitis from propylene glycol in ECG electrodes, complicated by medicament allergy," Contact Dermatitis, vol. 50, p. 42, Feb. 2004, doi: 10.1111/j.0105-1873.2004.00271c.x.

[69] A. Searle and L. Kirkup, "A direct comparison of wet, dry and insulating bioelectric recording electrodes," Physiol. Meas., vol. 21, no. 2, pp. 271–283, May 2000, doi: 10.1088/0967-3334/21/2/307.

[70] H. Hussin, N. Soin, S. F. W. M. Hatta, F. A. M. Rezali, and Y. A. Wahab, "Review—Recent Progress in the Diversity of Inkjet-Printed Flexible Sensor Structures in Biomedical Engineering Applications," J. Electrochem. Soc., vol. 168, no. 7, p. 077508, Jul. 2021, doi: 10.1149/1945-7111/ac0e4b.

[71] Y.-T. Tseng et al., "Morphology and properties of PEDOT:PSS/soft polymer blends through hydrogen bonding interaction and their pressure sensor application," J. Mater. Chem. C, vol. 8, no. 18, pp. 6013–6024, May 2020, doi: 10.1039/D0TC00559B.

[72] L. M. Ferrari, U. Ismailov, J.-M. Badier, F. Greco, and E. Ismailova, "Conducting polymer tattoo electrodes in clinical electro- and magneto-encephalography," Npj Flex. Electron., vol. 4, no. 1, Art. no. 1, Mar. 2020, doi: 10.1038/s41528-020-0067-z.

[73] G. Acar, O. Ozturk, A. J. Golparvar, T. A. Elboshra, K. Böhringer, and M. K. Yapici, "Wearable and Flexible Textile Electrodes for Biopotential Signal Monitoring: A review," Electronics, vol. 8, no. 5, Art. no. 5, May 2019, doi: 10.3390/electronics8050479.

[74] H.-L. Peng et al., "Flexible dry electrode based on carbon nanotube/polymer hybrid micropillars for biopotential recording," Sens. Actuators Phys., vol. 235, Sep. 2015, doi: 10.1016/j.sna.2015.09.024.

[75] M. Eklund and N. Kjäll, Silicone-based Carbon Black Composite for Epidermal Electrodes. 2019. Accessed: May 19, 2022. [Online]. Available: http://urn.kb.se/resolve?urn=urn:nbn:se:uu:diva-401868

[76] W. Luo, "Fabrication and Characterization of Porous CNF/PDMS Nanocomposite for Sensing Application," Aug. 2018, Accessed: May 19, 2022. [Online]. Available: https://shareok.org/handle/11244/301321

[77] H. C. Jung et al., "CNT/PDMS composite flexible dry electrodesfor long-term ECG monitoring," IEEE Trans. Biomed. Eng., vol. 59, no. 5, pp. 1472–1479, May 2012, doi: 10.1109/TBME.2012.2190288.

[78] G.-L. Li, J.-T. Wu, Y.-H. Xia, Q.-G. He, and H.-G. Jin, "Review of semi-dry electrodes for EEG recording," J. Neural Eng., vol. 17, no. 5, p. 051004, Oct. 2020, doi: 10.1088/1741-2552/abbd50.

[79] Y. Hou, Z. Li, Z. Wang, and H. Yu, "Miura-ori structured flexible microneedle array electrode for biosignal recording," Microsyst. Nanoeng., vol. 7, no. 1, Art. no. 1, Jul. 2021, doi: 10.1038/s41378-021-00259-w.

[80] T. Takeshita et al., "Relationship between Contact Pressure and Motion Artifacts in ECG Measurement with Electrostatic Flocked Electrodes Fabricated on Textile," Sci. Rep., vol. 9, no. 1, Art. no. 1, Apr. 2019, doi: 10.1038/s41598-019-42027-x.

[81] "Introduction to Polymer Science," in Introduction to Physical Polymer Science, John Wiley & Sons, Ltd, 2005, pp. 1–28. doi: 10.1002/0471757128.ch1.

[82] Z. Zhou, H. Zhang, J. Liu, and W. Huang, "Flexible electronics from intrinsically soft materials," Giant, vol. 6, p. 100051, Jun. 2021, doi: 10.1016/j.giant.2021.100051.

[83] R. Ariati, F. Pereira Sales, A. Souza, R. Lima, and J. Ribeiro, "Polydimethylsiloxane Composites Characterization and Its Applications: A Review," Polymers, vol. 13, p. 4258, Dec. 2021, doi: 10.3390/polym13234258.

[84] J. Brandrup, E. H. Immergut, and E. A. Grulke, Polymer handbook. New York: Wiley, 1999.

[85] K. Sun et al., "Flexible polydimethylsiloxane/multi-walled carbon nanotubes membranous metacomposites with negative permittivity," Polymer, vol. 125, Jul. 2017, doi: 10.1016/j.polymer.2017.07.083.

[86] H. Kim, E. Kim, C. Choi, and W.-H. Yeo, "Advances in Soft and Dry Electrodes for Wearable Health Monitoring Devices," Micromachines, vol. 13, no. 4, p. 629, Apr. 2022, doi: 10.3390/mi13040629.

[87] E. Dal Lago, E. Cagnin, C. Boaretti, M. Roso, A. Lorenzetti, and M. Modesti, "Influence of Different Carbon-Based Fillers on Electrical and Mechanical Properties of a PC/ABS Blend," Polymers, vol. 12, p. 29, Dec. 2019, doi: 10.3390/polym12010029.

[88] R. N. Rothon, Particulate-filled polymer composites. Harlow, Essex, England; New York: Longman Scientific & Technical; J. Wiley, 1995.

[89] D. C. Kim, H. J. Shim, W. Lee, J. H. Koo, and D.-H. Kim, "Material-Based Approaches for the Fabrication of Stretchable Electronics," Adv. Mater., vol. 32, no. 15, p. 1902743, 2020, doi: 10.1002/adma.201902743.

[90] T. Khan, M. S. Irfan, M. Ali, Y. Dong, S. Ramakrishna, and R. Umer, "Insights to low electrical percolation thresholds of carbon-based polypropylene nanocomposites," Carbon, vol. 176, pp. 602–631, May 2021, doi: 10.1016/j.carbon.2021.01.158.

[91] K. Ke, L. Yue, H. Shao, M.-B. Yang, W. Yang, and I. Manas-Zloczower, "Boosting electrical and piezoresistive properties of polymer nanocomposites via hybrid carbon fillers: A review," Carbon, vol. 173, pp. 1020–1040, Mar. 2021, doi: 10.1016/j.carbon.2020.11.070.

[92] S. Peng, Y. Yu, S. Wu, and C.-H. Wang, "Conductive Polymer Nanocomposites for Stretchable Electronics: Material Selection, Design, and Applications," ACS Appl. Mater. Interfaces, vol. 13, no. 37, pp. 43831–43854, Sep. 2021, doi: 10.1021/acsami.1c15014.

[93] V. Kumar, M. N. Alam, A. Manikkavel, M. Song, D.-J. Lee, and S.-S. Park, "Silicone Rubber Composites Reinforced by Carbon Nanofillers and Their Hybrids for Various Applications: A Review," Polymers, vol. 13, no. 14, Art. no. 14, Jan. 2021, doi: 10.3390/polym13142322.

[94] "Three Main Properties of Carbon Black." http://www.carbonblack.jp/en/cb/tokusei.html (accessed May 19, 2022).

[95] G. Eastmond, A. Ledwith, S. Russo, and P. Sigwalt, Eds., Comprehensive Polymer Science: The Synthesis, Characterization, Reactions & Applications of Polymers - Chain Polymerization Part I, Vol.3, 1st edition. Oxford: Pergamon Press, 1990.

[96] S. Mirdehghan, "Fibrous polymeric composites," 2021, pp. 1–58. doi: 10.1016/B978-0-12-824381-7.00012-3.

[97] M. Meo and M. Rossi, "Prediction of Young's modulus of single wall carbon nanotubes by molecular-mechanics based finite element modeling," Compos. Sci. Technol., vol. 66, pp. 1597–1605, Sep. 2006, doi: 10.1016/j.compscitech.2005.11.015.

[98] S. Iijima, "Helical microtubules of graphitic carbon," Nature, vol. 354, no. 6348, pp. 56–58, Nov. 1991, doi: 10.1038/354056a0.

[99] P. M. Ajayan, O. Stephan, C. Colliex, and D. Trauth, "Aligned Carbon Nanotube Arrays Formed by Cutting a Polymer Resin—Nanotube Composite," Science, vol. 265, no. 5176, pp. 1212–1214, Aug. 1994, doi: 10.1126/science.265.5176.1212.

[100] "Carbon nanotube, single-walled (6,5) chirality, = 95 carbon 95 as carbon nanotubes, average diameter 0.78nm 308068-56-6." http://www.sigmaaldrich.com/ (accessed Oct. 21, 2022).

[101] S. Azizi, E. David, M. F. Fréchette, P. Nguyen-Tri, and C. M. Ouellet-Plamondon, "Electrical and thermal conductivity of ethylene vinyl acetate composite with graphene and carbon black filler," Polym. Test., vol. 72, pp. 24–31, Dec. 2018, doi: 10.1016/j.polymertesting.2018.09.031.

[102] K.-W. Kim, W. Han, and B.-J. Kim, "Effects of Mixing Ratio of Hybrid Carbonaceous Fillers on Thermal Conductivity and Mechanical Properties of Polypropylene Matrix Composites," Polymers, vol. 14, no. 10, p. 1935, May 2022, doi: 10.3390/polym14101935.

[103] A. Kasgoz, D. Akın, A. İ. Ayten, and A. Durmus, "Effect of different types of carbon fillers on mechanical and rheological properties of cyclic olefin copolymer (COC) composites," Compos. Part B Eng., vol. 66, pp. 126–135, Nov. 2014, doi: 10.1016/j.compositesb.2014.05.010.

[104] "Merck | Life Science Products & Service Solutions." https://www.sigmaaldrich.com/EE/en (accessed Oct. 21, 2022).

[105] G. Faiella et al., "Monitoring the Dispersion Process of SWNTs in Aqueous Solutions by UV-Vis and Raman Spectroscopies," J. Nanosci. Nanotechnol., vol. 9, no. 10, pp. 6026–6033, Oct. 2009, doi: 10.1166/jnn.2009.1561.

[106] J.-Y. Hwang, H.-S. Kim, J. H. Kim, U. S. Shin, and S.-H. Lee, "Carbon Nanotube Nanocomposites with Highly Enhanced Strength and Conductivity for Flexible Electric Circuits," Langmuir, vol. 31, no. 28, pp. 7844–7851, Jul. 2015, doi: 10.1021/acs.langmuir.5b00845.

[107] G. Mittal, V. Dhand, K. Y. Rhee, S.-J. Park, and W. R. Lee, "A review on carbon nanotubes and graphene as fillers in reinforced polymer nanocomposites," J. Ind. Eng. Chem., vol. 21, pp. 11–25, Jan. 2015, doi: 10.1016/j.jiec.2014.03.022.

[108] D. G. Papageorgiou, I. A. Kinloch, and R. J. Young, "Graphene/elastomer nanocomposites," Carbon, vol. 95, pp. 460–484, Dec. 2015, doi: 10.1016/j.carbon.2015.08.055.

[109] L.-C. Tang, L. Zhao, F. Qiang, Q. Wu, L.-X. Gong, and J.-P. Peng, "Chapter Twelve - Mechanical Properties of Rubber Nanocomposites Containing Carbon Nanofillers," in Carbon-Based Nanofillers and Their Rubber Nanocomposites, S. Yaragalla, R. K. Mishra, S. Thomas, N. Kalarikkal, and H. J. Maria, Eds. Elsevier, 2019, pp. 367–423. doi: 10.1016/B978-0-12-817342-8.00012-3.

[110] M. H. Al-Saleh and U. Sundararaj, "A review of vapor grown carbon nanofiber/polymer conductive composites," Carbon, vol. 47, no. 1, p. 2, 2009.

[111] Y. Li et al., "A review of the electrical and mechanical properties of carbon nanofiller-reinforced polymer composites," J. Mater. Sci., vol. 54, Jan. 2019, doi: 10.1007/s10853-018-3006-9.

[112] S. Chowdhury, M. Olima, Y. Liu, M. Saha, J. Bergman, and T. Robison, "Poly dimethyl-siloxane/carbon nanofiber nanocomposites: fabrication and characterization of electrical and thermal properties," Int. J. Smart Nano Mater., vol. 7, no. 4, pp. 236–247, Oct. 2016, doi: 10.1080/19475411.2016.1269027.

[113] E. M. Ahmed, "Hydrogel: Preparation, characterization, and applications: A review," J. Adv. Res., vol. 6, no. 2, pp. 105–121, Mar. 2015, doi: 10.1016/j.jare.2013.07.006.

[114] S. Bashir et al., "Fundamental Concepts of Hydrogels: Synthesis, Properties, and Their Applications," Polymers, vol. 12, no. 11, p. 2702, Nov. 2020, doi: 10.3390/polym12112702.

[115] G. Li, D. Zhang, S. Wang, and Y. Y. Duan, "Novel passive ceramic based semi-dry electrodes for recording electroencephalography signals from the hairy scalp," Sens. Actuators B Chem., vol. 237, pp. 167–178, Dec. 2016, doi: 10.1016/j.snb.2016.06.045.

[116] G. Shen et al., "A novel flexible hydrogel electrode with a strong moisturizing ability for long-term EEG recording," J. Neural Eng., vol. 18, no. 6, Dec. 2021, doi: 10.1088/1741-2552/ac41ab.

[117] M. Wang et al., "Tough and stretchable ionogels by in situ phase separation," Nat. Mater., vol. 21, no. 3, Art. no. 3, Mar. 2022, doi: 10.1038/s41563-022-01195-4.

[118] J. Tie, Z. Mao, L. Zhang, Y. Zhong, X. Sui, and H. Xu, "Conductive ionogel with underwater adhesion and stability as multimodal sensor for contactless signal propagation and wearable devices," Compos. Part B Eng., vol. 232, p. 109612, Mar. 2022, doi: 10.1016/j.compositesb.2022.109612.

[119] Y. Wu et al., "Highly Conductive, Transparent, Adhesive, and Self-Healable Ionogel Based on a Deep Eutectic Solvent with Widely Adjustable Mechanical Strength," Macromol. Rapid Commun., vol. n/a, no. n/a, p. 2200480, doi: 10.1002/marc.202200480.

[120] C. Lu and X. Chen, "Piezoionic strain sensors enabled by force-voltage coupling from ionogels," Chem. Phys. Lett., vol. 803, p. 139872, Sep. 2022, doi: 10.1016/j.cplett.2022.139872.

[121] J. Han, "What is Potassium Acetate E261(i) and its Uses in Food and Pharmaceutical?," Jul. 24, 2020. https://foodadditives.net/acidity-regulator/potassium-acetate/ (accessed May 20, 2022).

[122] F. J. He and G. A. MacGregor, "Beneficial effects of potassium on human health," Physiol. Plant., vol. 133, no. 4, pp. 725–735, 2008, doi: 10.1111/j.1399-3054.2007.01033.x.

[123] "Saturated Salt Solutions and control of Air Humidity." https://www.engineeringtoolbox.com/salt-humidity-d_1887.html (accessed May 20, 2022).

[124] X. Wu, Y. Gong, S. Xu, Z. Yan, X. Zhang, and S. Yang, "Electrical Conductivity of Lithium Chloride, Lithium Bromide, and Lithium Iodide Electrolytes in Methanol, Water, and Their Binary Mixtures," J. Chem. Eng. Data, vol. 64, Sep. 2019, doi: 10.1021/acs.jced.9b00405.

[125] C. Lei, Y. Guo, W. Guan, H. Lu, W. Shi, and G. Yu, "Polyzwitterionic Hydrogels for Efficient Atmospheric Water Harvesting," Angew. Chem. Int. Ed., vol. 61, no. 13, p. e202200271, 2022, doi: 10.1002/anie.202200271.

[126] P. J. Worsfold, A. Townshend, and C. F. Poole, Eds., Encyclopedia of Analytical Science, 2nd edition. Amsterdam; Boston: Elsevier, 2005.

[127] T. Mohammad, M. Freire, B. Saramago, J. N. Canongia Lopes, and L. P. N. Rebelo, "Surface Tension of Ionic Liquids and Ionic Liquid Solutions," Chem. Soc. Rev., vol. 41, pp. 829–868, Jan. 2012, doi: 10.1039/c1cs15146k.

[128] S. A. Forsyth, J. M. Pringle, and D. R. MacFarlane, "Ionic liquids: an overview," Aust. J. Chem., vol. 57, no. 2, pp. 113–119, Feb. 2004, doi: 10.1071/CH03231.

[129] A. Asakawa, M. Kohara, C. Sasaki, C. Asada, and Y. Nakamura, "Comparison of choline acetate ionic liquid pretreatment with various pretreatments for enhancing the enzymatic saccharification of sugarcane bagasse," Ind. Crops Prod., vol. 71, pp. 147–152, Sep. 2015, doi: 10.1016/j.indcrop.2015.03.073.

[130] N. Muhammad et al., "Synthesis and Physical Properties of Choline Carboxylate Ionic Liquids," J. Chem. Eng. Data, vol. 57, no. 8, pp. 2191–2196, Aug. 2012, doi: 10.1021/je300086w.

[131] J. A. L. Willcox, H. Kim, and H. J. Kim, "A molecular dynamics study of the ionic liquid, choline acetate," Phys. Chem. Chem. Phys., vol. 18, no. 22, pp. 14850–14858, Jun. 2016, doi: 10.1039/C6CP01031H.

[132] "volatility noun - Definition, pictures, pronunciation and usage notes | Oxford Advanced Learner's Dictionary at OxfordLearnersDictionaries.com." https://www.oxfordlearnersdictionaries.com/definition/english/volatility (accessed May 20, 2022).

[133] D. Rengstl, "Choline as a Cation for the Design of Low-toxic and Biocompatible Ionic Liquids, Surfactants, and Deep Eutectic Solvents," Universität Regensburg. Accessed: May 20, 2022. [Online]. Available: https://epub.uni-regensburg.de/28285/1/Dissertation_Doris_Rengstl.pdf

[134] P. Berton, K. Bica, and R. Rogers, "Ionic liquids for consumer products: Dissolution, characterization, and controlled release of fragrance compositions," Fluid Phase Equilibria, vol. 450, Jul. 2017, doi: 10.1016/j.fluid.2017.07.011.

[135] F. M. F. Vallana et al., "Ionic liquids as modulators of fragrance release in consumer goods," New J. Chem., vol. 40, no. 12, pp. 9958–9967, Nov. 2016, doi: 10.1039/C6NJ01626J.

[136] B. Clare, A. Sirwardana, and D. R. MacFarlane, "Synthesis, Purification and Characterization of Ionic Liquids," in Ionic Liquids, B. Kirchner, Ed. Berlin, Heidelberg: Springer, 2010, pp. 1–40. doi: 10.1007/128_2008_31.

[137] K. Põhako-Esko, M. Timusk, K. Saal, R. Lõhmus, I. Kink, and U. Mäeorg, "Increased conductivity of polymerized ionic liquids through the use of a nonpolymerizable ionic liquid additive," J. Mater. Res., vol. 28, no. 22, pp. 3086–3093, Nov. 2013, doi: 10.1557/jmr.2013.330.

[138] J. Lu, F. Yan, and J. Texter, "Advanced applications of ionic liquids in polymer science," Prog. Polym. Sci., vol. 34, no. 5, pp. 431–448, May 2009, doi: 10.1016/j.progpolymsci.2008.12.001.

[139] P. Leleux et al., "Ionic liquid gel-assisted electrodes for long-term cutaneous recordings," Adv. Healthc. Mater., vol. 3, no. 9, pp. 1377–1380, Sep. 2014, doi: 10.1002/adhm.201300614.

[140] S. Velasco-Bosom et al., "Conducting Polymer-Ionic Liquid Electrode Arrays for High-Density Surface Electromyography," Adv. Healthc. Mater., vol. 10, no. 17, p. 2100374, 2021, doi: 10.1002/adhm.202100374.

[141] M. Isik et al., "Cholinium-based ion gels as solid electrolytes for long-term cutaneous electrophysiology," J. Mater. Chem. C, vol. 3, no. 34, pp. 8942–8948, 2015, doi: 10.1039/C5TC01888A.

[142] F. Elhi et al., "Electromechanically active polymer actuators based on biofriendly choline ionic liquids," Smart Mater. Struct., vol. 29, no. 5, p. 055021, Apr. 2020, doi: 10.1088/1361-665X/ab7f24.

[143] A. Moretti, M. Paoletta, S. Liguori, M. Bertone, G. Toro, and G. Iolascon, "Choline: An Essential Nutrient for Skeletal Muscle," Nutrients, vol. 12, no. 7, p. 2144, Jul. 2020, doi: 10.3390/nu12072144.

[144] Institute of Medicine (US) Standing Committee on the Scientific Evaluation of Dietary Reference Intakes and its Panel on Folate, Other B Vitamins, and Choline, Dietary Reference Intakes for Thiamin, Riboflavin, Niacin, Vitamin B6, Folate, Vitamin B12, Pantothenic Acid, Biotin, and Choline. Washington (DC): National Academies Press (US), 1998. Accessed: May 20, 2022. [Online]. Available: http://www.ncbi.nlm.nih.gov/books/NBK114310/

[145] J. K. Blusztajn and R. J. Wurtman, "Choline and Cholinergic Neurons," Science, vol. 221, no. 4611, pp. 614–620, Aug. 1983, doi: 10.1126/science.6867732.

[146] D. Rengstl, B. Kraus, M. Van Vorst, G. D. Elliott, and W. Kunz, "Effect of choline carboxylate ionic liquids on biological membranes," Colloids Surf. B Biointerfaces, vol. 123, pp. 575–581, Nov. 2014, doi: 10.1016/j.colsurfb.2014.09.057.

[147] M. Petkovic et al., "Novel biocompatible cholinium-based ionic liquids—toxicity and biodegradability," Green Chem., vol. 12, no. 4, pp. 643–649, Apr. 2010, doi: 10.1039/B922247B.

[148] A. Santos, B. D. Ribeiro, D. Alviano, and M. A. Coelho, "Toxicity of ionic liquids toward microorganisms interesting to the food industry," RSC Adv, vol. 4, Aug. 2014, doi: 10.1039/C4RA05295A.

[149] S. P. M. Ventura, F. A. e Silva, A. M. M. Gonçalves, J. L. Pereira, F. Gonçalves, and J. A. P. Coutinho, "Ecotoxicity analysis of cholinium-based ionic liquids to Vibrio fischeri marine bacteria," Ecotoxicol. Environ. Saf., vol. 102, pp. 48–54, Apr. 2014, doi: 10.1016/j.ecoenv.2014.01.003.

[150] S. P. F. Costa, P. C. A. G. Pinto, R. A. S. Lapa, and M. L. M. F. S. Saraiva, "Toxicity assessment of ionic liquids with Vibrio fischeri: An alternative fully automated methodology," J. Hazard. Mater., vol. 284, pp. 136–142, Mar. 2015, doi: 10.1016/j.jhazmat.2014.10.049.

[151] I. Juneidi, M. Hayyan, and M. Hashim, "Evaluation of toxicity and biodegradability of cholinium-based deep eutectic solvents," RSC Adv., vol. 5, pp. 83636–83647, Sep. 2015, doi: 10.1039/C5RA12425E.

[152] S. A. Chowdhury, M. C. Saha, S. Patterson, T. Robison, and Y. Liu, "Highly Conductive Polydimethylsiloxane/Carbon Nanofiber Composites for Flexible Sensor Applications," Adv. Mater. Technol., vol. 4, no. 1, p. 1800398, 2019, doi: 10.1002/admt.201800398.

[153] H. Kõiv, K. Pesti, M. Min, and R. Land, "Investigation of cost-effective carbon nanofiber/carbon fiber and silicone polymer composite material for wearable bioimpedance device," in 2019 IEEE Sensors Applications Symposium (SAS), Mar. 2019, pp. 1–6. doi: 10.1109/SAS.2019.8706026.

[154] "NOVOCS safety data sheet."
https://www.smooth-on.com/msds/files/NOVOCS_Matte.pdf
(accessed May 20, 2022).

[155] J. H. Kim et al., "Simple and cost-effective method of highly conductive and elastic carbon nanotube/polydimethylsiloxane composite for wearable electronics," Sci. Rep., vol. 8, no. 1, p. 1375, Jan. 2018, doi: 10.1038/s41598-017-18209-w.

[156] F. W. Low, "The Effect of Chemical Solutions (Isopropyl Alcohol, Dichloromethane, Acetone and Triton X-100) on the Dispersion of Single-Walled Carbon Nanotubes," J. Appl. Sci. Res., vol. 9, pp. 3411–3416, Aug. 2013.

[157] T. R. Michel et al., "Evaluation of porous polydimethylsiloxane/carbon nanotubes (PDMS/CNTs) nanocomposites as piezoresistive sensor materials," Microsyst. Technol., vol. 26, no. 4, pp. 1101–1112, Apr. 2020, doi: 10.1007/s00542-019-04636-4.

[158] S. Wu et al., "Novel Electrically Conductive Porous PDMS/Carbon Nanofiber Composites for Deformable Strain Sensors and Conductors," ACS Appl. Mater. Interfaces, vol. 9, no. 16, pp. 14207–14215, Apr. 2017, doi: 10.1021/acsami.7b00847.

[159] L. Feng, N. Xie, and J. Zhong, "Carbon Nanofibers and Their Composites: A Review of Synthesizing, Properties and Applications," Materials, vol. 7, no. 5, pp. 3919–3945, May 2014, doi: 10.3390/ma7053919.

[160] X. Gao et al., "Mechanically Enhanced Electrical Conductivity of Polydimethylsiloxane-Based Composites by a Hot Embossing Process," Polymers, vol. 11, no. 1, Art. no. 1, Jan. 2019, doi: 10.3390/polym11010056.

[161] S. Grassini, "16 - Electrochemical impedance spectroscopy (EIS) for the in-situ analysis of metallic heritage artefacts," in Corrosion and Conservation of Cultural Heritage Metallic Artefacts, P. Dillmann, D. Watkinson, E. Angelini, and A. Adriaens, Eds. Woodhead Publishing, 2013, pp. 347–367. doi: 10.1533/9781782421573.4.347.

[162] Y. Gao, X. Fang, J. Tan, T. Lu, L. Pan, and F. Xuan, "Highly sensitive strain sensors based on fragmentized carbon nanotube/polydimethylsiloxane composites," Nanotechnology, vol. 29, no. 23, p. 235501, Apr. 2018, doi: 10.1088/1361-6528/aab888.

[163] M. Amjadi, Y. J. Yoon, and I. Park, "Ultra-stretchable and skin-mountable strain sensors using carbon nanotubes-Ecoflex nanocomposites," Nanotechnology, vol. 26, no. 37, p. 375501, Sep. 2015, doi: 10.1088/0957-4484/26/37/375501.

[164] Y.-T. Wu, T. Yan, and Z.-J. Pan, "Wearable Carbon-Based Resistive Sensors for Strain Detection: A Review," IEEE Sens. J., vol. 21, no. 4, pp. 4030–4043, Feb. 2021, doi: 10.1109/JSEN.2020.3034453.

[165] L. Wang et al., "Highly stretchable, anti-corrosive and wearable strain sensors based on the PDMS/CNTs decorated elastomer nanofiber composite," Chem. Eng. J., vol. 362, pp. 89–98, Apr. 2019, doi: 10.1016/j.cej.2019.01.014.

[166] D. Miklavcic, N. Pavselj, and F. Hart, "Electric Properties of Tissues," in Wiley Encyclopedia of Biomedical Engineering, vol. 6, 2006.
doi: 10.1002/9780471740360.ebs0403.

[167] C. Assambo, A. Baba, R. Dozio, and M. Burke, "Determination of the parameters of the skin-electrode impedance model for ECG measurement," Feb. 2007, pp. 90–95.

[168] S. Kim, R. F. Yazicioglu, T. Torfs, B. Dilpreet, P. Julien, and C. Van Hoof, "A 2.4µA continuous-time electrode-skin impedance measurement circuit for motion artifact monitoring in ECG acquisition systems," in 2010 Symposium on VLSI Circuits, Jun. 2010, pp. 219–220. doi: 10.1109/VLSIC.2010.5560290.

[169] T. Degen and T. Loeliger, "An improved method to continuously monitor the electrode-skin impedance during bioelectric measurements," Annu. Int. Conf. IEEE Eng. Med. Biol. Soc. IEEE Eng. Med. Biol. Soc. Annu. Int. Conf., vol. 2007, pp. 6295–6298, 2007, doi: 10.1109/IEMBS.2007.4353794.

[170] M. S. Spach, R. C. Barr, J. W. Havstad, and E. C. Long, "Skin-Electrode Impedance and Its Effect on Recording Cardiac Potentials," Circulation, vol. 34, no. 4, pp. 649–656, Oct. 1966, doi: 10.1161/01.CIR.34.4.649.

[171] G. Medrano, A. Ubl, N. Zimmermann, T. Gries, and S. Leonhardt, "Skin Electrode Impedance of Textile Electrodes for Bioimpedance Spectroscopy," 2007. doi: 10.1007/978-3-540-73841-1_69.

[172] B. Taji, S. Shirmohammadi, V. Groza, and I. Batkin, "Impact of Skin–Electrode Interface on Electrocardiogram Measurements Using Conductive Textile Electrodes," IEEE Trans. Instrum. Meas., vol. 63, no. 6, pp. 1412–1422, Jun. 2014, doi: 10.1109/TIM.2013.2289072.

[173] F. Xiong, D. Chen, Z. Chen, C. Jin, and S. Dai, "Impedance Characteristics of the Skin-Electrode Interface of Dry Textile Electrodes for Wearable Electrocardiogram," in Advances in Body Area Networks I, Cham, 2019, pp. 343–356. doi: 10.1007/978-3-030-02819-0_26.

[174] L. Euler, L. Guo, and N.-K. Persson, "Textile Electrodes: Influence of Knitting Construction and Pressure on the Contact Impedance," Sensors, vol. 21, no. 5, p. 1578, Feb. 2021, doi: 10.3390/s21051578.

[175] B. C. Fortune, C. G. Pretty, C. J. Cameron, L. R. McKenzie, L. T. Chatfield, and M. P. Hayes, "Electrode–skin impedance imbalance measured in the frequency domain," Biomed. Signal Process. Control, vol. 63, p. 102202, Jan. 2021, doi: 10.1016/j.bspc.2020.102202.

[176] G. Li, S. Wang, and Y. Y. Duan, "Towards gel-free electrodes: A systematic study of electrode-skin impedance," Sens. Actuators B Chem., vol. 241, pp. 1244–1255, Mar. 2017, doi: 10.1016/j.snb.2016.10.005.

[177] B. Taji, A. D. C. Chan, and S. Shirmohammadi, "Effect of Pressure on Skin-Electrode Impedance in Wearable Biomedical Measurement Devices," IEEE Trans. Instrum. Meas., vol. 67, no. 8, pp. 1900–1912, Aug. 2018, doi: 10.1109/TIM.2018.2806950.

[178] O. G. Martinsen and S. Grimnes, "Facts and myths about electrical measurement of stratum corneum hydration state," Dermatol. Basel Switz., vol. 202, no. 2, pp. 87–89, 2001, doi: 10.1159/000051604.

[179] H. F. Posada-Quintero, R. Rood, Y. Noh, K. Burnham, J. Pennace, and K. H. Chon, "Dry carbon/salt adhesive electrodes for recording electrodermal activity," Sens. Actuators Phys., vol. 257, pp. 84–91, Apr. 2017, doi: 10.1016/j.sna.2017.02.023.

[180] H. Kõiv, K. Pesti, M. Min, R. Land, and I. Must, "Comparison of the Carbon Nanofiber-/Fiber- and Silicone-Based Electrodes for Bioimpedance Measurements," IEEE Trans. Instrum. Meas., vol. 69, no. 4, pp. 1455–1463, Apr. 2020, doi: 10.1109/TIM.2019.2962297.

[181] J. Sandby-Møller, T. Poulsen, and H. C. Wulf, "Epidermal thickness at different body sites: relationship to age, gender, pigmentation, blood content, skin type and smoking habits," Acta Derm. Venereol., vol. 83, no. 6, pp. 410–413, 2003, doi: 10.1080/00015550310015419.

[182] L. Euler, "Impedance and Stimulation Comfort of Knitted Electrodes for Neuromuscular Electrical Stimulation (NMES): Influence of electrode construction and pressure application to the electrode," 2020. Accessed: Jul. 07, 2022. [Online]. Available: http://urn.kb.se/resolve?urn=urn:nbn:se:hb:diva-23896

[183] M. A. Aizat and F. Aziz, "12 - Chitosan Nanocomposite Application in Wastewater Treatments," in Nanotechnology in Water and Wastewater Treatment, A. Ahsan and A. F. Ismail, Eds. Elsevier, 2019, pp. 243–265. doi: 10.1016/B978-0-12-813902-8.00012-5.

[184] J. Alipal et al., "A review of gelatin: Properties, sources, process, applications, and commercialisation," Mater. Today Proc., vol. 42, pp. 240–250, Jan. 2021, doi: 10.1016/j.matpr.2020.12.922.

[185] K. Liu et al., "Artificial Sensitive Skin for Robotics Based on Electrical Impedance Tomography," Adv. Intell. Syst., vol. 2, no. 4, p. 1900161, 2020, doi: 10.1002/aisy.201900161.

[186] T.-J. Kao, G. J. Saulnier, D. Isaacson, T. L. Szabo, and J. C. Newell, "A Versatile High-Permittivity Phantom for EIT," IEEE Trans. Biomed. Eng., vol. 55, no. 11, pp. 2601–2607, Nov. 2008, doi: 10.1109/TBME.2008.2001287.

[187] M. A. Kandadai, J. L. Raymond, and G. J. Shaw, "Comparison of electrical conductivities of various brain phantom gels: Developing a 'Brain Gel Model,'" Mater. Sci. Eng. C Mater. Biol. Appl., vol. 32, no. 8, pp. 2664–2667, Dec. 2012, doi: 10.1016/j.msec.2012.07.024.

[188] S. de Gelidi et al., "Towards a thoracic conductive phantom for EIT," Med. Eng. Phys., vol. 77, pp. 88–94, Mar. 2020, doi: 10.1016/j.medengphy.2019.10.008.

[189] D. Peterson, "Tissue Equivalent Phantom Development for Biomedical Applications," University of Florida, Gainesville, 2009. Accessed: Jul. 07, 2022. [Online]. Available: https://ufdc.ufl.edu/UFE0025025/00001

[190] V. Gaubert, H. Gidik, and V. Koncar, "Proposal of a Lab Bench for the Unobtrusive Monitoring of the Bladder Fullness with Bioimpedance Measurements," Sensors, vol. 20, no. 14, Art. no. 14, Jan. 2020, doi: 10.3390/s20143980.

[191] G. Anand, A. Lowe, and A. Al-Jumaily, "Tissue phantoms to mimic the dielectric properties of human forearm section for multi-frequency bioimpedance analysis at low frequencies," Mater. Sci. Eng. C Mater. Biol. Appl., vol. 96, pp. 496–508, Mar. 2019, doi: 10.1016/j.msec.2018.11.080.

[192] A. Hellerbach, V. Schuster, A. Jansen, and J. Sommer, "MRI Phantoms – Are There Alternatives to Agar?," PLOS ONE, vol. 8, no. 8, p. e70343, Aug. 2013, doi: 10.1371/journal.pone.0070343.

[193] A. M. R. Pinto, P. Bertemes-Filho, and A. Paterno, "Gelatin: a skin phantom for bioimpedance spectroscopy," Biomed. Phys. Ampmathsemicolon Eng. Express, vol. 1, no. 3, p. 035001, Sep. 2015, doi: 10.1088/2057-1976/1/3/035001.

[194] H. Kõiv, K. Pesti, and R. Gordon, "Electric Impedance Measurement of Tissue Phantom Materials for Development of Medical Diagnostic Systems," in Electric Impedance Measurement of Tissue Phantom Materials for Development of Medical Diagnostic Systems, De Gruyter Oldenbourg, 2016, pp. 131–137. doi: 10.1515/9783110449822-013.

[195] H. Kõiv, M. Rist, and M. Min, "Development of bioimpedance sensing device for wearable monitoring of the aortic blood pressure curve," Tm - Tech. Mess., vol. 85, no. 5, pp. 366–377, May 2018, doi: 10.1515/teme-2017-0113.

[196] A. Barui, "3 - Synthetic polymeric gel," in Polymeric Gels, K. Pal and I. Banerjee, Eds. Woodhead Publishing, 2018, pp. 55–90. doi: 10.1016/B978-0-08-102179-8.00003-X.

[197] K. C. Chu and B. K. Rutt, "Polyvinyl alcohol cryogel: an ideal phantom material for MR studies of arterial flow and elasticity," Magn. Reson. Med., vol. 37, no. 2, pp. 314–319, Feb. 1997, doi: 10.1002/mrm.1910370230.

[198] M. Kobayashi and H. S. Hyu, "Development and Evaluation of Polyvinyl Alcohol-Hydrogels as an Artificial Atrticular Cartilage for Orthopedic Implants," Materials, vol. 3, no. 4, pp. 2753–2771, Apr. 2010, doi: 10.3390/ma3042753.

[199] synjosh, "What SynDaver Makes | SynDaver," Jan. 08, 2019. https://syndaver.com/what-we-do/ (accessed Jul. 07, 2022).

[200] I. Mano, H. Goshima, M. Nambu, and M. Iio, "New polyvinyl alcohol gel material for MRI phantoms," Magn. Reson. Med., vol. 3, no. 6, pp. 921–926, Dec. 1986, doi: 10.1002/mrm.1910030612.

[201] L. Gautam, S. G. Warkar, S. I. Ahmad, R. Kant, and M. Jain, "A review on carboxylic acid cross-linked polyvinyl alcohol: Properties and applications," Polym. Eng. Sci., vol. 62, no. 2, pp. 225–246, 2022, doi: 10.1002/pen.25849.

[202] J. M. Harris, "Introduction to Biotechnical and Biomedical Applications of Poly(Ethylene Glycol)," in Poly(Ethylene Glycol) Chemistry: Biotechnical and Biomedical Applications, J. M. Harris, Ed. Boston, MA: Springer US, 1992, pp. 1–14. doi: 10.1007/978-1-4899-0703-5_1.

[203] M. F. A. Cutiongco et al., "Submillimeter Diameter Poly(Vinyl Alcohol) Vascular Graft Patency in Rabbit Model," Front. Bioeng. Biotechnol., vol. 4, p. 44, 2016, doi: 10.3389/fbioe.2016.00044.

[204] M. Chaouat et al., "A Novel Cross-linked Poly(vinyl alcohol) (PVA) for Vascular Grafts," Adv. Funct. Mater., vol. 18, no. 19, pp. 2855–2861, 2008, doi: 10.1002/adfm.200701261.

[205] I. del Agua, D. Mantione, N. Casado, A. Sanchez-Sanchez, G. G. Malliaras, and D. Mecerreyes, "Conducting Polymer Iongels Based on PEDOT and Guar Gum," ACS Macro Lett., vol. 6, no. 4, pp. 473–478, Apr. 2017, doi: 10.1021/acsmacrolett.7b00104.

Acknowledgements

Firstly, I want to express my gratitude to my supervisor Prof. Mart Min who initiated this project and has been really supportive throughout the years by encouraging and motivating me.

A big thank you goes to my co-supervisor Raul Land, who has advised me at every step along the way – from LabVIEW to spelling. Also, a warm thank you goes to my other co-supervisor, Indrek Must, who has a remarkably wide knowledge specter making the conversations with him fruitful and fascinating. In addition, I would like to thank Kaija Põhako-Esko from Tarty University for all the chemistry-based insight and for being a fantastic role model.

Furthermore, I want to thank everybody in TalTech, TJS department of electronics, who have helped me with their skills and knowledge during my Ph.D. studies; without your guidance, this work would not have been possible.

A big thank you goes to my fellow Ph.D. students Julia Berdnikova, Sander Ulp, Maksim Butšenko, Egon Astra, Eiko Priidel, Kaiser Pärnamets, Marek Rist, Margus Metshein, Rauno Jõemaa, Collins Burton Mwakwata, and Rida Khan. They have made this experience more enjoyable. Thank you for your helpful advice, encouragement, and jokes. Huge thanks go to Ksenija Pesti for being amazingly supportive from the very beginning and also for being such a great friend.

Finally, I want to thank my family and friends for their endless encouragement and for always being there. Thank you, Liisi Tagel, my dear friend, for editing my work and helping me to find motivation. Your dark humor and intelligence have pushed me through the most complex challenges.

Abstract
Development and analysis of carbon-based dry-contact electrodes for bioimpedance measurements

This thesis focuses on developing and testing carbon-based dry-contact electrodes for bioimpedance measurements on biological tissues. In this work, I describe a method for fabricating and testing microneedle-like carbon fiber electrodes that outperform smooth surface carbon electrodes. For this, an effective electrode-skin interface impedance measurement system was developed to provide valuable information about contact quality while allowing tissue characterization to occur almost simultaneously. In addition, multi-layer test phantom material is produced to test alternative semi-dry ionogel carbon electrodes.

Electrodes are a crucial part and still an open study area in the field of non-invasive bioimpedance wearables. In my work, the carbon-silicone composite material was fabricated, and microneedle-like carbon nanofiber and carbon fiber electrodes were formed. The material was tested under cyclic compressive and stretching load, and the electrodes' interface impedance was thoroughly tested with a unique measurement setup. In addition to self-made carbon electrodes, a comparative study was conducted with conventional Ag/AgCl pre-gelled electrodes, Ag/AgCl "dry" metal electrodes, carbon textile electrodes, and FLEXCon® OMNI-WAVE™ carbon sticker electrodes. The comparative results showed that the Ag/AgCl hydrogel electrodes are the most stable (interface impedance does not change remarkably over time, nor is it prone to external influences, like sweat, heat, pressure, or skin condition) and have the shortest stabilization time. "Dry" electrodes showed higher stabilization time and greater variance between interface impedance. The results were similar between self-made CNF/CF-PDMS, OMNI-WAVE™ carbon stickers, and Ag/AgCl "dry" metal electrodes. As CNF/CF-PDMS and OMNI-WAVE™ electrodes are not as rigid as metal electrodes, they have a significant advantage in the world of wearables. However, unlike the dry-contact CNF/CF-PDMS electrodes I developed, OMNI-WAVE™ adhesive electrodes are not reusable.

In addition to developing dry electrodes, semi-dry ionogel electrodes were introduced. Proposed electrolytic gels improved the contact between the electrode and the skin, but the reusability of the developed electrodes was not fully convincing. As the ionic liquid's toxicity level (choline acetate) is still under research, a layered PVA-gelatin test phantom was proposed for comparative measurements. Also, the phantom had one extra feature: a PVA tube to mock an artery. Phantom material proved to be a relatively stable and easy-to-use alternative for the real human hand. Furthermore, PVA mock artery showed a similar pressure-impedance response as real arteries impedance and pressure are inversely proportional. However, for interface impedance measurements and electrode contact assessment, future development is needed to make the top layer of the phantom more dry-skin-like.

The novel electrode interfacial impedance measurement setup used in this study provides a straightforward and quick tool to compare the measurements' quality and electrodes. It is possible to register 4 electrodes' impedances almost simultaneously (4 impedances are registered in 3 seconds). Additionally, give a quick assessment of the placement and contact of the electrodes with the subject under the test; this reveals the contact's quality and whether or not the electrodes are placed correctly.

Furthermore, tissue characterization (e.g., registering impedance change of pulsating artery from the wrist) is possible at the same time. This method contributes comprehensively to the quality assessment of electrodes in bioimpedance measurements, and the technique is applied successfully in current research.

Kokkuvõte
Süsinikmaterjalil põhinevate kuivkontakt-elektroodide arendus ja analüüs bioimpedantsi mõõtmiseks

Antud väitekiri keskendub süsinikul põhinevate kuivkontakt-elektroodide väljatöötamisele ja testimisele, et mõõta bioloogiliste kudede bioimpedantsi. Töös kirjeldan ma meetodit, mis võimaldab valmistada ja testida mikronõelalaadseid süsinikkiud-elektroode, mille kontaktimpedants on sileda pinnaga süsinikelektroodidest oluliselt madalam. Selleks töötasin välja tõhusa elektroodi ja naha ühenduskoha impedantsi mõõtmise süsteemi, mis annab väärtuslikku teavet kontakti kvaliteedi kohta, võimaldades samal ajal mõõta kudede bioimpedantsi. Lisaks arendasin välja mitmekihilise testfantoommaterjali, et testida alternatiivseid poolkuivi ionogeel süsinikelektroode.

Üks äärmiselt oluline osa kantavate, mitteinvasiivsete ja bioimpedantsil põhinevate meditsiiniliste seadmete juures on elektroodid. Nahaga kokkupuutuvate pindelektroodide arendamine on endiselt väljakutsuv ja põnev uurimisvaldkond. Oma töös valmistasin süsinik-silikoon komposiitmaterjali ning valmistasin sellest mikronõelalaadsed süsiknanofiiber ja süsinkfiiberelektroodid. Materjali testisin tsükliliselt surve- ja venituskoormuse all ning elektroodide kontaktimpedantsi analüüsisin põhjalikult uudse arendatud mõõtemeetodiga.

Lisaks isevalmistatud süsinikelektroodidele viisin läbi võrdleva uuringu Ag/AgCl hüdrogeelelektroodide, Ag/AgCl metallelektroodide, süsiniktekstiilelektroodide ja FLEXCon® OMNI-WAVE™ süsinikkleebis-elektroodidega. Võrdlustulemused näitasid, et Ag/AgCl hüdrogeelelektroodid on kõige töökindlamad (kontaktimpedants ei muutu aja jooksul märkimisväärselt, elektroodid ei ole altid välismõjudele nagu niiskus/higi, temperatuuri muutus, surve mõõtmiskohal või naha üleüldine seisund) ja neil on lühim stabiliseerumisaeg. "Kuivad"elektroodid näitasid pikemat stabiliseerumisaega ja suuremat kontaktimpedantsi väärtust. Tulemused olid sarnased isevalmistatud CNF/CF-PDMS, OMNI-WAVE™ süsinikkleebiste ja Ag/AgCl metallelektroodide puhul, aga kuna CNF/CF-PDMS ja OMNI-WAVE™ elektroodid on painduvad ning ei ole nii jäigad kui metallelektroodid, on neil kantavate seadmete maailmas märkimisväärne eelis, sest nad sobituvad paremini liikuvale ja muutuvale kontaktpinnale. OMNI-WAVE™ kleepselektroodid kinnituvad tugevalt naha pinnale ja pärast eemaldamist on elektrood kasutuskõlbmatu, kuid minu välja töötatud kuivkontaktiga CNF/CF-PDMS elektroodidel on korduvkasutatavus võimalik.

Lisaks kuivelektroodide väljatöötamisele võtsin kasutusele poolkuivad ioonvedeliku geelil põhinevad süsinikelektroodid. Valmistatud elektrolüütilised geelid parandasid elektroodi ja naha vahelist kontakti märkimisväärselt, kuid väljatöötatud elektroodide korduvkasutatavus ei olnud täielikult veenev. Edaspidine uurimistöö on vajalik, et täiustada neid uudseid poolkuivi ionogeel elektroode.

Kuna kasutatud ioonse vedeliku (koliinatsetaadi) toksilisuse tase ja ohutus inimkudedele pole veel täielikult selge, siis valmistasin võrdlevateks mõõtmisteks kihilise PVA-l ja želatiinil põhineva testfantoomi. Arendatud testmaterjal osutus üsna stabiilseks ja hõlpsasti kasutatavaks alternatiiviks bioloogilisele koele, kuid kontaktimpedantsi mõõtmiseks ja elektroodide kvaliteedi hindamiseks on vaja fantoomi pealmist kihti edasi arendada, et muuta see kuivale nahale sarnasemaks.

Fantoom sisaldab ka lisafunktsiooni materjali paigutatud PVA toru imiteerib pulseerivat arterit. PVA kunstarter ja fantoom näitasid sarnast rõhu-impedantsi vahelist seost nagu päris arter – impedants ja rõhk on pöördvõrdelises seoses.

Selles töös kasutatud uudne kontaktimpedantsi mõõtemeetod on lihtne ja kiire vahend mõõtmiste ja elektroodide kvaliteedi hindamiseks. Peaaegu üheaegselt on võimalik registreerida nelja elektroodi impedantsi (3 sekundi jooksul registreeritakse 4 impedantsi väärtust) ning anda kiire hinnang elektroodide paigutusele ja kontaktile (milline on kontakti kvaliteet ja kas elektroodid on õigesti paigutatud). Lisaks on samal ajal võimalik mõõta bioimpedantsi (näiteks randmelt pulseeriva arteri impedantsi muutuse registreerimine). Kirjeldatud meetodiga annab antud doktoritöö tervikliku panuse elektroodide kvaliteedi hindamise süsteemi bioimpedantsi mõõtmistel ning seda tehnikat on ka töös edukalt kasutatud.

Appendix 1

I

H. Kõiv, K. Pesti, M. Min, and R. Land. Investigation of cost-effective carbon nanofiber/ carbon fiber and silicone polymer composite material for wearable bioimpedance device. IEEE Sensors Applications Symposium (SAS), pages 1–6, Mar. 2019

Investigation of cost-effective carbon nanofiber/carbon fiber and silicone polymer composite material for wearable bioimpedance device

Hip Kõiv*, Ksenija Pesti, Mart Min, Raul Land

Thomas Johann Seebeck department of electronics
Tallinn University of Technology
Tallinn, Estonia
*hip.koiv@taltech.ee

Abstract—Wearable health monitoring devices have gained more popularity in recent years, but there are still many challenges that need to be solved. Sensors and electrodes that these devices are using are often uncomfortable and not suitable for long-time measurements. This paper investigates carbon nanofiber/carbon fiber and silicone composite material that could be employed as electrodes to register bioimpedance change in the wrist area. Flexible, low-cost and electrically conductive sensors, showed good linear strain sensitivity response when stretched to 100%, but the gauge factor was fairly low (~0.7). Also, investigating impedance change of the composite under compressive loading/unloading presented regular and continuous downward shift suggesting instability. We demonstrate the potential application of fabricated material as electrodes by registering bioimpedance change and comparing it with widely used Ag/AgCl electrodes. Prepared carbon nanofiber and silicone mixture showed promising results as an electrode for wearable device.

Index Terms—bioimpedance, PDMS, carbon nanofiber, carbon fiber.

I. INTRODUCTION

Wearable sensors and monitors are becoming more important in personal health applications because the possibility to make long-time measurements accurately and comfortably is appealing to patients, as well as to health professionals. High blood pressure, also called hypertension, has been recognized as a major health burden and a leading risk factor for stroke [1]. To discover this deadly disease at an early stage, it is necessary to monitor the patient's blood pressure continuously for a longer period. Our research group is working on a wearable device that detects changes in bioimpedance in the wrist area. The hypothesis behind the method says that the bioimpedance signal is similar to aortic blood pressure curve. Therefore, by using transfer functions, we can translate impedance signal into pressure waveform [2]. One problem with correctly detecting the blood pressure from the radial artery, lays in the fact that the used electrodes are stiff and uncomfortable. To measure the bioimpedance change, it is important to have a proper contact with the skin. We want to increase the correct result probability, thus, using electrodes that are stretchable, tightly around the measuring site, but still comfortable for the user, are needed. This paper analyses flexible and stretchable conductive material that could replace the existing electrodes currently in use. Frequent technique how to achieve this kind of stretchable composite, is to add highly conductive fillers into polymer matrix. Polydimethylsiloxane (PDMS), also known as silicone rubber, is often considered as the base material. From the first years when carbon nanotubes were discovered in 1991 by Iijima [3], there have been constant rise in the amount of published papers about different flexible polymers incorporated with carbon nanofillers [4]. These fillers are usually carbon nanotubes (CNT), carbon nanofibers (CNF) and carbon fibers (CF). Carbon nanomaterials have excellent electrical and mechanical properties. In addition, carbon fillers have high aspect ratio (proportional relationship between length and diameter) – CNTs having the highest and CF the lowest. Bigger aspect ratio of the fillers help to form greater number of conductive pathways inside the non-conductive polymeric matrices and as a result, the electrical properties of the composite improve remarkably. However, carbon based fillers tend to agglomerate due to firm van der Waals forces between individual fibers [5]. It is important to disperse these carbon clumps homogeneously inside the polymer to achieve better conductivity on lower concentration of fillers. There are many methods reported to effectively fabricate flexible conductive CNT/CNF/CF composites: acid treatment, grafting modification, treatment by ionic surfactants, milling, and shear mixing [4,6], but herein, we are using less complex and more cost-effective approach. We prepare CNF/CF-PDMS and CF-PDMS mixtures with different filler concentrations and investigate fabricated material's response to strain and pressure loading, electrical properties, stability in time and applicability as bioimpedance electrodes. The goal is to achieve cheap, controllable, and conductive material to use it as comfortable smart electrodes and flexible strain sensors.

II. Materials and Methods

A. Materials

To prepare the flexible conductive material, we are using carbon nanofibers (diameter 100 nm, length 20-200 μm, conical, >98% carbon basis) supplied by Sigma-Aldrich (St. Louis, MO, USA). In addition we used carbon fiber (diameter 7 μm, length 6 mm, SIGRAFIL® C30), which was obtained from GRM Systems (Slatinky, Czech Republic). The silicone elastomer was two part platinum cure liquid silicone (Dragon Skin, Shore 10A) purchased from Smooth-on, Inc. (Macungie, PA, USA). Quickly evaporating silicone oil (SO) solvent, hexamethyldisiloxane (purity 98%) by Sigma-Aldrich (St. Louis, MO, USA) was used to lower the viscosity of the silicone, simplify the mixing process and vacuum degassing. In addition, isopropylalcohol (IPA), also from Sigma-Aldrich, was used as the solvent to break the van der Waals forces between the carbon particles and disperse them better in PDMS.

B. Preparation of simple CNF/CF-PDMS samples

Two-part silicone, A and B part were mixed separately with carbon nanofibers, carbon fibers, and silicone oil using magnetic stirrer for 2 hours. Then the A and B part of the two similar composites were mixed together and mechanically stirred for few minutes. Vacuum degassing removed the trapped air bubbles and the sample cured for 24 hours in room temperature (23°C). Various CNF/CF-PDMS samples were prepared with different carbon filler concentrations (from 2 wt% to 7.7 wt%) to compare the electrical conductivity and mechanical property changes.

C. Preparation of the CNF-PDMS samples

For comparison, samples without CF were prepared to try to improve the stability of the electrical resistivity response. First procedure is similar to CNF/CF-PDMS mixture presented in the previous section, but to enhance the properties even more, we changed the mixing method and used surfactant to disperse the CNFs better. Samples were made using reliable techniques introduced in various published articles [7,8,9]. First, the CNFs were dispersed in IPA solution using sonicator (frequency of 40 kHz, power 30 W) for 15 minutes. Silicone part A was added to the mixture together with silicone oil, and sonicated for another 10 minutes. The mixture becomes homogeneous black paste. Next, IPA is evaporated by placing the composite into vacuum chamber on a hot plate that is heated to IPAs boiling point, which is 82.6°C. Same procedure was repeated to make the B component. To stir the two parts (A part and B part) together more silicone oil (20 wt%) was required for less viscous mixture. After 5 minutes of strong mechanical stirring, the material was vacuum degassed for few minutes to remove the air bubbles and as a last step it cured overnight before the characterisation. Fabricated samples have carbon filler concentrations from 2 to 7.7 wt%.

D. Measurements

Samples were cut into 2x2 cm squares with the thickness of 2 mm (Figure 1a), and placed between two gold-coated electrodes. To apply pressure to the specimens, we used a custom-made CNC device for cyclic loading/unloading (Figure 1b).
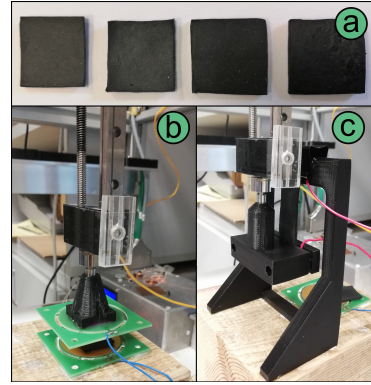

Fig. 1. a - samples cut into 2x2 cm, b – CNC load sensor and sample between two gold-coated electrodes, c – strain sensitivity measurement setup.

Measurements were conducted under the changing load of 0 to 1200g (approximately 0-30 kPa). Top electrode was pressed against the sample at the rate of 5 μm per second, the impedance values (by Impedance Analyzer 6500B series, Wayne Kerr Electronics), and the load values (by CNC load sensor) were registered simultaneously through LabVIEW program. Measurement frequency (10 kHz) was picked so that the the sample would show purely resistive response (phase angle approximately 0°C). Volume resistivity was calculated from the measured impedance with the formula:

$$\rho = R * \frac{A}{l} \tag{1}$$

where ρ is volume resistivity, R is the measured impedance, A is the area of the sample and l is the thickness. For strain measurements, composite with the dimensions of 5 cm (length) x 2 cm (width) x 2 mm (thickness), was strapped between two gold-coated electrodes and tested under cyclic tensile loading/unloading (Figure 1c). The sample was stretched to 100% strain with the rate of 0.1 mm per second and released back to 0% strain with the same step.

III. Results and Discussion

When there is enough carbon nanofibers dispersed inside the PDMS substrate, the effective conductive network is formed and material becomes electrically conductive. Figure 2 shows how resistivity changes with CNF concentrations.

At low CNF content (2 wt%), the resistivity is very high and sparse conductive network is formed. When CNF wt% increases, resistivity rapidly decreases. Samples with CNF concentration of 7.7 wt% depict resistivity values as low as 1.5 Ωm.
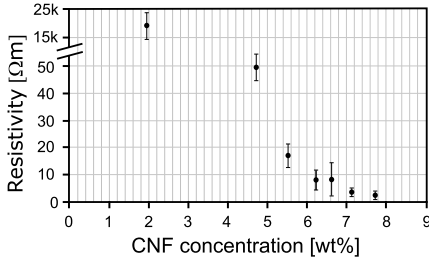
Fig. 2. Different samples with various carbon nanofiber concentrations and their resistivity response.

A. Compressive loading/unloading

Figure 3 shows CNF/CF-PDMS (7 wt%) samples' impedance change with compressive loading/unloading cycles. At first, the contact between the electrode and the sample is light and impedance shows very high values. With every 5 µm step the contact improves and impedance decreases until it reaches the smallest value with maximum loading.
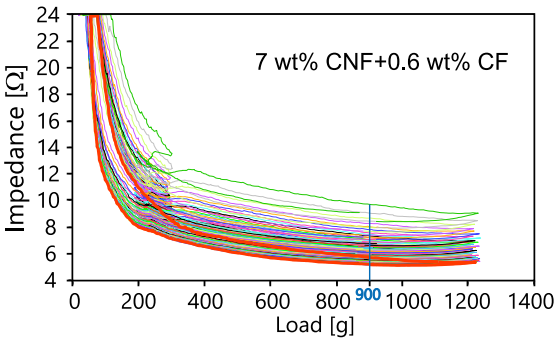

Fig. 3. One sample under 50 compressive loading/unloading cycles and its impedance response.

With stronger compression, more filler particles are pushed together and consequently, numerous conductive pathways are formed inside the composite. Tests revealed the presence of hysteresis because the unloading part of the cycle shows small delay in recovering into its original state forming noticeable impedance loops on the graph (Figure 3). Around 200g of load, the pressure sensor of the CNC machine, displays strong nonlinearity (Figure 3). This is a defect of the device and can be overlooked because the region we are interested in is not influenced. We prepared CNF/CF-PDMS samples with different CNF concentrations and studied their conductivity response to compression. CF concentration varied less between the samples (from 0.55 wt% to 0.6 wt%) and are not brought out separately. If figure 3 depicts one sample with its 50 cycles, then figure 4 depicts conductivity change with each compressive unloading cycle of six different samples. To distinguish between the materials, with every cycle one impedance point

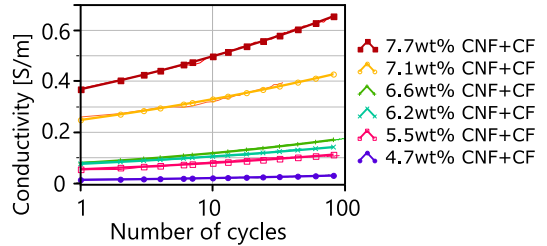is picked when the load is 900g (Figure 3, blue vertical line) and presented on the graph.

Fig. 4. Six different samples with varying concentrations from 4.7 wt% to 7.7% and their conductivity changes with every consecutive cycle.

The thin solid line is the raw data and the dotted line is the fitted trend line of the measured points (Figure 4). The graph confirms that with every consecutive cycle the conductivity increases rapidly suggesting exponential growth. This drift in values slows down, but is not arrested even after 200 cycles, which is the longest data log registered (Figure 8). The results correlate fairly well with previous findings in the literature [10]. Figure 4 also clearly shows how concentration of carbon fillers increase the conductivity remarkably, which is in good agreement with similar researches.
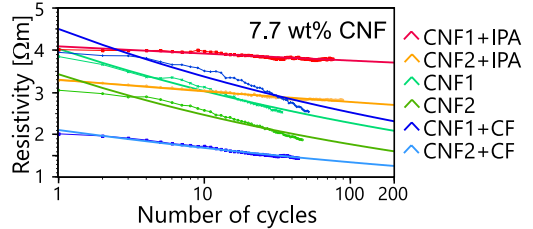

Fig. 5. CNF+IPA (red and orange lines) samples have more stable resistivity response with each consecutive cycle than CNF and CNF+CF mixtures.

Now, if we compare two techniques and different fillers used to make flexible conductive composite material, we see some interesting trends. The first set of analyses depicted on Figure 5 shows samples with the same nanofiber concentration (7.7 wt%) but:

- CNF1+IPA and CNF2+IPA is prepared according to the method introduced in chapter IIC where the ultrasonication is used to disperse the nanofibers inside the IPA;
- CNF1 and CNF2 are fabricated by the method introduced in chapter IIB but without the carbon fiber strands;
- CNF1+CF and CNF2+CF samples are made using the same method as previous, but carbon fibers are added to the composite.

Resistivity values taken from the 10th cycle show a slight difference between the materials. Two separate CNF+CF samples with the same concentrations (Figure 5 - dark blue and light blue lines) show bigger variance in resistivity, 3.4 Ωm and 1.7

Ωm (50%), than CNF samples (Figure 5 – light green and dark green lines), 3 Ωm and 2.5 Ωm (17%) and CNF+IPA samples (Figure 5 – red and orange lines), 4 Ωm and 3 Ωm (25%).

CFs are significantly bigger than CNF particles and it is more difficult to disperse them inside the PDMS uniformly with magnetic stirrer to reach a good repeatability between different mixtures. More interesting observation to emerge from the data comparison was that the CNF+IPA sample resistivity change with compressive cycles was significantly less than with other composites. For example, the CNF1 resistivity changes about 40% from 1-100 cycle, but CNF1+IPA change is as low as 5%. This lets to speculate that the CNF+IPA samples are more stable due to better dispersion of filler particles. Given that our findings are based on limited number of samples it is important to treat these results with considerable caution. Further data collection is required to determine if material produced with IPA and sonication are showing more reliable response. Another instability appeared when the composite that was measured repeatedly during last few months, depicted different resistivity values. Figure 6 presents how resistivity is increasing rapidly with time – after 4.5 months the resistivity is 10.5 times higher than during the first measurement on 25th compressive cycle and slightly less, 9.7 times higher on 200th cycle.
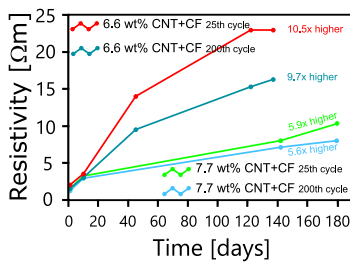

Fig. 6. Aging effect of two separate samples on 25th cycle and 200th cycle.

Aging effect of the samples with IPA and only CNF, are not analysed here, because the time between the first measurement and the last is not so long to make any strong implications. Possible reason for this phenomenon is not completely clear, but one explanation could be that the earlier conductive pathways formed during compressive loading are now blocked because the material is getting more rigid and filler particles are not connecting so easily anymore. Most studies have not focused on the aging issue and research into solving this matter is in progress.

B. Strain sensitivity

To investigate the strain sensing capability of the composed materials, tensile loading tests were conducted and three different samples are depicted in Figure 7 with their relative resistance, $\Delta R/R_0$, and strain, ε. When the specimen is stretched to 100% strain, the relative resistance increases 75% and the response is fairly linear.
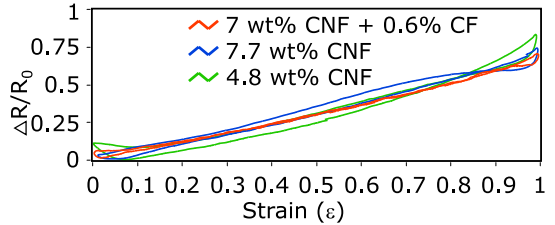

Fig. 7. All tested samples have similar response to stretching and releasing cycles.

All tested samples had similar piezoresistive response and sensitivity to strain. On low strain percentage, the conductive fillers are still attached and resistance is lower, but when strain starts to increase, the fillers are losing their connections with each other and resistance grows. Gauge factor was calculated to describe the sensitivity of samples by using formula:

$$K = (\Delta R/R_0)/\varepsilon \qquad (2)$$

where K is gauge factor, $\Delta R/R_0$ relative resistance change and ε is strain. Gauge factors of all samples are similar, $\sim$ 0.7. Despite the fact that the sensitivity is a great deal lower than reported by other researchers, Wu et al. [8] and Wang et al. [11], the material is still applicable to detect some movements. However, current composite can not be considered as an strain sensor with an expected quality. If it is possible to reduce the filler concentration inside the mixture and still maintain good conductivity, the samples become less rigid and probably the strain sensitivity is better as well [12]. Durability of the fabricated material was tested by repeating the stretching (from unstretched condition) and releasing cycles. After the stretching part of the cycle, the sample showed a small hysteresis effect similarly as it was with compressive loading tests, but returned slowly to its initial state. Figure 8 depicts 207 stretching cycles and its impedance response. With each cycle a stable drift towards lower impedance is observed. The sample does not show signs of stabilizing even after 200th stretching cycle.
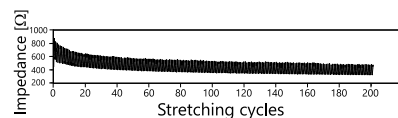

Fig. 8. Impedance is decreasing with every consecutive cycle.

C. Application of CNF/CF-PDMS and CNF-PDMS composite as electrodes

We compared commercially available Ag/AgCl gel electrodes with the prepared flexible and stretchable conductive material. The goal of the experiment was to discover bioimpedance change from the wrist area. For this, four rectangular pieces of the fabricated composite with dimensions

of 1 cm (width) x 1.5 cm (length) x 1.5 mm (thickness) were used as alternative electrodes. They were placed longitudinally on the radial artery and fixed against the wrist with some elastic band for a better contact. To register the bioimpedance change, MFLI Lock-in amplifier (Zürich Instruments), was used. Three simple measurements were conducted on 10 kHz frequency with:

- Ag/AgCl gel electrodes on the wrist;
- CNF/CF-PDMS mock electrodes on the wrist;
- CNF-PDMS mock electrodes on the wrist.

As the production of the stretchable alternative electrode material is still under development, the best result and the cleanest impedance signal was expected from the Ag/AgCl electrodes. We hypothesize that the fabricated electrode material, mixed with carbon fibers, gives also a good response because the long fibers that are sticking out of the base (Figure 9) make good skin-electrode contact by pressing themselves little bit inside the skin.
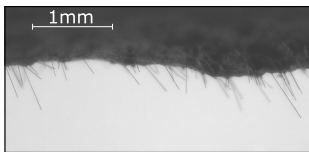
Fig. 9. Carbon fiber strands are sticking out of the base material.

Ag/AgCl electrodes showed reasonably good signal, which can be seen from the Figure 10a. Unfortunately, two experimental electrode materials did not show any understandable impedance change without preparing the skin first. Slightly abrading the wrist to remove the stratum corneum layer improved the signal remarkably and the pulse rate was clearly distinguishable. So far, we got the best response by adding conductive ECG gel for a better contact and this gave a comparable result with Ag/AgCl electrodes (Figure 10b and 10c) as all three sets display impedance variation of $\sim$ 0.1%.

However, this is not particularly surprising, given the fact that the material itself is quite conductive. The problem is not the material, but the skin-electrode interface and special consideration must be given to the contact medium. CNF/CF-PDMS material did not perform better than CNF-PDMS as was hypothesized because the soft carbon fibers probably do not have the strength to impede the skin surface. First preliminary application experiments were not fully successful. Nevertheless, the CNF/CF-PDMS and CNF/PDMS proved to be a stretchable and conductive versatile material that has a prospect as electrodes on wearable devices [13]. Future work will focus on lowering the CNF concentration in the mixture and overcoming the contact problem with the skin. In addition, further data collection is required to verify the biocompatiblity of the proposed electrodes during long-term measurements.

IV. CONCLUSION

Stretchable and flexible carbon nanofiber/carbon fiber silicone rubber composite material was developed by using
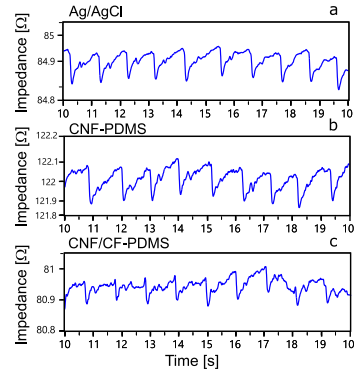

Fig. 10. a - Ag/AgCl electrodes used to measure impedance change, b – carbon nanofiber and PDMS electrodes detecting impedance change, and c – CNF/CF-PDMS electrodes showing the least favorable result in impedance measurements.

simple and cost-effective methods. Material's compressive response to resistivity and strain sensing was investigated. Strain showed linear response but gauge factor was fairly low. The compressive loading/unloading tests revealed that with every consecutive cycle, resistivity of the sample decreases, during unloading, material returns to its initial state. When carbon nanofiber concentration is increased to 7.7 wt%, the conductivity grows as well (to 0.7 S/m) due to bigger number of conductive pathways formed inside. Produced composite was used as electrodes on the radial artery to detect impedance changes with every cardiac cycle. The performance was poor when the skin was not prepared but abrading the measuring site or adding conductive gel improved the electrode-skin contact and impedance change was comparable with Ag/AgCl electrodes. Our investigations into this area are still ongoing, but the first results revealed that with some modifications in the fabricating part, this approach has the potential to improve the wearable health monitoring electronics.

REFERENCES

[1] D. Lackland and M. Weber, "Global Burden of Cardiovascular Disease and Stroke: Hypertension at the Core", Canadian Journal of Cardiology, vol. 31, no. 5, pp. 569-571, 2015.

[2] M. Min, P. Annus, H. Kõiv, A. Krivošei, T. Uuetoa and J. Lamp, "Bioimpedance sensing - a viable alternative for tonometry in non-invasive assessment of central aortic pressure", in 2017 IEEE International Symposium on Medical Measurements and Applications (MeMeA), Rochester, MN, USA, 2017, pp. 373–378.

[3] S. Iijima, "Helical microtubules of graphitic carbon", Nature, vol. 354, no. 6348, pp. 56-58, 1991.

[4] B. Mensah, H. Kim, J. Lee, S. Arepalli and C. Nah, "Carbon nanotube-reinforced elastomeric nanocomposites: a review", International Journal of Smart and Nano Materials, vol. 6, no. 4, pp. 211-238, 2015.

[5] R. Atif and F. Inam, "Reasons and remedies for the agglomeration of multilayered graphene and carbon nanotubes in polymers", Beilstein Journal of Nanotechnology, vol. 7, pp. 1174-1196, 2016.

[6] L. Feng, N. Xie and J. Zhong, "Carbon Nanofibers and Their Composites: A Review of Synthesizing, Properties and Applications", Materials, vol. 7, no. 5, pp. 3919-3945, 2014.

[7] J. Kim, J. Hwang, H. Hwang, H. Kim, J. Lee, J. Seo, U. Shin and S. Lee, "Simple and cost-effective method of highly conductive and elastic carbon nanotube/polydimethylsiloxane composite for wearable electronics", Scientific Reports, vol. 8, no. 1, 2018.

[8] S. Wu, J. Zhang, R. Ladani, A. Ravindran, A. Mouritz, A. Kinloch and C. Wang, "Novel Electrically Conductive Porous PDMS/Carbon Nanofiber Composites for Deformable Strain Sensors and Conductors", ACS Applied Materials Interfaces, vol. 9, no. 16, pp. 14207-14215, 2017.

[9] D. Chung, Carbon composites. Polymer/Matrix Composites: Structure and Processing, 2nd ed. New York: Butterworth-Heinemann, 2017, pp. 161-217.

[10] P. Huang, Z. Xia and S. Cui, "3D printing of carbon fiber-filled conductive silicon rubber", Materials Design, vol. 142, pp. 11-21, 2018.

[11] X. Wang, J. Li, H. Song, H. Huang and J. Gou, "Highly Stretchable and Wearable Strain Sensor Based on Printable Carbon Nanotube Layers/Polydimethylsiloxane Composites with Adjustable Sensitivity", ACS Applied Materials Interfaces, vol. 10, no. 8, pp. 7371-7380, 2018.

[12] Y. Zeng, H. Liu, J. Chen and H. Ge, "Effect of strain on the electrical resistance of carbon nanotube/silicone rubber composites", Journal of Wuhan University of Technology-Mater. Sci. Ed., vol. 26, no. 5, pp. 812-816, 2011.

[13] Y. Liu, H. Wang, W. Zhao, M. Zhang, H. Qin and Y. Xie, "Flexible, Stretchable Sensors for Wearable Health Monitoring: Sensing Mechanisms, Materials, Fabrication Strategies and Features", Sensors, vol. 18, no. 2, p. 645, 2018.

Appendix 2

II

H. Kõiv, K. Pesti, M. Min, R. Land, I. Must. Comparison of the carbon nanofiber-/fiber- and silicone-based electrodes for bioimpedance measurements. In IEEE Transactions on Instrumentation and Measurement, vol. 69, no. 4, pages 1455-1463. IEEE, 2020.

Comparison of the Carbon Nanofiber-/Fiber- and Silicone-Based Electrodes for Bioimpedance Measurements

Hip Kõiv, Ksenija Pesti, Mart Min, *Senior Member, IEEE*, Raul Land, *Member, IEEE*, and Indrek Must

Abstract—**Electrodes for bioimpedance measurements remain a challenge. In practice, commercially available nonpolarizable silver/silver chloride (Ag/AgCl) gel electrodes prove to be the best option for bioimpedance-based testing. The hydrogel layer reduces the problematic electrode–skin interface impedance, which results in a highly reliable signal. Our workgroup is developing a wearable device that estimates aortic blood pressure from the bioimpedance taken from the wrist area. Understandably, wet electrodes do not suit for a wearable, and there is a need for dry, soft, reusable, and stable electrodes. This study proposes stretchable carbon nanofiber/carbon fiber silicone electrodes as an alternative for cardiac signal measurements with bioimpedance. Five different electrode materials are tested and analyzed: Ag/AgCl gel, Ag/AgCl dry, two carbon and silicone composite materials, and carbon textile. To compare the electrodes' characteristics, the current through the tissue under the changing pressure, frequency, contact duration, and skin preparation is registered, and the electrode–skin impedance is calculated. The soft and stretchable carbon fiber silicone electrodes proved to have similar response as rigid nonpolarizable Ag/AgCl dry electrodes. Selected methods and proposed instrumentation ensure acceptable reproducibility of the base value and the modulation depth of the measured impedance despite the different electrode materials, large variation of the electrode–skin impedance, and the actual measurement current.**

Index Terms—**Bioimpedance, carbon nanofiber, carbon fiber, electrodes, electrode–skin interface impedance.**

I. INTRODUCTION

BIOIMPEDANCE measures tissue's resistance to the externally applied electrical current flow and its ability to store electrical charge. Our workgroup is developing a wristwatch that registers impedance change from the radial artery and estimates central aortic blood pressure using transfer

functions. This is a serious challenge because the magnitude of the fluctuating bioimpedance signal registered from the wrist is extremely low and difficult to measure in practice. Besides, the current has to pass two electrode–skin interfaces, but more than 99% of the body's resistance to electrical current flow is at the skin [1]. It is well known that the choice of electrodes will influence the electrical signals that are measured [2], and picking an appropriate electrode for intended use is important. The silver-silver chloride (Ag/AgCl) wet electrodes are mostly used in different bioimpedance applications due to their nonpolarizable nature and excellent contact with the skin [3]. For wearable technology, the Ag/AgCl gel electrodes are not a reasonable choice because desired electrodes have to be reusable, soft, flexible, nonirritable to the patient, and convenient for long-term measurements. Developed cost-effective and stretchable carbon nanofiber-/fiber- and silicone-based material could be used as an alternative. The proposed material was characterized in a previous work published in IEEE Sensors Applications Symposium 2019 Conference Proceedings [4]. We hypothesize that using longer carbon fiber strands that stick out from the carbon–silicone composite will reduce the electrode–skin interface impedance, which will result in stronger and more reliable bioimpedance signals. Previous work on the potential of carbon-based dry electrodes has been carried out, but it tends to focus on ECG, EEG, and EMG electrodes [5]–[8]. Unfortunately, only a few studies target electrodes applicable for bioimpedance-based measurements [9]–[12]. This article investigates how well the developed carbon nanofiber and carbon fiber together with polydimethylsiloxane (CNF/CF-PDMS) material suit for demanding bioimpedance measurements. The aim of this work is to compare and analyze the electrode–skin impedance of newly produced electrodes at different frequencies. In addition, the interface impedance dependence on time, pressure, and skin preparation is determined.

II. MATERIALS AND METHODS

A. Electrode–Skin Impedance

The electrode is the site of the shift from electronic to ionic conduction where the electronic part is the metallic or carbon (electrons as the charge carriers) and the ionic part is the electrolyte gel or tissue liquid (ions as the charge carriers) [13]. Human skin consists of three main layers: stratum
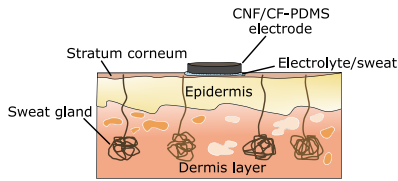
Fig. 1. Three main skin layers: dermis, epidermis, and stratum corneum. CNF/CF-PDMS electrode is placed on the SC, and sweat is accumulating under the electrode through the sweat glands.
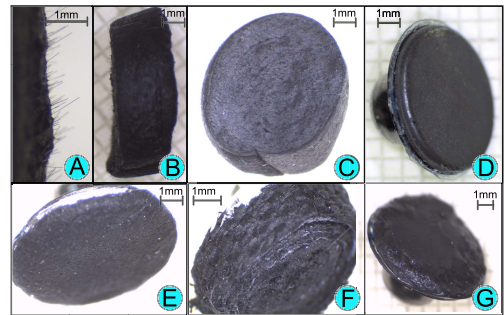

Fig. 2. (a) Close-up of CNF/CF-PDMS electrode from the side when carbon fiber strands are sticking out from the base material. (b) CNF/CF-PDMS electrode from the side. (c) CNF/CF-PDMS electrode pictured from the top. (d) Ag/AgCl dry electrode. (e) CNF/CF-PDMS smooth electrodes without the fiber strands. (f) rolled carbon textile electrode. (g) Ag/AgCl pregelled electrode. Gel is on top of the electrode metal base.

corneum (SC), epidermis, and dermis layer (see Fig. 1). The stratum corneum is the driest layer, and its moisture content is only about 20%, making it a serious obstacle for the current to go through. Luckily, sweat glands that are located in the dermis collect the ions and transport them through the duct into the skin surface lightly moisturizing the SC [14].

The area of the skin that is in contact with the electrolyte solution is called an effective electrode area (EEA) of the electrode, and it is the dominating factor determining electrode–skin impedance [13]. The electrode–skin impedance ($Z_{\text{Electrode–Skin}}$) can be represented by separating it into three different impedances: impedance of electrode material itself ($Z_{\text{Electrode}}$), impedance of the contact medium between the electrode and the tissue (Z_{Contact}), and impedance of the skin under the electrode (Z_{Skin}). Summing them up gives us the total impedance that can be called electrode–skin interface impedance, as mentioned earlier ($Z_{\text{Electrode–Skin}} = Z_{\text{Electrode}} + Z_{\text{Contact}} + Z_{\text{Skin}}$).

High electrode–skin impedance will result in poor signal quality and low signal-to-noise ratio, and it is important to make the contact between the tissue and the electrode as good as possible to minimize the probability of disturbances. Abrading the skin slightly (four to five scrapes with a rough cloth) removes the dead skin cells to some extent, and in theory, this should improve the interface contact [15], [16]. The impedance difference between the abraded and not abraded skin is evaluated in this study.

B. Developed Carbon-Based Dry Electrodes

In the previous article [4], carbon nanofiber and carbon fiber-silicone polymer (CNF/CF-PDMS) was prepared and characterized to test as a possible dry electrode material for bioimpedance measurements. Carbon nanofibers (diameter: 100 nm; length: 20–200 μm; and conical: >98% carbon basis) supplied by Sigma-Aldrich (St. Louis, MO, USA), carbon fibers (diameter: 7 μm and length: 6 mm, SIGRAFIL C30), obtained from GRM Systems (Slatinky, Czech Republic) were mixed with silicone (PDMS) to prepare flexible conductive electrodes. The silicone elastomer was a two-part platinum cure liquid silicone (Dragon Skin, Shore 10A) purchased from Smooth-on, Inc. (Macungie, PA, USA). Quickly evaporating silicone oil (SO) solvent, hexamethyldisiloxane (purity >98%), by Sigma-Aldrich was used to lower the viscosity of the mixture and simplify the mixing process and vacuum degassing. In addition, isopropylalcohol (IPA), also from Sigma-Aldrich, was used as the solvent to break the van der

Waals forces between the carbon particles with sonicator or magnetic stirrer and disperse them better in PDMS.

To compare the developed electrodes and evaluate the suitability of dry carbon material, measurements were made simultaneously with commercial Ag/AgCl gel electrodes and Ag/AgCl dry electrodes (Comepa, France). Ag/AgCl gel electrodes have electrolyte (hydrogel) on the Ag metal base (snap coated with Ag/AgCl), but the dry Ag/AgCl electrodes do not.

Altogether, five different electrodes were assessed (see Fig. 2):

1) CNF/CF-PDMS fiber electrodes [see Fig. 2(a)–(c)];
2) Ag/AgCl dry electrodes [see Fig. 2(d)];
3) CNF/CF-PDMS electrodes with the smooth surface [see Fig. 2(e)];
4) Carbon textile electrodes (Zorflex FM101L100— 0.4 mm) [see Fig. 2(f)];
5) Ag/AgCl gel electrodes [see Fig. 2(g)].

The difference between the smooth surface electrodes and fiber electrodes is not the material itself but rather the material's preparation for further usage. In the case of fiber electrodes, the sample is rolled into a solid cylinder, and round electrodes are cut from it with a sharp scalpel. This method is used to make the carbon textile electrodes as well. The cutting edge reveals longer fiber strands (originally 6 mm) that are now sticking out from the base material [see Fig. 2(a)]. Smooth CNF/CF-PDMS does not have the cut edge, which means that the fiber strings are only inside the sample.

C. Measurement Setup

The most important variable when comparing the dry electrodes is the electrode–skin impedance [17], [18]. It is valuable to know what is happening between the skin and the electrodes to assess the measurement itself and the materials used.

The measurements were conducted on room temperature (approximately 23 °C) by using a four-electrode setup to minimize the effect of the electrodes' polarization [13] during determining the base impedance (Z_0). The forearm of a healthy female (Northern European white) was cleaned with
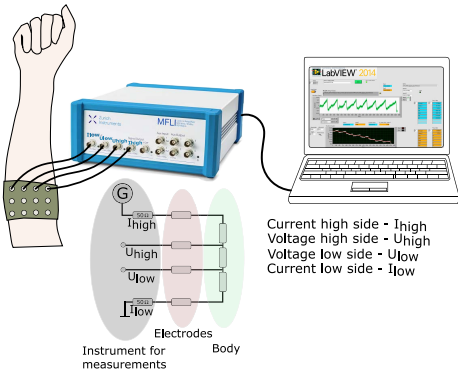
Fig. 3. Measurement setup consisting of MFLI lock-in amplifier, electrode sets on the forearm, and a computer for LabVIEW software.
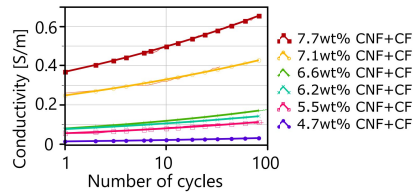

Fig. 4. Six different CNF/CF-PDMS samples with varying carbon concentrations from 4.7 wt% to 7.7%, and their conductivity change with every consecutive cycle.

III. RESULTS

A. Electrode Material Characterization

In the previous work [4], the proposed electrode material was characterized. Developed material was first tested under the compressive loading/unloading cycles and stretched/released for the strain response. These experiments showed much instability, such as aging effect, hysteresis, and impedance decrease, with consecutive loading/unloading cycles. However, the prepared composite showed good conductivity (up to 0.7 S/m), gauge factor around 0.7, and a preliminary application as bioimpedance electrodes showed promising results. Fig. 4. shows the CNF/CF-PDMS material with different carbon concentrations and conductivity change under the changing load from 0-30 kPa.

B. Frequency Response

As the bioimpedance parameter is frequency dependent [20]–[22], the impedance spectrum of the whole electrode-body system should be characterized. Fig. 5 depicts the above-mentioned spectra (from 10 kHz to 10 MHz) for five different electrode sets (introduced in Section II-B).

The CNF/CF-PDMS electrode set was tested twice—on abraded and not abraded skin. Four out of five electrode sets give very similar base impedance (Z_0—measured between the two sensing electrodes U_{low} and U_{low}) response over the frequency sweep. At 10 kHz, the base impedance is around 100 Ω. It starts to decrease until it reaches 25 Ω at 10 MHz. The phase angle is around $-20°$ (in frequency range from 70 kHz to 1.5 MHz), which means that the imaginary part of the impedance is about 1/3 of the real part. At frequencies above 1.5 MHz, the capacitive effect becomes more prominent.

At 1.5 MHz, the observable strong discontinuity of the impedance curves is caused by the Keysight E4990A autoranging function and can be ignored in our experiments. The textile electrode set shows a different response than others (see Fig. 5—brown line). Until 100 kHz, the base impedance is much higher (at 10 kHz twice as much) compared with other electrodes even though all the measurement conditions were the same. Besides, the phase angle displays bigger capacitive behavior (starts from $-60°$ at 10 kHz). Presumably, the capacitive behavior can be explained by the fact that there is an unreliable contact with the skin because the textile has air between the threads. As carbon textile is hydrophilic, it absorbs the moisture into its yarns not leaving enough

ethanol prior 30 min to the testing. The subject under the test had no cardiovascular diseases, the body temperature was 36.6°, body mass was 61 kg, and body mass index (BMI) was 20.9. In all cases, the participant's consent was obtained.

Fig. 3 depicts the measurement setup. Measurements were arranged so that it was possible to evaluate three different electrodes sets sequentially without removing or moving the electrodes from the skin surface (during every measurement series only one electrode set was connected to the instrument).

Three columns (four electrodes of the same material in a row) of electrodes are placed on the inner side of the forearm where the skin is less hairy and more homogeneous [19]. The electrodes were attached to a stretchy textile for comfortable quick setup and for a firm hold around the arm. The distance between the electrodes was 1 cm for both directions. The wires were soldered to the metal buttons that hold the metal circular snap (7 mm), making the same contact surface dimensions for all the tested electrodes. The actual electrode is glued with Ag-based conductive paint on the metal base snap.

MFLI lock-in amplifier (Zürich Instruments) configured as the four-electrode measurement system registers the potential difference between the two sensing electrodes (depicted as U_{low} and U_{low} in Fig. 3) and the current through the current electrodes (depicted as I_{low} and I_{low} in Fig. 3).

The excitation voltage was 3 V_{pk}, and two different frequencies (10 and 70 kHz) were applied. Given the fact that the impedance signal taken from the forearm showed a cardiac pulse, the MFLI instrument was configured to operate with 100-Hz sixth-stage low-pass filter; 100 points per period proved to be enough to assess the resulting signals. Keeping the excitation voltage constant, it was possible to check which electrode set provides the best contact with the skin (has the highest current value flowing through the tissue—named "measured current" on the graphs). All the registered values were saved by LabVIEW software, where the electrode–skin interface impedance is estimated. In addition to measurements made with the MFLI amplifier, the Keysight E4990A impedance analyzer was used to determine the frequency response from 10 kHz to 10 MHz.
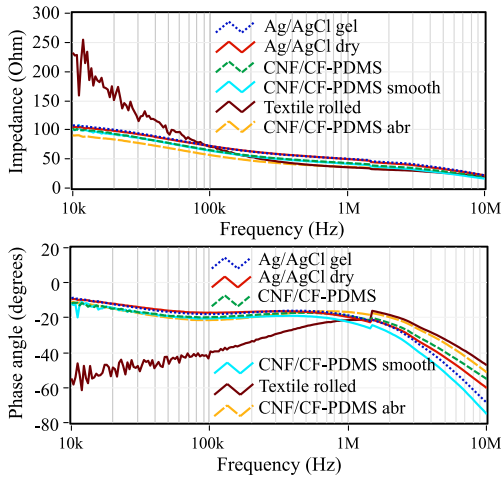
Fig. 5. Upper graph showing base impedance change from 10 kHz to 10 MHz, and a lower graph shows the phase angle change between the same frequency areas. Four electrode sets show a very similar response, but textile electrode has strong capacitive behavior until around 100 kHz.

Fig. 6. Time dependence of the measured current of five different electrodes that are measured on 10 and 70 kHz.

electrolytes (sweat) on the surface of the skin. At first glance (from the results in Fig. 5), this effect is not desired, but in theory, the interface impedance between two hydrophilic environments (skin and textile) is lower. Moisture absorption in the carbon textile increases the conductive ionic components in the material, and already existing ions become mobile. To emphasize this effect, the textile will be infused with various liquid agents in future research for an improved result.

The stratum corneum layer gives large impedance in series with the viable skin, dominating the measurement at low frequencies (below 10 kHz) [23]. From the conducted frequency sweep, the distinctive moment (phase angle of the Z_0 reaches saturation) of base impedance (Z_0) is at 70 kHz. Based on these two criteria, the frequencies 10 and 70 kHz were selected for further experiments.

C. Time Dependence of the Measurements

When sweat accumulates under the electrodes, it fills the caps between the electrode and the skin layer, making an effective electrolyte area. This reduces the electrode–skin impedance and is strongly dependent on time [24]. To observe the change, the electrodes were placed on the forearm, and currents at 10 and 70 kHz were registered every few minutes (as shown in Fig. 6). The measured current response with time is very similar on both frequencies except that at 70 kHz, the current values are almost twice as much as on 10 kHz. With gray, the measured dependence on time is depicted for textile electrodes. It shows the lowest current that is going through the skin compared with other tested electrodes (less than 0.1 mA at 10 kHz and around 0.25 mA at 70 kHz). The current does not change significantly with the time, suggesting that there is no effective electrolyte layer composing after 95 min. With red, the current through the CNF/CF-PDMS
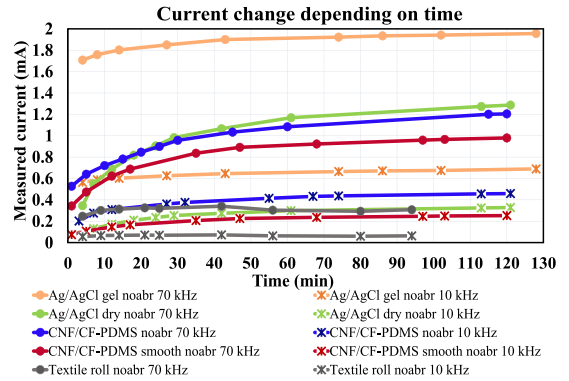
smooth electrode is presented. The current is higher than it was with textile—starts from 0.1 mA and reaches 0.25 mA (from 0.35 to 0.9 mA at 70 kHz) with 120 min. With first 30 min, since the electrodes are placed on the hand, electrode–skin impedance reduces remarkably. After that, it starts to reach its saturation point, and the measured current stabilizes. This behavior is evident for three dry electrode variants (CNF/CF-PDMS smooth, CNF/CF-PDMS fiber, and Ag/AgCl dry), suggesting their similar interface impedance rate change in time. At 70 kHz, CNF/CF-PDMS fiber electrodes (blue line with circles) have a comparable response as Ag/AgCl dry electrodes (green line with circles)—measured current magnitude reaches to 1.2 mA with 120 min. At 10 kHz, Ag/AgCl dry electrodes' measured current values are more similar to CNF/CF-PDMS smooth electrodes. Ag/AgCl gel electrodes have a noticeably different response. First, when the electrodes are placed on the skin, the measured current is around 0.6 and 1.8 mA (at 10 and 70 kHz accordingly), but with few minutes, the electrodes start to reach their saturation point, and the current going through the tissue is as high as 0.7 mA at 10 kHz and around 2 mA at 70 kHz. This is 50%–75% higher than the dry electrodes' values.

D. Abrading the Skin

Abrading the stratum corneum and removing the dry outermost layer of the dead skin cells reduce the skin impedance. At 10 kHz, the average $Z_{Electrode-Skin}$ is for most of the tested electrodes roughly 12% lower and at 70 kHz, about 16% lower than without abrading. In Fig. 7, the lines show the same electrodes' average electrode–skin impedance change with time.

The lines with circles are measured when the skin was abraded (abr) and the lines with diamonds when no prior abrasion (noabr) was used. The electrode–skin impedance for one textile electrode when the skin is not abraded is, on average, approximately 30 kΩ at 10 kHz (6 kΩ at 70 kHz). Abrading the skin reduces the impedance to around 22 and 5.5 kΩ at 10 and 70 kHz accordingly. Textile electrode response is not
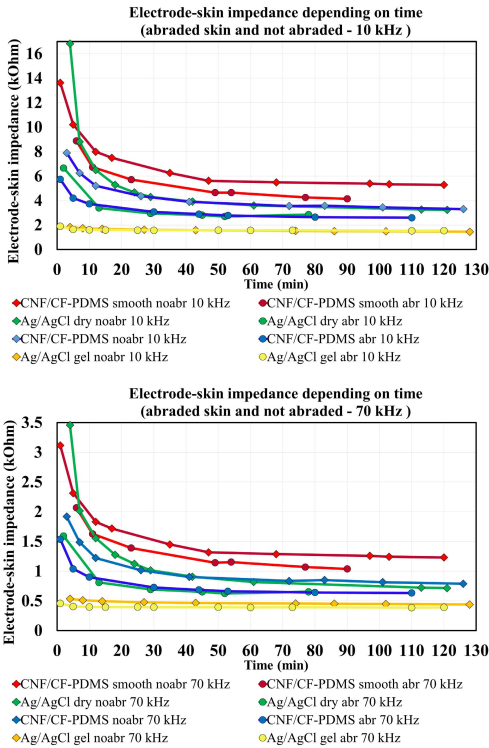
Fig. 7. Electrode–skin impedance for abraded skin and not abraded skin. Comparison between four different electrodes: Ag/AgCl gel, Ag/AgCl dry, CNF/CF-PDMS smooth, and CNF/CF-PDMS fiber.

Fig. 8. Measured current dependence on time when 10.6 kPa of pressure is applied on the contact electrodes, and no external pressure is applied.

depicted on the graph because its average impedance is many times larger than for the other electrodes.

Again, the response is more similar between the CNF/CF-PDMS and Ag/AgCl dry electrodes. Average $Z_{Electrode-Skin}$ without abrasion is 3.8 kΩ at 10 kHz and 900 Ω at 70 kHz. Abrading the skin reduces the contact impedance approximately 23% and 24% on different measurement frequencies. Smooth electrodes have higher average electrode–skin impedance (red lines in Fig. 7), but abrading improves the contact as well (approximately 17% at 10 kHz and 15% at 70 kHz). Gel electrodes are not significantly influenced by abrading; for both, the average impedance is around 1.6 kΩ and 400 Ω at 10 and 70 kHz, respectively.

E. Pressure Dependence

Previous researches [12], [25] have noticed that the pressure on the electrodes improves the effective contact area and reduces interface impedance. Two separate measurements were conducted where the pressure on the electrodes influenced current through the tissue:

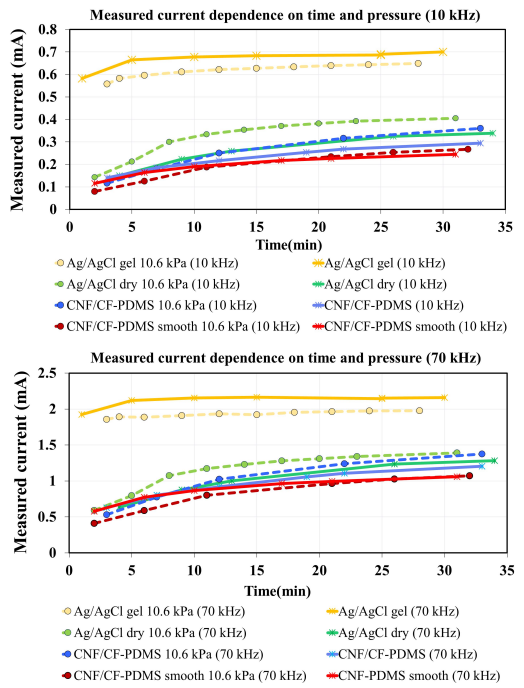1) constant pressure (10.6 kPa) applied on the electrodes (see Fig. 8);

2) external pressure from 0 to 32 kPa with the step of 2.1 kPa applied to the electrodes (see Fig. 9).

The forearm part of the hand was laying on the armrest, and a long plastic band was placed over the electrodes so that it was possible to hang weights on the extra strap. The weights varied from 100 to 1500 g, and the pressure on the electrodes was distributed according to the area that the strap covered. One set of electrodes (four electrodes) had a maximum of 32 kPa of force applied to them, and it was assumed that the applied pressure distributes evenly.

Four different electrode sets were compared: Ag/AgCl dry, Ag/AgCl gel, CNF/CF-PDMS smooth, and CNF/CF-PDMS fiber electrodes. Table I gives an overview, in percentages, on how the actual measured current is changing with the pressure and without the external pressure in approximately 30 min. In Fig. 8 (70 kHz), yellow lines are representing Ag/AgCl gel electrodes having the least effect on the current when pressure is applied—current increases 12% with 30 min.

When only the textile band is holding, the gel electrodes in place (around 2 kPa, which is considered as "no pressure") current increased 7%. The soft CNF/CF-PDMS fiber and smooth electrodes are more dependent on pressure. Blue dotted line (see Fig. 8) shows the fiber electrode's difference in the measured current when 10.6 kPa is applied—change is as high as 160%. Without the pressure, the measured current increases 56% in 33 min. Smooth carbon polymer gives a similar response (see the red lines in Fig. 8). At 70 kHz,

TABLE I

MEASURED CURRENT DEPENDENCE ON TIME IN PERCENTAGES WHEN
PRESSURE IS APPLIED ON THE CONTACT ELECTRODES AND
NO PRESSURE IS APPLIED

	Pressure 10.6 kPa	No pressure	Pressure 10.6 kPa	No pressure
	10 kHz		70 kHz	
Ag/AgCl gel	16%	20%	7%	12%
Ag/AgCl dry	185%	190%	140%	137%
CNF/CF-PDMS	120%	110%	160%	56%
CNF/CF-PDMS smooth	233%	111%	185%	86%

TABLE II

MEASURED CURRENT GROWTH WHEN INCREASING PRESSURE
IS APPLIED ON THE ELECTRODES (IN %)

	10 kHz	70 kHz
Ag/AgCl gel	4.4%	4.7%
Ag/AgCl dry	4.5%	2.2%
CNF/CF-PDMS	9.9%	8.3%
CNF/CF-PDMS smooth	17.8%	16.0%

Ag/AgCl dry electrode values grow approximately 140% with 32 min, when pressure is applied, and 137%, when external pressure is not affecting the measurements. As these percentages are almost the same, it gives the expression that the rigid silver electrodes are not so pressure dependent as soft carbon electrodes. With the second pressure experiment, the electrode sets that have reached to their interface impedance saturation were compared. The electrodes had been on the hand for 2.5 h before growing pressure with the step of 2.1 kPa was applied on the electrodes until it became uncomfortable for the subject under the test (the maximum pressure was 32 kPa). The change with the pressure is depicted in Fig. 9, and changes in percentages are given in Table II.

The change in current is small (approximately 5%) for Ag/AgCl gel and Ag/AgCl dry electrodes. The measured current through the CNF/CF-PDMS fiber electrodes increased around 10% with growing pressure and through smooth CNF/CF-PDMS electrodes slightly more—approximately 18%.

These two experiments do not give a fully comprehensive understanding how much the pressure is influencing the electrode–skin contact, but it has a positive effect to some extent. Especially, when the dry electrodes are freshly placed on the hand, it reduces the time until the measured current reaches its saturation point. It is valuable to have some reasonable pressure on the dry electrodes, but it should not cause distress to the person under the test. Level of pressure can be different for various electrodes; as for rigid metal ones, it has to be lower, and for stretchable soft CNF/CF-PDMS electrodes, it can be higher. However, it should not be more than 6 kPa according to our experiments conducted.

F. Cardiac Signal

All of the above-mentioned properties (time, abrasion, and pressure) change the electrode–skin interface impedance, but the base impedance signal (Z_0) can be influenced as well.
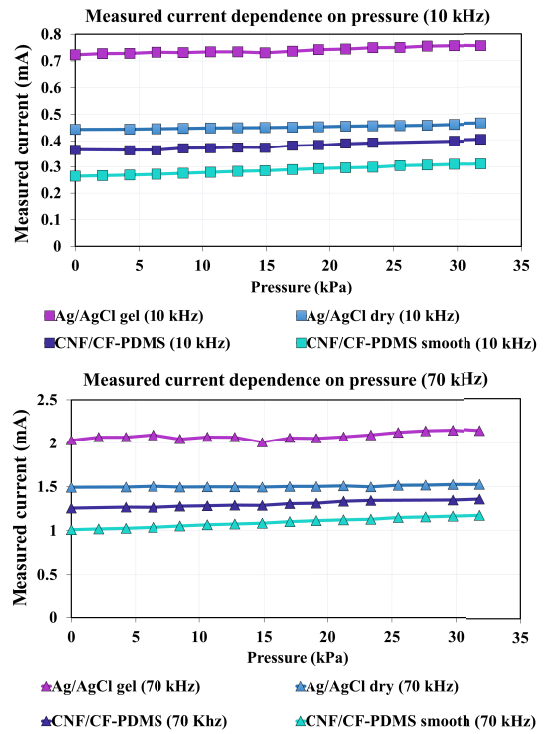

Fig. 9.   Measured current dependence on the changing pressure. The electrodes stayed on the skin for 2.5 h before applying the external pressure.

It can appear in the signal-to-noise ratio (rms noise, %) or impedance signal change (ΔZ) due to cardiac pulse (max–min, %). In Fig. 10, three base impedance signals that were registered with the CNF/CF-PDMS, Ag/AgCl dry, and Ag/AgCl gel electrodes are compared. All three variants clearly show a cardiac signal. The ΔZ is very minuscule—around 0.060%, but it is evident already 1 min after the electrodes were placed on the forearm. The impedance change is so small because there are no arteries close to the surface under the sensing electrodes. When the same electrodes are placed on the wrist area, where the radial artery is very close to the surface, it will show ΔZ around 0.2%, as shown in previous research [4]. With time, the noise (rms, % value from the desired signal) decreases, and the signal becomes clearer. For all three signals, these values (rms% and max–min%) are very similar. Except that the gel electrode signal is more stable and reliable. For dry electrodes, it depends more on the placement and time on the hand, and the cardiac signal is not so straightforward and predictable as it is with gel electrodes.

IV. DISCUSSION

Five different electrode materials were compared to evaluate the developed CNF/CF-PDMS fiber electrodes. When observing the change in current through the tissue, which depends on the electrode–skin impedance, it is possible to get a quick
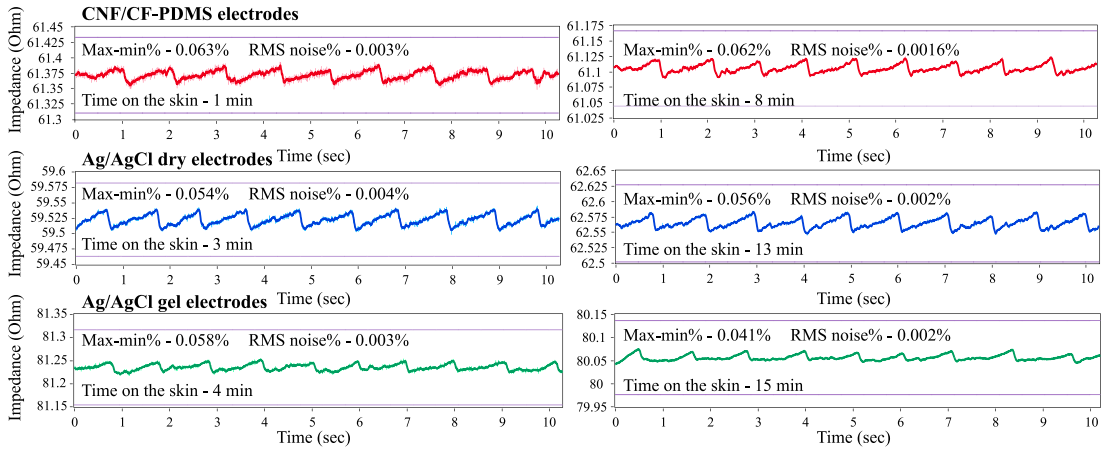
Fig. 10. Typical base impedance (Z_0) signals that are measured with the CNF/CF-PDMS, Ag/AgCl dry, and Ag/AgCl gel electrodes. All the measurements show a small cardiac pulse (measured from the inner side of the forearm). Graphs show how, with time, the signal gets slightly less noisy.

and valuable overview of the quality and suitability of the electrodes. The electrode–skin impedance of all the tested materials depends on the pressure on the electrodes, contact duration, preparation of the skin beforehand (abrasion), and frequency.

Other factors can influence $Z_{\text{Electrode}-\text{Skin}}$, especially the different physiological or health conditions the subject under the test can have, for example, hyperthermia, hypothermia, the thickness of the fat layer on the forearm, and the age. In addition, electrode positions and moving artifacts can become a major concern. These points were not discussed in the scope of this article but will be addressed in future studies.

The measurements showed that Ag/AgCl gel electrodes have the lowest $Z_{\text{Electrode}-\text{Skin}}$ and pass the current with less overvoltage than most other electrodes. In addition, the hydrogel on top of the electrode plate fills out spaces between the tissue and the base making the contact more stable. Dry electrodes, such as CNF/CF-PDMS, do not have the extra layer of electrolyte or hydrogel added to the base material, and contact problems can occur. Besides, this results in higher electrode–skin interface impedance. Fortunately, the tissue has a tendency to produce sweat making natural electrolyte between the electrode and the skin, leading to reduced interface impedance and improving the signal quality to some extent. This phenomenon takes time to develop and has multiple uncertainties. However, the primary goal was to evaluate the dry CNF/CF-PDMS fiber electrode's quality by comparing the results with other possible materials. Textile electrodes showed very high impedance values, but in future research, the moisture level of the electrode itself will be increased to enhance the contact with the skin. As the texture of the carbon textile is rougher than the silicone electrodes. it has a good advantage when making semidry electrodes. Tests revealed that Ag/AgCl dry electrode and CNF/CF-PDMS fiber electrode have very similar time dependence of the interface impedance response, abrasion, and force. On the

other hand, similar CNF/CF-PDMS smooth electrodes gave higher $Z_{\text{Electrode}-\text{Skin}}$ values in every experiment, suggesting that our hypothesis proves to be correct. Fibers sticking out from the base material enhance the contact interface between the skin and the electrode, making CNF/CF-PDMS dry fiber electrodes a considerable alternative for bioimpedance measurements. Also, as soft electrodes adapt well to different shapes, stretchable material has a clearly favored position for wearable applications. To further the current research, we will concentrate on the process of investigating and producing nondryable gel that can be used between the carbon fiber strands for more stable contact with the skin. This small amount of gel would turn the dry electrodes into semidry electrodes [26]; nevertheless, they would be reusable and applicable for long-term use.

V. CONCLUSION

A stretchable carbon nanofiber/carbon fiber silicone rubber composite material to use as electrodes for bioimpedance measurements was developed. To test the quality of the electrodes, five different materials were compared, and their electrode–skin interface impedance change with contact duration, abrasion of the skin, frequency, and pressure was determined. The CNF/CF-PDMS fiber electrodes proved to be comparable to nonpolarizable Ag/AgCl dry electrodes. Textile electrodes and the CNF/CF-PDMS smooth electrodes showed higher electrode–skin impedance due to poor contact with the measurement site. Ag/AgCl gel electrodes were indisputably the best electrodes tested as the electrode–skin impedance was the lowest—1.6 kΩ at 10 kHz and 500 Ω at 70 kHz. Results, so far, have been encouraging, and even though the nonpolarizable Ag/AgCl dry electrodes had a similar response as CNF/CF-PDMS fiber electrodes, the developed material is more suitable for the wearable type of devices considering the softness and stretchability.

REFERENCES

[1] R. M. Fish and L. A. Geddes, "Conduction of electrical current to and through the human body: A review," *Eplasty*, vol. 9, p. e44, Oct. 2009.

[2] M. Rahal, J. Khor, A. Demosthenous, A. Tizzard, and R. Bayford, "A comparison study of electrodes for neonate electrical impedance tomography," *Physiolog. Meas.*, vol. 30, no. 6, pp. S73–S84, 2009, doi: 10.1088/0967-3334/30/6/s05.

[3] M. R. Neuman, "Biopotential electrodes," in *Medical Instrumentation: Application and Design*, J. G. Webster, Ed., 3rd ed. New York, NY, USA: Wiley, 1998, pp. 183–232, doi: 10.1201/9781420003864.ch47.

[4] H. Kõiv, K. Pesti, M. Min, and R. Land, "Investigation of cost-effective carbon nanofiber/carbon fiber and silicone polymer composite material for wearable bioimpedance device," in *Proc. IEEE Sensors Appl. Symp. (SAS)*, Mar. 2019, pp. 1–6, doi: 10.1109/SAS.2019.8706026.

[5] F. J. Romero *et al.*, "Inexpensive and flexible nanographene-based electrodes for ubiquitous electrocardiogram monitoring," *NPJ Flexible Electron.*, vol. 3, no. 1, p. 12, 2019, doi: 10.1038/s41528-019-0056-2.

[6] T. Kim, J. Park, J. Sohn, D. Cho, and S. Jeon, "Bioinspired, highly stretchable, and conductive dry adhesives based on 1D-2D hybrid carbon nanocomposites for all-in-one ECG electrodes," *ACS Nano*, vol. 10, no. 4, pp. 4770–4778, 2016, doi: 10.1021/acsnano.6b01355.

[7] A. A. Chlaihawi, B. B. Narakathu, S. Emamian, B. J. Bazuin, and M. Z. Atashbar, "Development of printed and flexible dry ECG electrodes," *Sens. Bio-Sens. Res.*, vol. 20, pp. 9–15, Sep. 2018, doi: 10.1016/j.sbsr.2018.05.001.

[8] H.-C. Jung *et al.*, "CNT/PDMS composite flexible dry electrodesfor long-term ECG monitoring," *IEEE Trans. Biomed. Eng.*, vol. 59, no. 5, pp. 1472–1479, May 2012, doi: 10.1109/TBME.2012.2190288.

[9] S. Kaufmann, G. Ardelt, and M. Ryschka, "Measurements of electrode skin impedances using carbon rubber electrodes-first results," *J. Phys., Conf. Ser.*, vol. 434, no. 1, 2013, Art. no. 012020, doi: 10.1088/1742-6596/434/1/012020.

[10] G. Medrano, A. Ubl, N. Zimmermann, T. Gries, and S. Leonhardt, "Skin electrode impedance of textile electrodes for bioimpedance spectroscopy," in *Proc. 13th Int. Conf. Electr. Bioimpedance 8th Conf. Electr. Impedance Tomogr.*, 2007, pp. 260–263, doi: 10.1007/978-3-540-73841-1_69.

[11] J. C. Marquez, F. Seoane, E. Välimäki, and K. Lindecrantz, "Comparison of dry-textile electrodes for electrical bioimpedance spectroscopy measurements," *J. Phys., Conf. Ser.*, vol. 224, no. 1, 2010, Art. no. 012140, doi: 10.1088/1742-6596/224/1/012140.

[12] R. Kusche, S. Kaufmann, and M. Ryschka, "Dry electrodes for bioimpedance measurements—Design, characterization and comparison," *Biomedical Phys. Eng. Express*, vol. 5, no. 1, 2018, Art. no. 015001, doi: 10.1088/2057-1976/aaea59.

[13] O. G. Martinsen and S. Grimnes, *Bioimpedance and Bioelectricity Basics*. New York, NY, USA: Academic, 2011, doi: 10.1016/b978-0-12-303260-7.x5000-x.

[14] F. Lu *et al.*, "Review of stratum corneum impedance measurement in non-invasive penetration application," *Biosensors*, vol. 8, no. 2, p. 31, 2018.

[15] W. Olson, D. Schmincke, and B. Henley, "Time and frequency dependence of disposable ECG electrode-skin impedance.," *Med. Instrum.*, vol. 13, no. 5, pp. 269–272, 1979.

[16] H. de Talhouet and J. G. Webster, "The origin of skin-stretch-caused motion artifacts under electrodes," *Physiolog. Meas.*, vol. 17, no. 2, p. 81, 1996, doi: 10.1088/0967-3334/17/2/003.

[17] A. Bosnjak, A. Kennedy, P. Linares, M. Borges, J. McLaughlin, and O. J. Escalona, "Performance assessment of dry electrodes for wearable long term cardiac rhythm monitoring: Skin-electrode impedance spectroscopy," in *Proc. 39th Annu. Int. Conf. IEEE Eng. Med. Biol. Soc. (EMBC)*, Jul. 2017, pp. 1861–1864, doi: 10.1109/EMBC.2017.8037209.

[18] B. Taji, S. Shirmohammadi, V. Groza, and I. Batkin, "Impact of skin–electrode interface on electrocardiogram measurements using conductive textile electrodes," *IEEE Trans. Instrum. Meas.*, vol. 63, no. 6, pp. 1412–1422, Jun. 2014, doi: 10.1109/tim.2013.2289072.

[19] Y. N. Kalia, F. Pirot, and R. H. Guy, "Homogeneous transport in a heterogeneous membrane: Water diffusion across human stratum corneum *in vivo*," *Biophys. J.*, vol. 71, no. 5, pp. 2692–2700, 1996. Avaialable: 10.1016/S0006-3495(96)79460-2.

[20] H. Caytak, A. Boyle, A. Adler, and M. Bolic, "Bioimpedance spectroscopy processing and applications," in *Encyclopedia of Biomedical Engineering*. Oxford, U.K.: Elsevier, 2019, pp. 265–279, doi: 10.1016/b978-0-12-801238-3.10884-0.

[21] L. Yang *et al.*, "The frequency spectral properties of electrode-skin contact impedance on human head and its frequency-dependent effects on frequency-difference EIT in stroke detection from 10Hz to 1MHz," *PloS ONE*, vol. 12, no. 1, 2017, Art. no. e0170563, doi: 10.1371/journal.pone.0170563.

[22] J. Rosell, J. Colominas, P. Riu, R. Pallas-Areny, and J. G. Webster, "Skin impedance from 1 Hz to 1 MHz," *IEEE Trans. Biomed. Eng.*, vol. 35, no. 8, pp. 649–651, Aug. 1988, doi: 10.1109/10.4599.

[23] Ø. Martinsen, S. Grimnes, and E. Haug, "Measuring depth depends on frequency in electrical skin impedance measurements," *Skin Res. Technol.*, vol. 5, no. 3, pp. 179–181, 1999, doi: 10.1111/j.1600-0846.1999.tb00128.x.

[24] D. E. Bahr *et al.*, "Miniature ambulatory skin conductance monitor and algorithm for investigating hot flash events," *Physiolog. Meas.*, vol. 35, no. 2, p. 95, 2014, doi: 10.1088/0967-3334/35/2/95.

[25] B. Taji, A. D. Chan, and S. Shirmohammadi, "Effect of pressure on skin-electrode impedance in wearable biomedical measurement devices," *IEEE Trans. Instrum. Meas.*, vol. 67, no. 8, pp. 1900–1912, Aug. 2018.

[26] G. Li, S. Wang, and Y. Y. Duan, "Towards conductive-gel-free electrodes: Understanding the wet electrode, semi-dry electrode and dry electrode-skin interface impedance using electrochemical impedance spectroscopy fitting," *Sens. Actuators B, Chem.*, vol. 277, pp. 250–260, 2018, doi: 10.1016/j.snb.2018.08.155.

Hip Kõiv was born in Kanepi, Estonia, in 1990. She received the B.S. degree in electronics and bionics and the M.Sc. degree in electronics and communication from the Tallinn University of Technology, Tallinn, Estonia, in 2013 and 2015, respectively, where she is currently pursuing the Ph.D. degree with the Thomas Johann Seebeck Department of Electronics.

Her research interests include the bioimpedance study, aortic blood pressure measurements, and the materials for developing biological phantoms.

Ksenija Pesti was born in Kunda, Estonia, in 1985. She received the B.S. degree in electronics and bionics and the M.Sc. degree in electronics and biomedical engineering from the Tallinn University of Technology (TalTech), Tallinn, Estonia, in 2006 and 2009, respectively, where she is currently pursuing the Ph.D. degree with the Thomas Johann Seebeck Department of Electronics.

Her current research interests are covering the fields of bioimpedance measurement, biomedical sensors, and simulation toward the medical sensor solutions.

Mart Min (Senior Member, IEEE) received the Diploma Engineer's qualification in electronics from the Tallinn University of Technology, Tallinn, Estonia, in 1969, and the Ph.D. degree in measurement science from the Kiev Polytechnic, Kiev, Ukraine, in 1984.

He has been with the Thomas Johann Seebeck Department of Electronics, Tallinn University of Technology, as a Professor and a Leading Scientist, since 1992. From 1992 to 1993, he was with the Technical University of Munich, Munich, Germany, and the Bundeswehr University Munich, Munich, as a Guest Scientist and a Professor. From 2007 to 2010, he was with the Institute of Bioprocessing and Analytical Measurement Technique, Heilbad Heiligenstadt, Germany. He is interested in the measurement and processing of biosignals with implementations in industry, including developing pacemakers for the following companies: St. Jude Medical, USA, Abbott, Stockholm, Sweden, and Guidant/Boston Scientific, Natick, MA, USA. He is the author of more than 200 articles. He holds tens of patents.

Dr. Min is also a Senior Member of the IEEE Instrumentation and Measurement Society and Engineering in Medicine and Biology Society. He is on the International Committee for Promotion of the Research in Bio-Impedance (ICPRBI). He has been a Professor Emeritus since 2016.

Raul Land (Member, IEEE) was born in Estonia in 1959. He received the Dipl.Eng. degree in automation and telemechanics and the Ph.D. degree from the Tallinn University of Technology (TUT), Tallinn, Estonia, in 1982 and 2002, respectively.

Since 1982, he has been working on research at TUT, where he is currently a Researcher and a Senior Researcher with the Thomas Johann Seebeck Department of Electronics.

Indrek Must was born in Tartu, Estonia, 1985. He received the M.Sc. degree in materials technology and the Ph.D. degree in physical engineering from the University of Tartu, Tartu.

The main topic of his work is the electromechanical characterization of the ionic electroactive polymer actuators, sensors, and energy harvesters. His other research interests include the engagement of ionically active materials in soft robotics for increased biocompatibility and for the efficient use of bio-inspired strategies.

Appendix 3

III

H. Kõiv, M. Rist, M. Min. Development of bioimpedance sensing device for wearable monitoring of the aortic blood pressure curve. In tm - Technisches Messen, vol. 85, no. 5, pages 366-377. De Gruyter/Oldenbourg, 2018.

H. Kõiv, M. Rist, and M. Min*

Development of bioimpedance sensing device for wearable monitoring of the aortic blood pressure curve

Entwicklung eines Bioimpedanz-Messgerätes für die mobile Erfassung des aortalen Blutdruck

Abstract: Wearable devices that monitor our vital signs have been gaining more importance with each year. Non-invasive, continuous, accurate and precise blood pressure assessment method integrated in a wearable is a multidisciplinary challenge. This work presents an electrical bioimpedance (EBI) unit for multi-frequency measurements on pulsating artery for central aortic pressure (CAP) estimation. The developed device provides low complexity in the electronics design with a frequency range between 1 kHz and 200 kHz. It is able to register the impedance of blood vessel volume change simultaneously at different locations. Experiments were carried out in vivo by using the four-electrode configuration on human thorax, axillary artery and radial artery. Preliminary results show the applicability of the proposed impedance spectroscopy system to measure blood vessel volume changes. The impedance data can be later interpreted into the aortic blood pressure wave by using a generalized transfer function. In addition, experimental test-phantom and electrode design are introduced for testing purposes of the impedance system.

Keywords: Hypertension, aortic blood pressure, electrical bioimpedance, impedance spectroscopy, wearable, gelatine phantom.

Zusammenfassung: Tragbare Messgeräte, welche unsere Vitalfunktionen aufzeichnen, gewinnen von Jahr zu Jahr an Bedeutung. Nicht-invasive, kontinuierliche, präzise und genaue Blutdruckmessverfahren, welche in einem tragbaren System realisiert werden, sind eine multidisziplinäre Herausforderung. Diese Arbeit präsentiert ein Messgerät, welches die elektrische Bioimpedanz (EBI) ei-

ner pulsierenden Arterie misst, um den zentralen aortalen Blutdruck (CAP) zu bestimmen. Das entwickelte Gerät basiert auf einem einfachen elektrischen Design und deckt einen Frequenzbereich zwischen 1 kHz und 200 kHz ab. Es ermöglicht die simultane Erfassung der Volumenänderung einer Arterie an mehreren Messpunkten. Die Experimente wurden in vivo mit einer Konfiguration aus vier Elektroden an einem menschlichen Thorax, Arteria axillaris und der Arteria radialis durchgeführt. Zwischenergebnisse zeigen die grundsätzliche Anwendbarkeit der Impedanzspektroskopie, welche die Volumenänderung der Blutgefäße erfasst. Die Daten der Impedanzmessung werden mittels einer generalisierenden Transferfunktion in arterielle Blutdruckkurven umgewandelt. Des Weiteren zeigen wir ein experimentelles Phantom und das Elektrodendesign für Testzwecke des Bioimpedanzsystems.

Schlagwörter: Arterielle Hypertonie, Bluthochdruck, elektrische Bioimpedanz, tragbare Impedanzspektroskopie, Gelatine-Phantom.

1 Introduction

Raised blood pressure, also called hypertension, is estimated to cause 3.9 million deaths in Europe each year [1] and it is sometimes called the "silent killer" because it has no warning symptoms [2]. Evaluation of hypertension involves careful measurement of patient's pressure in the aorta, which is the best indicator showing the real load on the heart. Also, it is not influenced by the wave reflections due to artery branching [3]. At the moment, the most accurate and precise method is the direct invasive measurement, when a pressure transducer is connected to the tube catheter, which is inserted into the aorta through radial or femoral artery. Unfortunately, invasive procedure can cause several complications to the patient: infections, hemorrhages, hematomas, and arterial embolization [4]. As invasiveness is not desired in clinical field, our research is now dealing with the ways to make trustable non-

*Corresponding author: M. Min, Tallinn University of Technology, Thomas Johann Seebeck Department of Electronics, Tallinn, Estonia, e-mail: mart.min@ttu.ee
H. Kõiv, M. Rist, Tallinn University of Technology, Thomas Johann Seebeck Department of Electronics, Tallinn, Estonia

Table 1: Comparison of different devices using tonometry method to measure central aortic pressure.

Device	Method of waveform recording	Sensor location	Pros+/Cons-	Method of estimation	Company
SphygmoCor [5]	Radial tonometry	wrist	+ industrial standard for non-invasive CAP estimation, operator can select the best possible reading, thus minimising artefacts. − compresses underlying artery, handheld, operator dependent and difficult to apply constant pressure, poor reproducibility.	GTF (radial-aortic)	AtCorMedical, Australia
BPro[9]	Radial tonometry	wrist	+ 24 h measuring possible at home environment, FDA and CE approved. − plunger compresses the artery, inconsistent pressure.	GTF (N-point average)	HealthSTATS, Singapore
TL-300 [10]	Radial tonometry	wrist	+ wrist bracelet system − moving artefacts, only measured by clinical personnel.	GTF (radial-aortic)	Tensys Medical, Inc., USA
HEM-9000AI [11]	Radial tonometry	wrist	+ array of sensors − inconsistent pressure, still needs more research.	Linear regression algorithm	Omron Healthcare, Inc., Japan

invasive measurements to evaluate central aortic pressure waveform continuously.

Currently, the "gold standard" to detect the central aortic pressure (CAP) non-invasively, is the radial artery applanation tonometry, which has the widest application in devices performing pulse wave analysis [5]. Typically, a pencil-like pressure sensor is placed manually onto the radial artery over the radius bone and a constant applanation is applied against the blood vessel for the waveform reading [6]. The intra-arterial forces, sensed by a pressure transducer, are then translated into the aortic pressure waveforms using generalized transfer function (GTF) [7].

Table 1 compares non-invasive tonometry devices for estimation of CAP. Comparison shows that every device has disadvantages and due to the absence of satisfactory solutions, we proposed bioimpedance measurement method as an alternative diagnostic tool for indirect assessment of the CAP. Electrical bioimpedance (EBI) is measured on the radial artery on the wrist and the changes of artery impedance are translated into the central aortic pressure curve using transfer function (TF) similarly as in applanation tonometry. The first results were published in 2013, where Krivoshei et al. [8] introduced EBI measurement system based on the CircMon circulation monitor from JR Medical (Tallinn, Estonia) with a bracelet-type tetra-polar sensor.

The 4-electrode sensor was placed onto the radial artery close to scaphoid bone with the 5 mm distance between the electrodes.
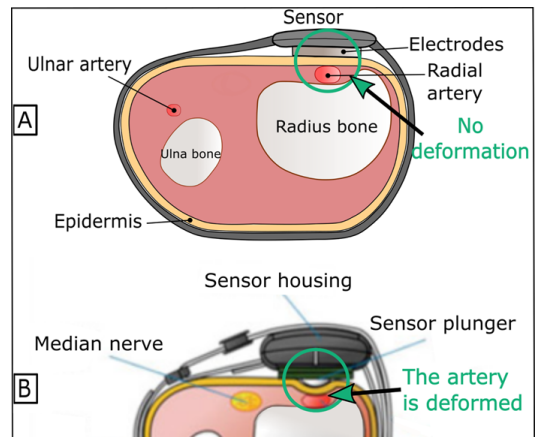

Figure 1: A – Bioimpedance electrodes placed on the artery to estimate the CAP. B – wearable tonometry sensor placed on the radial artery, which uses a plunger pressing against the blood vessel.

Using impedance electrodes instead of applanation tonometry plunger, does not require artery deformation. Figure 1 shows clearly how the tonometry plunger system is pressing the radial artery against the radius bone (Figure 1B), but the impedance electrodes do not (Figure 1A). We expect that the need for an artery deformation is a serious drawback of the method. However, the contact between EBI electrodes and skin must be excellent to avoid motion artefacts as well.

A prototype of the applied bioimpedance sensing system can be seen in Figure 2, where impedance cardiograph
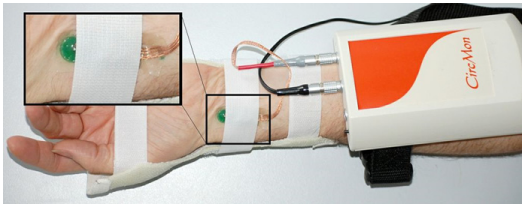
Figure 2: CircMon BT101 based bioimpedance measurement system.

is depicted together with the wearable wrist gantry. Four electrodes are used for impedance registering: 2 for voltage pick-up and 2 for current excitation. The frequency of the measurement signals was 120 kHz. In addition to EBI measurements, simultaneous recording of the central pressure was taken invasively using pressure sensor catheter [12]. Also, SphygmoCor tonometry device (Australia) was used to compare the results with invasive and bioimpedance measurements. Experiments were made with 53 voluntary patients in East-Tallinn Central Hospital, Estonia. Proposed generic transfer function between EBI and the CAP showed surprisingly good results and these can be seen in before-published articles [8, 13] and [14].

While many advancements of the system are still needed, the first clinical experiments are encouraging. In this light, the present paper focuses on improvements we have been doing for better bioimpedance measurements. This includes new impedance analysis unit for multi-frequency and multi-site measurements on pulsating artery, test-phantom preparation and development of new bending electrode system.

2 Unsolved problems and advancement ideas

Although the methods for non-invasive monitoring of CAP have evolved substantially, implementations in wearable technology for continuous tracking of the pressure curve are still not reliable enough.

Motion artefacts are one major obstacle in application of the tonometry, and this is problematic also for the given bioimpedance sensor. Electrode location and the applied force clearly affect the motion artefact [15], which means that the electrodes must be strictly fixed on the wrist on radial artery and the patient cannot move his/her hand without restraints during the measurement. For the continuous and long-lasting pressure analysis, convenience is particularly important, but the patient not being able to

move, will give us no advantage in front of already clinically approved tonometry method. Conductive textile or silicone would be a good flexible and stretchable alternative to traditional metal electrodes, which tend to corrode and require stiff contact. Additional studies are required, both research and experimentations.

For our specific method, one main unsolved and important fact is that we don't know why the radial artery bioimpedance signal correlates (through the mathematically expressed transfer function [13]) so firmly with the central aortic pressure. Patient's vascular distinctiveness like age, sex, illness, and augmentation index can be extremely variating, but in practice, the generalized transfer function [16], which associate the bioimpedance changing waveform with the aortic blood pressure curve, work satisfactorily in spite of the above given disparities.

One hypothesis is that although the fluidic impedance of the vascular system from the aorta to the radial artery is indeed different for individual patients, the vascular resistance of palm's capillary system is definitely greater than radial artery's fluidic impedance. If the heart ventricle provides the blood pressure in the aorta (analogous to electrical voltage), then we can expect that the blood pressure on the radial artery does not depend much on the properties of the blood vessels from the aorta to radial artery. The situation is similar to voltage measurements, where the measured voltage does not depend on the impedance of the cables (circuitry). This very simplified model does not take into account reflections and the activity of blood vessels themselves, but gives an insightful explanation to the problem. To prove our hypothesis, an experimental model of simplified vascular system and physical hand phantom are under development. Also, a new multi-frequency measurement unit is proposed to get more real-time information about the blood pressure variations and suppress motion artefacts. In addition, a guarded electrode system is proposed to reduce uncertainties of current flow in the wrist area.

3 Phantom for testing

3.1 Phantom background

One interesting part is to develop a tissue-similar phantom of wrist with radial artery to solve some of the raised problems in the last chapter.

Phantoms are objects that mimic living tissues and they are often used in different medical diagnostic fields

such as optical spectroscopy, ultrasound, impedance tomography and magnetic resonance imaging to name few. Phantoms that are reproducible and stable with well-controlled properties, are useful for calibrating, testing or controlling existing techniques or new developments. Also, it is possible to reduce animal and human experiments when proper tissue-similar sample is available [17].

Many bioelectrical non-invasive impedance-based methods such as bioelectrical impedance analysis (BIA), impedance plethysmography (IPG), impedance cardiography (ICG), electrical impedance spectroscopy (EIS) and electrical impedance tomography (EIT) have been proposed and applied for clinical, medical and biomedical applications. The phantoms are usually required to calibrate, compare and evaluate these systems before applying them on the real subject under the test for practical imaging purposes [18].

In the given study, we are interested in a phantom that allows in-lab investigation of the tetra-polar bioimpedance electrodes. For this, the phantom base should have similar electrical conductivity as hand muscle, it should have pulsating radial artery and its pressure and frequency must be controllable. In addition, artificial radial artery should be elastic, slightly conductive and have small diameter. Overall, it is expected to have features that are as anatomically realistic as possible. The electrical properties (relative permittivity, ε_r and conductivity, σ) of different tissues of human body are varying according to their types [17]. Gabriel et al. [19] have identified dielectric properties of different tissues in the range of 10 Hz to 100 GHz and information about the parameters are taken from it.

Firstly, we are designing a hand model that has muscle tissue, blood vessel, blood and cortical bone. Goal in the future is to make a more accurate model with extra layers on the muscle – skin and fat. This broadens the phantom's usage possibilities.

Questions to be answered by developing a phantom:
– How other tissues around the pulsating radial artery, for example radial veins around the artery and bigger cephalic vein near it, influence components of the model, hence how this can be detected with impedance change;
– Why does radial artery bioimpedance signal correlate so well with the central aortic pressure in spite of the different patients?

3.2 Phantom preparation

Phantom is made of gelatine material because gelatine is formed by natural macromolecules, it is biodegradable,

can be easily manipulated with NaCl for desired dielectric properties and has a low cost [20]. Gelatine is very suitable for phantoms that need to hold its figure and have different shapes as it is easily formable with different molds and water-gelatine solutions closely simulate the density and viscosity of the human tissue [21]. It is needed to simulate realistic situation of soft tissues and its layers, so, in first proposed hand model we are using gelatine as a base material.

The fabrication process of the hand phantom:
– dilating gelatine powder (225 PS18, Rousselot) in distilled water;
– heating it on water bath (around 70 °C) and letting it to melt into unified liquid;
– adding NaCl (99+ %, Sigma-Aldrich) into the water to adjust the electrical conductivity;
– adding formaldehyde solution (37 wt%, Sigma-Aldrich) to rise the melting point of the mixture (gelatine's melting point is quite low, 35 °C) so it could be used at room temperature for longer time;
– adding preservative Ethyl 4-hydroxybenzoate (99+ %, Sigma-Aldrich) to avoid bacterial growth.

3.3 Experiments with phantom

The gelatine mixture is poured into the silicone mold and PVC forearm skeletal is placed inside it together with very flexible and small silicone tube for artery mimicking. After solidifying of gelatine, outcome is seen in Figure 3B – experimental physical forearm phantom. In addition, Stöckert SIII Heart Lung System (Figure 3A) was used to pump coloured water through the artificial radial artery to imitate pulse. It was possible to palpate for the pulse near the scaphoid bone and overall, the hand looked satisfactorily realistic. Few experiments were made to get an insight on how impedance change occurs on gelatine phantom with pulsating artery and how reliable it is. For radial artery mimicking, conductive silicone tube is currently under development. Radial artery is characterized with low conductivity (approximately 0.3 S/m [19]) and it is quite elas-
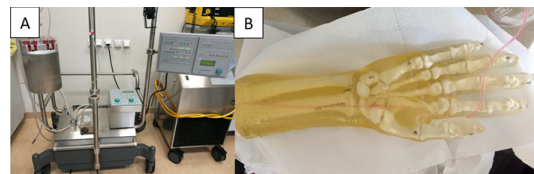

Figure 3: A – Stöckert SIII Heart Lung System. B – First experimental hand phantom.

tic. At the moment, silicone tube was used for the blood flow, but as silicone is not a conductive matter, it is not useful for our impedance sensor measurements as electrical current is not passing through it. Past researches suggest that carbon fibre or carbon nanotubes added to the silicone mixture could give us needed outcome – flexible and marginally conductive tube [22, 23]. Since the electrical conductivity of carbon nanotubes is known to be extremely high (~18000 S/cm [24]), a significant increase of the conductivity of elastomers can be expected when they are properly dispersed. Adding the fillers is challenging because the end material should be very homogeneous for evenly distributed conductivity throughout the silicone tube. As the silicone mock artery is still under development, cavity inside the phantom was used as an alternative. Gelatine mixture was poured inside the box, which had aluminium rod crossed through it. After solidifying of the mixture, the rod was carefully removed and cavity was left inside the sample. In this study, we used current injection and voltage measurements between adjacent electrodes to register impedance change on pulsating "artery". Four electrodes were attached to the surface of phantom and impedance change was registered with MFLI Lock-in Amplifier (Zürich Instruments AG, Switzerland). Artificial pulsating blood flow was generated with Stöckert SIII Heart Lung System and pressure sensor was attached to the system to read pressure variations.

Two experiments were prepared:

1. gelatine test object with silicone tube inside and water pumped through it;
2. gelatine test object with cavity inside and saltwater pumped through it.

First experiment showed minimal impedance change with every pulsation as expected because silicone tube is non-conductive and electrical current cannot pass it. Though, small change was registered due to the slight movement of the test object (capacitive current) and electrodes having a better contact with every pulsation. For second experiment setup, saltwater with 10 wt/vol% NaCl was pumped through the cavity. This time when pressure increased, impedance decreased unlike in the previous experiment. Now, electrical current can move through the conductive gelatine and saltwater, thus impedance change is registered. Unfortunately, due to gelatine's properties, it cannot go under large deformation without cracking. Every test object with cavity as an artery, split approximately after 20 minutes of work. Nevertheless, experiments with proposed dynamic model insightfully depicted how pressure and impedance change are connected. When pressure grows, cavity dilates and volume of saltwater is big-

ger, which means that the impedance value is slightly lower. These preliminary results suggest that given phantom is geometry-dependent. Volume increase results in a swelling of the cross-sectional area of the cavity and the conductance will increase slightly as is needed. If the volume increase would have occurred outside the measured tissue volume, the measured conductance would not have changed with the geometrical volume increase and if the volume increase would have resulted in a swelling of length, conductance would have decreased [25].

4 Development of the wearable measurement unit

Although the medically approved impedance cardiograph CircMon BT101 showed a good capability during special diagnostic procedures in hospital, it is not appropriate for wearable use. Therefore, a low complexity impedance measurement unit with lower power consumption and smaller size was designed based on Quadra impedance spectrometer introduced in [26, 27]. A similar approach was successfully used for the design of a real time EBI measurement system for Finnish company, Injeq Oy [28]. The present unit (see Figure 4) is built up on the basis of TMS320F28069 signal processor from Texas Instruments (USA), containing, besides the digital computing part, also built-in 12-bit analog-to-digital converter (ADC). Especially important is the high resolution (150 ps) pulse width modulator (PWM) for generating the binary excitation voltage U_{EXC} at 100 MHz clock, and a dual multiply-accumulate (MAC) 16×16 bit processing unit for performing the discrete Fourier transform (DFT) of the digitized response voltage U_{OUT}. As a result, a real time spectral analysis after every 1 ms time interval is available. Task specific analog input/output interfaces have to be designed for individual applications. Unfortunately, the simple voltage excitation and response current measurement principle is not applicable for two reasons, 1) four-electrode system with excitation from current source is needed to reduce the role of uncertain skin impedance, and 2) the level of current through a living tissue must be determined definitely below the allowed level [29].

Therefore, a more complicated solution is proposed (Figure 5), where a voltage-to-current converter (U-to-I) is added to receive more stable excitation current through the sample under test (SUT). This converter uses a symmetric current sensing negative feedback from R_{REF1}, which turns the generated voltage U_{EXC} into the excitation current I_{EXC}. Spreading of I_{EXC} throughout the human tissue is
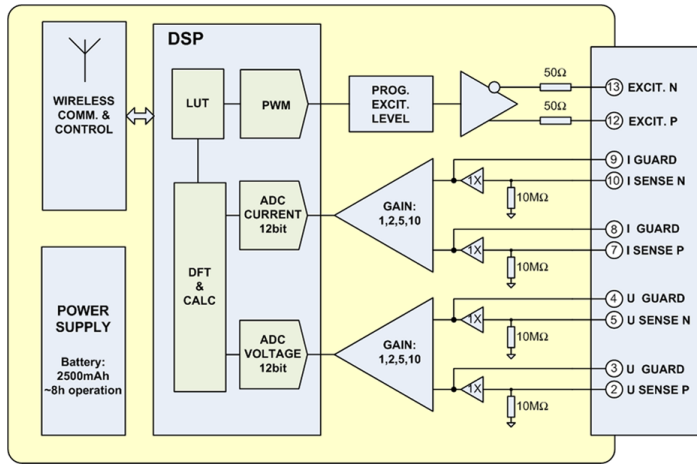
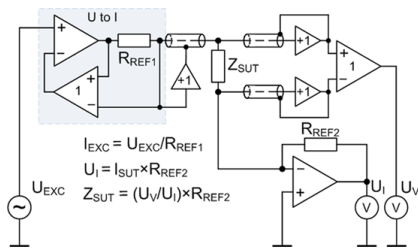**Figure 4:** Block diagram of the impedance measurement unit.

Figure 5: Voltage excitation (U_{EXC}) with voltage to current (U-to-I) conversion and current (I_{EXC}) measurement; guarding against the spreading of the excitation current is applied.
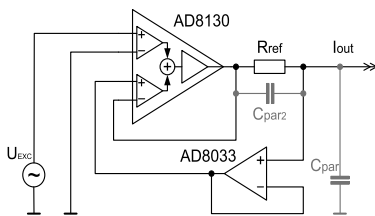

Figure 6: An electronic circuit for converting the excitation voltage into current excitation (U-to-I converter).

Figure 7: Binary multi-frequency excitation voltage with the amplitude of 1 V, generated for conversion into excitation current I_{EXC}.

avoided by using potential guarding on the shielded output, achieved with the unity gain voltage following amplifier.

The developed U-to-I converter in Figure 6 is built up on the basis of the differential difference amplifier AD8130 from Analog Devices, USA. An operational amplifier AD8033 (also from Analog Devices) with 100 % 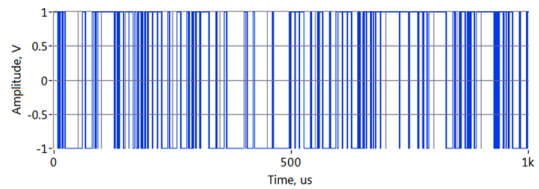feedback operates as a unity gain and high input impedance voltage follower for receiving a general current feedback from the resistor R_{REF}. The characteristics are given at two values of R_{REF}: 1 kΩ and 10 kΩ. For obtaining the current with 1 mA peak value with the 1 V excitation voltage (Figure 7), R_{REF}=1 kΩ was chosen for the U-to-I converter. The capacitances C_{par} and C_{par2} in Figure 6 denote inevitable stray capacitances, which are found to be 10 pF. Albeit the current I_{EXC} through the Z_{SUT} is stabilized (see Figure 5 and Figure 6), the designed I-to-U converter (Figure 6) is still far from an ideal current source with infinite output impedance.

In Figure 8, there is characterized, how the output impedance of the current source (voltage-to-current converter) decreases with the frequency. It is less than 100 kΩ at the frequencies over 100 kHz but still acceptable, because the Z_{SUT} remains below 1 kΩ. Furthermore, undesirable leakage current through the stray capacitances and resistances takes place. For that reason, the connections from SUT to the input of differential voltage pick-up amplifier are shielded and guarded by equipotentials through voltage followers with unit gain (+1). This method reduces the current runaway from Z_{SUT}, but does not pre-
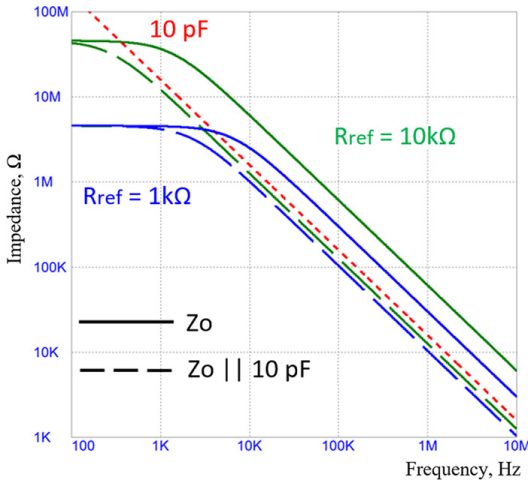
Figure 8: Output impedance of the U-to-I converter without Cpar =10 pF (Zo, continuous lines) and with Cpar (Zo||10 pF, dashed lines) in two cases: Rref = 1 kΩ (green lines) and Rref = 10 kΩ (blue lines).
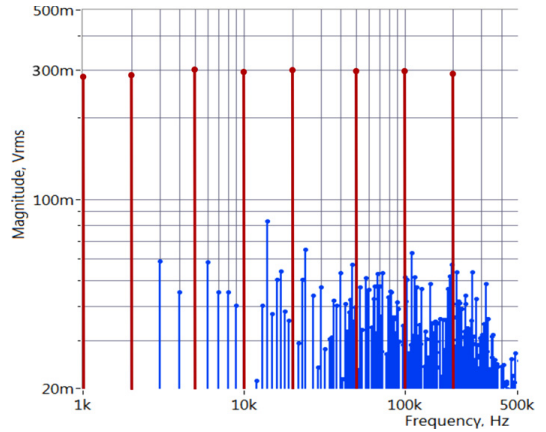

Figure 10: Spectrum of the used binary multi-frequency excitation containing the useful spectral components at the frequencies of 1, 2, 5, 10, 20, 50, 100 and 200 kHz. Root-mean-square (RMS) value of individual spectral components of the excitation voltage is 300 mV.
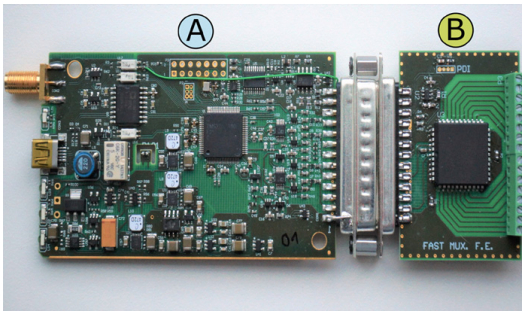

Figure 9: A photo of the prototyped impedance measurement unit (A) together with a multiplexer (B) connected to the input.

vent it entirely. Therefore, the current from Z_{SUT} is measured through U_I obtained with the aid of an operational amplifier with negative feedback via the resistor R_{REF2} in Figure 5 (forms an inverting current-to-voltage converter, $U_I = -I \cdot R_{REF2}$).

The prototyped measurement unit A together with input multiplexor B is shown in Figure 9. The prototype contains the digital part (see Figure 4) as well as analog parts, given in Figures 5 and 6.

The original Quadra device covers 1 kHz to 349 kHz simultaneously at 15 frequencies by generating a pulse width modulated (PWM) binary multi-frequency (BMF) excitation packages with 1 ms duration [27]. The developed prototype uses the same proprietary technology but within

more narrow frequency range – up to 200 kHz (see the binary waveform in Figure 10), which is covered by maximally 8 semi-logarithmically distributed frequencies.

We limited the frequency range keeping in mind the simple assemble and low power consumption of the device. Wider frequency range will not add any additional information to our scope. Nevertheless, measurements at several frequencies enable to extract the useful information more dependably while introducing soft computing methods like fuzzy logic and principle component analysis (PCA) [28].

The prototype was tested for uncertainty and repeatability of the measurement results. Results showed that the 0.5 % relative error is inherent to the measurement system, but the repeatability of changes falls into 0.1 % error zone, which extends up to 200 kHz frequency, if measuring the impedances ranging from 60 Ω to 10 kΩ.

5 Multipoint measurements

Although the measurements with CircMonBT101 impedance cardiograph are currently underway in Tallinn Central Hospital with different patients needing coronary angiography, we are carrying out multipoint measurements to get a better hindsight what could make ongoing research more valuable, keeping in mind the development of wearable devices for continuous monitoring. An idea was to obtain impedance signals from three different
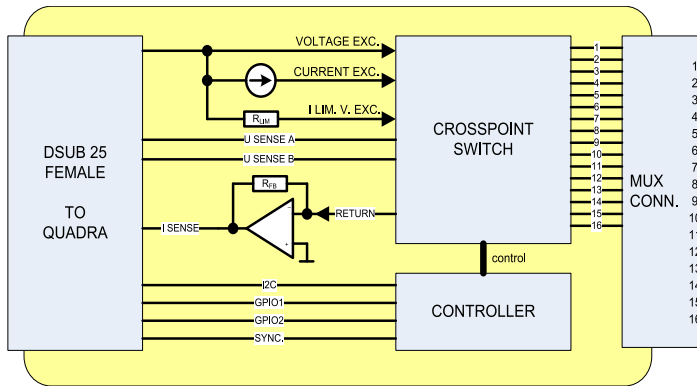
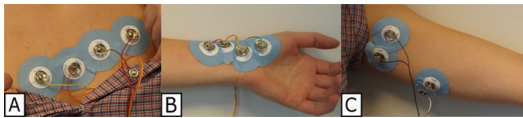**Figure 11:** High-speed multiplexer frontend.

Figure 12: Different placements to measure impedance. A – thorax. B – radial artery. C – axillary artery.

places on human body at the same time. The most desirable signal pick-up location for us is a forearm as many comfortable wearables are usually worn on the wrist. With performed experiments we tried to compare different measurement positions on a human body for signal analysis.

For this, the developed fast impedance measurement unit was used (see Figure 9). Multiplexer (Figure 9B) allows the device to switch between different sets of electrodes placed in the predetermined locations. It is performed using a cross-point switch CD22M3494 from Intersil. This is an analog switch that allows switching any of its input pins to any of its output pins. All the 16 inputs/outputs are bi-directional and can be used for passing both excitation and sense signals. Simplified block diagram of the multiplexer is shown in Figure 11.

The multiplexer operates semi-independently of the measurement device by including a dedicated microcontroller that is configured to perform user defined switching patterns. The switching time and patterns are programmed into the multiplexer's microcontroller and the automated switching is enabled. The process takes ~100 µs together with the step response after switching. As a result, one 1 ms acquisition cycle will be flawed and the minimum acquisition takes two cycles (2 ms per position).

The introduced spectroscopy device together with multiplexer is accustomed to measure from three different places near the arteries that could theoretically give

us impedance waveforms with complementary information. First multiplexer position is used to measure from the thorax, near the heart (Figure 12A). Second position is on the wrist, near the radial artery (Figure 12B). The third position is near the axillary artery on the upper arm (Figure 12C). Four wet pregelled Ag/AgCl electrodes were applied to get minimally corrupted impedance waveforms from the picked places. The aim of the setup is to analyse impedance changes and study the three different waveforms that are registered from various locations.

6 Preliminary results

Figure 13 shows the impedance curves of three positions simultaneously. X-axis represents the time period and y-axis shows the relative trend of the magnitude from the initial average value (near to 102.84 Ω seen in Figure 14). As an example, the measurements shown in Figures 13 and 14 were performed at the frequency of 50 kHz.
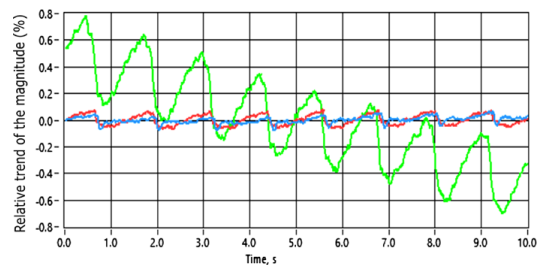

Figure 13: Measured impedance variation waveforms: green line – chest impedance when breathing withheld; blue line – variations measured on the wrist; red line – variations measured near the axillary artery.
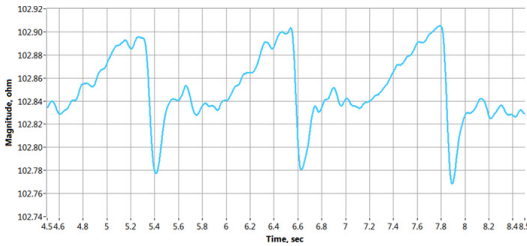
Figure 14: Waveform of the wrist impedance measured on the radial artery (extracted out, filtered and zoomed from the blue line from Figure 13).

Figure 15: Two pairs (A and B) of guarded electrodes for injection of excitation current IEXC (A) and pick-up of the response voltage VOUT (B).

Noticeably, the best result is obtained from the thorax (green line) – variations are clear and strong. The signals from the axillary (red line) and radial artery (blue line) are weaker and their bio-modulation is lower, but the beat-to-beat changes of impedance are still visible and can be acquired reliably. If the measurement conditions are good (electrodes are placed near the artery and are fixed sufficiently, the subject under the test is not moving and holding breath) then the pulse wave is clear and distinctive. Figure 14 shows a signal, which is taken from the radial artery and Savitzky-Golay filter was applied to the raw signal to suppress additive noise. The extracted and filtered waveform is presented in ohms – how the magnitude of radial bioimpedance changes during three heart cycles. When pulse wave comes in, the pressure in the artery rises and impedance descends quickly. After the fall, impedance increases continuously until the next pulse wave appears.

With these results we can recognize that under given conditions the designed impedance measurement unit can execute the tasks of wearable devices for continuous monitoring of central blood pressure waveforms. The signal measured from the wrist has smaller bio-modulation than the signal from the thorax but it is still informative and usable for later signal processing to compare it with aortic pressures.

At the same time, the performed experiments showed also that the careful electrode design should be included to the development. The level of skin hydration, motion artefacts and the extent of gel penetration in the tissue change the impedance significantly in unknown manner and uncertain rate. As a result, badly defined current leakage on the skin surface and uncertain spreading of the excitation current in the tissue, both make the stable measurements problematic with used electrodes – the stainless steel electrodes in CircMon system and the pregelled Ag/AgCl electrodes in Quadra based system.
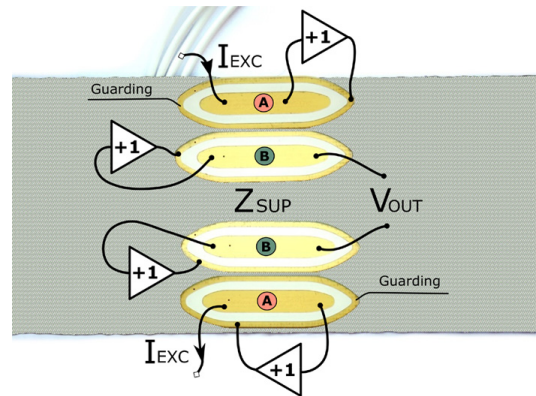
We propose flexible gold coated electrodes with guarding strips (Figure 15) to overcome the measurement instability. These tetra-polar electrodes have a pair A for current excitation I_{EXC}, and another pair B to pick-up the voltage U_{OUT} as a response from the impedance to be measured Z_{SUT}. The guarding of electrodes with voltage followers (unit gain amplifiers in Figure 15) is expected to reduce the instability significantly. Equipotential guarding is required not only for preventing the leakage of the excitation current from electrode pair A, but also for avoiding the non-informative signal intrusion to voltage electrodes B. At the moment, the electrode design introduced is at an idea level as some technical aspects still need to be solved. Especially, how to make the electrode material flexible as softer materials have the advantage of fitting easily against the skin and with this increase the contact area.

7 Discussion

Estimating aortic pressure from peripheral arteries has been a tedious task for many researchers and the work in this field continues. Currently, most reliable and non-invasive devices used to estimate the CAP are based on applanation tonometry and there are no commercial devices using impedance method for similar goal to the best of our knowledge. There are numerous reasons for that: significant motion artefacts, signal to noise ratio, weak signal and unclear electrode placement.

Our study introduces new development ideas to improve bioimpedance measurements on radial artery. This

includes first attempts on developing a physical phantom for EBI sensor testing and preliminary results demonstrate a good prospect on used materials and methods. The phantom gives a competitive advantage in controlling the variables that are affecting the measurement of artery fluctuations. Also, introduced guarded flexible electrodes used in impedance sensing could make moving artefacts insignificant but experiments are needed to prove the efficiency of the design.

Further, developed impedance analysis unit that is used for multipoint measurements with multiplexing give a new side to the ongoing data collection. Low-power and fast bioimpedance spectroscopy is especially useful when impedance value of the measured test object is changing rapidly. This technique enhances the detection of blood volume changes in different arteries simultaneously. Fast device can detect the diversities more reliably and this improves overall results greatly. As biological tissue shows a frequency-dependent behaviour to an applied alternating electrical signal, it is only reasonable to see the impedance response in wider spectra. In our case, from 1 kHz to 200 kHz. Also, spectroscopy could help to see if the electrode-skin contact is sufficient for the measurement. When the contact is not stable enough, the current will flow between the electrodes on the skin and not through the tissue – impedance base value is small due to the sweat on the skin which acts as a natural electrolyte. If current moves inside the tissue, then with increasing frequency the impedance base value changes according to the tissue's beta-dispersion graph [25]. This could give us certainty that the current is definitely flowing through the needed sample.

From recent literature we can find some prototype devices using impedance measurements to successfully register blood volume changes on forearm [30, 31, 32]. These devices can be used only for one frequency measurements and our proposed multi-site spectroscopy method has many beneficial features compared to others: fast impedance spectroscopy enables to conduct time-variant impedance spectral analysis, low power consumption allows cheaper manufacturing and multi-site measurements make signal correlation more reliable. Recent spectroscopy devices found in literature [33, 34] are usually using multi-sine as excitation but our presented prototype uses much simpler solution – sequence of binary pulses introduced in Chapter 4.

One downside regarding our methodology is that the current study was limited by the small number of various experiments and further data collection is required to determine exactly how beneficial introduced device for non-invasive aortic blood pressure estimation from radial

artery is. Future work involves the development of silicone material with controllable conductivity and testing its applicability inside the artificial gel phantom together with impedance measurements. Final ambition is to test the designed measurement unit and novel electrode system on a phantom, changing the properties of the test object according to the specific needs (different arteries, blood pressure, layers of tissues, electrode placement, materials etc.). To further our research and validate the impedance spectroscopy device, we intend to compare invasive pressure measurement results from the human aorta to interpreted bioimpedance curve taken simultaneously from peripheral arteries. For this, proposed device has to be medically approved and reliable enough for accurate and precise measurements on patients. In order to achieve that, firstly, the moving artefacts need to be minimized for patient monitoring possibilities and flexible electrodes with guarding, introduced in Chapter 6, will be prepared and tested on various human wrists (big, small, hairy, fatty, bony etc.).

8 Conclusion

Our work has led us to conclude that measuring impedance on radial artery with developed fast impedance spectroscopy device is more beneficial than impedance cardiograph which allows measurements only on one frequency. It may give valuable information about quality of electrode-skin contact in addition to dynamic volume changes of blood in artery. Besides, introduced flexible electrodes with guarding enable to avoid current leakage on the skin and define exact current flow inside the tissue. We believe that including the spectroscopy, multisite measurements and flexible guarded electrodes enable both – increased repeatability and minimized disturbances. Also, the developed phantoms allow to understand the blood flow and pressure processes in arteries more deeply. As a result measurement system parameters and working regime can be better determined.

Further experimental investigations are needed to make the bioimpedance fast spectroscopy useful for continuous aortic blood pressure estimation.

References

1. ESC, "European cardiovascular disease statistics 2017 edition, " Tech. Rep., 2017.
2. "High Blood Pressure (Hypertension) Information | cdc.gov," Cdc.gov, 2017 [Online]. Available: https://www.cdc.gov/bloodpressure/index.htm [Accessed: 10-Sep-2017].
3. C. M. McEniery, J. R. Cockcroft, M. J. Roman, S. S. Franklin and I. B. Wilkinson, "Central blood pressure: current evidence and clinical importance," *Eur. Heart J.*, vol. 35, no. 26, pp. 1719–1725, Jul. 2014.
4. B. Freeman and J. Berger, Anesthesiology Core Review: Part 2, Chapter 1: Invasive Arterial Blood Pressure Monitoring, Cenveo® Publisher Services, 2016.
5. A. Avolio, M. Butlin, and A. Walsh, "Arterial blood pressure measurement and pulse wave analysis – their role in enhancing cardiovascular assessment," *Physiological Measurement*, vol. 31, no. 1, pp. R1–R47, 2009.
6. L. Nainggolan, "New Devices to Measure Central Aortic Pressure: Interesting But Premature," *Medscape*, 2011.
7. S. DeLoach and R. Townsend, "Vascular Stiffness: Its Measurement and Significance for Epidemiologic and Outcome Studies," *Clinical Journal of the American Society of Nephrology*, vol. 3, no. 1, pp. 184–192, 2008.
8. A. Krivoshei, J. Lamp, M. Min, T. Uuetoa, H. Uuetoa and P. Annus, "Non-invasive method for the aortic blood pressure waveform estimation using the measured radial EBI," *Journal of Physics: Conference Series*, vol. 434, 012048, 2013.
9. "Home – HealthSTATS," Healthstats.com, 2017 [Online]. Available: http://www.healthstats.com/index3.php?page=product_bppro_intro [Accessed: 3-Feb-2017].
10. "Tensys Medical – cetrixtablets," *cetrixtablets*, 2018 [Online]. Available: http://www.cetrixtablets.com/project-details/tensys-medical/ [Accessed: 10-Jan-2018].
11. O. monitor, "Omron HEM-9000AI blood pressure mon," *Medi-Shop*, 2018 [Online]. Available: http://www.medi-shop.gr/en/patient-monitors/omron-hem-9000ai [Accessed: 07-Jan-2018].
12. "The intelligent pressure monitoring system, CODAN, Xtrans, Brochure" [Online]. Available: https://www.codan.de/documents/website/GB/CODAN_Xtrans_GB.pdf [Accessed: 3-Nov-2017].
13. A. Krivošei, H. Uuetoa, M. Min, P. Annus, T. Uuetoa and J. Lamp, "Adaptive Algorithm for Cardiac Period Normalization in Time," in *Book of Abstracts: 16th International Conference on Electrical Bio-Impedance (ICEBI) and the 17th Conference on Electrical Impedance Tomography (EIT) 2016*, pp. 66, 2016.
14. A. Krivošei, M. Min, P. Annus, H. Kõiv, A. Aabloo and T. Uuetoa, "Analysis of Instantaneous Cardiac EBI Signal Variability over the Heart Cycle(s): Non-Linear Time-Scale Approach," in *Joint Conference of European Medical and Biological Engineering Conference (EMBEC) and Nordic-Baltic Conference on Biomedical Engineering and Medical Physics (NBC) (EMBEC2017), Tampere, Finland*, pp. 940–943, 2017.
15. A. Cömert and J. Hyttinen, "Investigating the possible effect of electrode support structure on motion artifact in wearable bioelectric signal monitoring," *BioMedical Engineering OnLine*, vol. 14, no. 1, 2015.
16. M. Min, A. Krivošei, P. Annus, H. Kõiv, T. Uuetoa and J. Lamp, "Bioimpedance sensing – a viable alternative for tonometry in non-invasive assessment of central blood pressure", in *Proc. 12th Annual IEEE International Symposium on Medical Measurements and Applications (MeMeA, Mayo Clinic, Rochester, MN, USA)*, IEEE, pp. 373–378, 2017, DOI:10.1109/MeMeA.2017.7985905.
17. A. T. Mobashsher and A.Ṁ. Abbosh, "Artificial Human Phantoms: Human Proxy in Testing Microwave Apparatuses That Have Electromagnetic Interaction with the Human Body," *IEEE Microwave Magazine*, vol. 16, no. 6, 2015.
18. T. K. Bera, "Bioelectrical Impedance Methods for Noninvasive Health Monitoring: A review," *Journal of Medical Engineering*, vol. 2014, Article ID 381251, 28 pages, 2014.
19. C. Gabriel, S. Gabriel and E. Corthout, "The dielectric properties of biological tissues: I. Literature survey," *Physics in Medicine and Biology*, vol. 41, no. 11, pp. 2231–2249, 1996.
20. A. Pinto, P. Bertemes-Filho and A. Paterno, "Gelatin: a skin phantom for bioimpedance spectroscopy," *Biomedical Physics & Engineering Express*, vol. 1, no. 3, 035001, 2015.
21. A. K. Dabrowska, G.-M. Rotaru, S. Derler, F. Spano, M. Camenzind, S. Annaheim, R. Stämpfli, M. Schmid and R. M. Rossi, "Materials used to simulate physical properties of human skin," *Skin Research and Technology*, vol. 22, pp. 3–14, 2016.
22. A. Katihabwa, W. Wang, Y. Jiang, X. Zhao, Y. Lu and L. Zhang, "Multi-walled carbon nanotubes/silicone rubber nanocomposites prepared by high shear mechanical mixing," *Journal of Reinforced Plastics and Composites*, vol. 30, no. 12, pp. 1007–1014, 2011.
23. A. Saleem, L. Frormann and A. Soever, "Fabrication of Extrinsically Conductive Silicone Rubbers with High Elasticity and Analysis of Their Mechanical and Electrical Characteristics," *Polymers*, vol. 2, no. 3, pp. 200–210, 2010.
24. B. Mensah, H. Kim, J. Lee, S. Arepalli and C. Nah, "Carbon nanotube-reinforced elastomeric nanocomposites: a review," *International Journal of Smart and Nano Materials*, vol. 6, no. 4, pp. 211–238, 2015.
25. S. Grimnes and Ø. G. Martinsen, Bioimpedance and bioelectricity basics, Academic Press, 2000.
26. R. Land, P. Annus, M. Min, et al.Method and device for broadband analysis of systems and substances. European Patent Application EP2565654A2, Bulletin 2013/10; US Application US2013054178A1, publ. Feb. 28, 2013. – Patent.
27. M. Rist, M. Reidla, M. Min, T. Parve, O. Märtens and R. Land, "TMS320F28069-based impedance spectroscopy with binary excitation," in *EDERC 2012 Proceedings of the 5th European DSP in Education & Research Conference*, pp. 217–220, 2012.
28. S. Halonen, K. Annala, J. Kari, S. Jokinen, A. Lumme, K. Kronström and A. Yli-Hankala, "Detection of spine structures with Bioimpedance Probe (BIP)," *Journal of Clinical Monitoring and Computing*, pp. 1–8, 2016.
29. IEC 60601 – TC 62/SC 62A – Common aspects of electrical equipment used in medical practice. International Standard, Edition 1.0, 2015.
30. J. Schneider, M. Schroth, M. Holzhey, T. Blocher and W. Stork, "An approach to improve impedance plethysmography on the wrist by using adaptive feedback control," in *2017 IEEE Sensors Applications Symposium (SAS)*, 2017.

31. J. Wang, W. Hu, T. Kao, C. Liu and S. Lin, "Development of forearm impedance plethysmography for the minimally invasive monitoring of cardiac pumping function," *Journal of Biomedical Science and Engineering*, vol. 04, no. 02, pp. 122–129, 2011.

32. J. Xu, X. Gao, A. Lee, S. Yamada, E. Yavari, V. Lubecke and O. Boric-Lubecke, "Wrist-worn heartbeat monitoring system based on bio-impedance analysis," in *2016 38th Annual International Conference of the IEEE Engineering in Medicine and Biology Society (EMBC)*, 2016.

33. B. Han, Y. Xu and F. Dong, "Design of current source for multi-frequency simultaneous electrical impedance tomography," *Review of Scientific Instruments*, vol. 88, no. 9, 094709, 2017.

34. B. Sanchez, E. Louarroudi and R. Pintelon, "Time-invariant measurement of time-varying bioimpedance using vector impedance analysis," *Physiological Measurement*, vol. 36, no. 3, pp. 595–620, 2015.
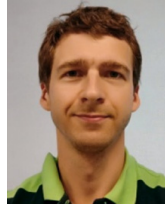
Bionotes

H. Kõiv
Tallinn University of Technology, Thomas Johann Seebeck Department of Electronics, Tallinn, Estonia
hip.koiv@gmail.com

Hip Kõiv was born in Kanepi, Estonia in 1990. She received the B. S. degree in electronics and bionics in 2013 and the M. S. degree in electronics and communication in 2015 from Tallinn University of Technology. She is currently pursuing the Ph. D. degree in Thomas Johann Seebeck Department of Electronics at Tallinn University of Technology and her current research interests include the bioimpedance study, aortic blood pressure measurements and the materials for developing biological phantoms.

M. Rist
Tallinn University of Technology, Thomas Johann Seebeck Department of Electronics, Tallinn, Estonia
marek.rist@ttu.ee

Marek Rist was born in Tallinn, Estonia, in 1980. He received the M. Sc. degree in electronics and biomedical engineering in 2007, in Tallinn University of Technology, Tallinn, Estonia with a thesis on technology for measurement of impedance of lithium-ion batteries. He is currently pursuing the Ph. D. degree in electronics engineering in Tallinn University of Technology where he is involved in several projects related to electrical impedance spectroscopy.

M. Min
Tallinn University of Technology, Thomas Johann Seebeck Department of Electronics, Tallinn, Estonia
mart.min@ttu.ee

Mart Min (M'95–SM'13) received the Diploma Engineer's qualification in electronics from Tallinn University of Technology (TUT), Estonia, in 1969 and the Ph. D. degree in measurement science from Kiev Polytechnic, Ukraine, in 1984. He has been with Thomas Johann Seebeck Department of Electronics of the TUT as a Professor and a Leading Scientist since 1992. During 1992–1993, he was with the Technical University of Munich and the Bundeswehr University in Munich, Germany, as a Guest Scientist and a Professor. During 2007–2010, he joined the Institute of Bioprocessing and Analytical Measurement Technique in Heilbad Heiligenstadt, Germany. He is interested in measurement and processing of bio-signals with implementations in industry, including developing of pacemakers for the companies St. Jude Medical (USA/Sweden) and Guidant/Cardiac Pacemakers (USA). He is a member of Instrumentation & Measurement and Engineering in Biology and Medicine Societies of the IEEE. Prof. Min belongs to the International Committee for Promotion of Research in Bio-Impedance (ICPRBI).

Curriculum Vitae

1. Personal data

Name	Hip Kõiv
Date and place of birth	2 February 1990, Põlva, Estonia
Nationality	Estonian

2. Contact information

Address	Tallinn University of Technology,
	School of Information Technology,
	Thomas Johann Seebeck Department of Electronics,
	Ehitajate tee 5, 19086 Tallinn, Estonia
E-mail	hip.koiv@taltech.ee

3. Education

2015–2022	Tallinn University of Technology, School of Information Technology, Information and Communication Technology, PhD studies
2013–2015	Tallinn University of Technology, Information and Communication Technology, MSc
2011–2012	Slovak University of Technology in Bratislava
2009–2013	Tallinn University of Technology, Electronics and bionics, BSc
1997–2009	Kanepi Gymnasium

4. Language competence

Estonian	native
English	fluent
Russian	basic
German	basic

5. Professional employment

2016–…	Tallinn University of Technology, School of Information Technologies, Thomas Johann Seebeck Department of Electronics, Junior Researcher

Elulookirjeldus

1. Isikuandmed

Nimi   Hip Kõiv
Sünniaeg ja -koht   02.02.1990, Põlva, Eesti
Kodakondsus   Eesti

2. Kontaktandmed

Aadress   Tallinna Tehnikaülikool,
                        Thomas Johann Seebecki elektroonikainstituut,
                        Ehitajate tee 5, 19086 Tallinn, Eesti
E-post   hip.koiv@taltech.ee

3. Haridus

2015–2022   Tallinna Tehnikaülikool,
                        Info- ja kommunikatsioonitehnoloogia, doktoriõpe
2013–2015   Tallinna Tehnikaülikool,
                        Info- ja kommunikatsioonitehnoloogia, MSc
2011–2012   Slovakkia Tehnikaülikool Bratislavas,
2009–2013   Tallinna Tehnikaülikool,
                        Elektroonika ja bioonika, BSc
1997–2009   Kanepi Gümnaasium

4. Keelteoskus

eesti keel   emakeel
inglise keel   kõrgtase
vene keel   algtase
saksa keel   algtase

5. Teenistuskäik

2016–...   Tallinna Tehnikaülikool, Infotehnoloogiateaduskond
                        Thomas Johann Seebecki elektroonikainstituut,
                        doktorant-nooremteadur